UNIVERSITÀ DEGLI STUDI DI PADOVA
Scuola di Dottorato in Scienze Molecolari

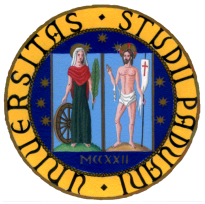

Atomistic modelling of liquid crystal materials properties: a theoretical and computational methodology

Mirko Cestari

Supervisore:
Prof.ssa Alberta Ferrarini

Direttore della Scuola:
Prof. Maurizio Casarin

2006-2008

Acknowledgements

I am particularly grateful to prof. Geoffrey R. Luckhurst who gave the chanche to visit Southampton, and for the interesting discussions about this work. Many thanks also to Alessandro Bosco for the excellent picture of the director deformation modes.

If, in some cataclysm, all scientific knowledge were to be destroyed,
and only one sentence passed on to the next generation of creatures,
what statement would contain the most information in the fewest words?
I believe it is the atomic hypothesis (or atomic fact, or whatever
you wish to call it) that all things are made of atoms little particles
that move around in perpetual motion, attracting each other when they
are a little distance apart, but repelling upon being squeezed into one another.
In that one sentence you will see an enormous amount of information
about the world, if just a little imagination and thinking are applied.

Richard P. Feynman

The Guide is definitive. Reality is frequently inaccurate.

Douglas Adams

Contents

1 Introduction **3**

1.1 Modelling of liquid crystals 3

1.2 Liquid crystals: properties 5

1.3 Liquid crystal dimers 7

1.4 Outline 10

2 Theoretical methods **11**

2.1 Bridging time- and length- scales 11

2.2 Theoretical methodologies: state of the art 11

2.3 The Surface Interaction model 13

2.4 Molecular expressions for LC properties in the SI framework 15

2.4.1 The Saupe ordering matrix 15

2.4.2 Properties at the Nematic-Isotropic (NI) transition 16

2.4.3 Dielectric permittivity 17

2.4.4 Flexoelectric coefficients 17

2.4.5 Molecular flexibility 18

3 Molecular expressions for the elastic constants **21**

3.1 Introduction 21

3.2 Abstract 24

3.3 Introduction 25

3.4 Theory: elastic constants of LC by the Surface Interaction method 28

3.4.1 Inclusion of molecular flexibility 32

3.5 Computational methodology 34

3.6 The elastic constants of 5CB 35

3.7 Conclusions 38

3.8 Appendices 41

3.9 References 51

4 Computational methodology and parametrisation for selected systems **65**

4.1 Introduction 65

4.2 Single molecule properties 66
4.2.1 Torsional potentials for CBOnOCB and CBOnOFF 66
4.2.2 Torsional potentials for CBnCB 71
4.2.3 Bond angles 73
4.2.4 Atomic charges 75
4.3 Definition of transferable fragments 76
4.4 Rotational Isomeric State approximation (RIS) 77
4.4.1 Geometry 78
4.4.2 Energy 78
4.4.3 The cut-off distance 80
4.5 Monte Carlo sampling of conformations 82
4.5.1 Scheme of the Monte Carlo sampling procedure 82
4.6 Computational scheme 86
4.7 Molecular surface 88

5 Results
Elastic constants of typical mesogens **89**
5.1 Introduction 89
5.2 Summary 92
5.3 Introduction 93
5.4 Elastic constants of LC by the Surface Interaction (SI) method 95
5.5 Results and discussion 98
5.6 Conclusions 103
5.7 References 106

6 Results
Rotational Isomeric State approximation **121**
6.1 Introduction 121
6.2 Order parameters and NI transition properties 122
6.3 Flexoelectric coefficients 126
6.4 Dielectric permittivity 131
6.5 Elastic constants 140

7 Results

Monte Carlo sampling of conformations **149**

7.1 Introduction 149

7.2 Flexoelectric coefficients 155

7.3 Dielectric permittivity 155

7.4 Elastic constants 161

7.5 Interpretation of experiments 161

List of abbreviations

QM	Quantum Mechanics
LC	Liquid Crystal
MC	Monte Carlo
MD	Molecular Dynamics
RIS	Rotational Isomeric State
NI	Nematic-Isotropic
DFT	Density Functional Theory
MP2	Moeller-Plesset 2nd order
SI	Surface Interaction
SES	Solvent Excluded Surface

1 Introduction

1.1 Modelling of liquid crystals

Liquid crystals (LCs) are a condensed phase between the isotropic liquid and the solid crystalline phases; for this reason they are also called *mesophases*. The constituting molecules, called *mesogens*, are preferentially aligned along a direction, the *director*, conventionally identified by a unit vector **n** (see Figure 1.1). This direction corresponds to the optical axis of macroscopically aligned samples. Mesophases with only orientational order are called *nematics*; if, in addition, some positional order is present, the phases are classified as *smectics*. Thus, in *nematics*, which are the simplest and most widely used LC phases, the molecular centres of mass are randomly distributed, like in ordinary (*isotropic*) liquids.

As a consequence of their mesoscale organisation, LCs exhibit great sensitivity to external fields; for instance electro-optical applications are based on the reorientation of the optical axis under the action of electric fields.

The molecules constituting LCs may exhibit different structures, but they have some common characteristics:

- a rather rigid and elongated core (mesogenic unit), usually made of aromatic rings, which gives molecules the typical anisometric shape;
- one or more flexible parts, generally an alkyl chains, which introduce some confor-

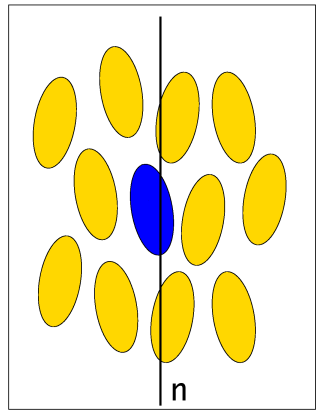

Figure 1.1: Cartoon of a nematic liquid crystal. The black line represents the director.

mational disorder.

The stability of mesophases is determined by the balance between shape anisotropy and flexibility.

The development of computational tools able to connect the molecular structure of mesogens to the properties of liquid crystals is motivated by several reasons. Of course, such methods would be useful to guide the synthetic design of materials with tailored properties. Furthermore, there are fundamental reasons of interest: liquid crystals, having properties which strongly depend on the molecular structure, can represent a benchmark for theoretical and computational approaches.

Methods suitable for the atomistic study of LC properties are Monte Carlo and Molecular Dynamics simulations [1, 2]. However, they also have time- and length-scale limitations: (i) due to the relative molecular complexity of mesogens, samples cannot contain more than some hundreds of molecules, and such dimensions may be insufficient to study collective properties like dielectric permittivity and elastic constants; (ii) trajectories of a few hundreds of nanoseconds, feasible at relatively high computational cost, may be insufficient to study collective properties, whose dynamics is characterised by time-scales longer than microseconds.

Therefore simulation techniques, though very important for the comprehension of the molecular origin of the liquid crystal behaviour, at present cannot be of great practical aid, in particular in relation to the design of materials. Alternative approaches, exploiting

some modelling of the interactions of single molecules with the environment, can be useful to this purpose; such approaches are very common in other contexts, for instance in the field of solvation [3].

The present thesis focuses on the development and the application of a computational methodology, based on a molecular field theory and atomistic modelling, to connect dielectric and elastic properties of nematic liquid crystals to the structure of the constituent molecules. The theoretical tool used to this purpose is a phenomenological model, known with the name of 'Surface Interaction' (SI) [4–6].

The following issues have been addressed in this thesis.

- Extension of the SI model: molecular expressions for the elastic constants of nematics have been derived, using the SI model and the continuum elastic theory.

- Development of an integrated computational procedure which, starting from molecular coordinates, by suitable handling of the conformational degrees of freedom, leads to the desired liquid crystal properties. A flexible procedure has been set up, using the Python programming language to glue together home-made Fortran codes and third-party software.

- Application of the methodology to the class of mesogens known as 'liquid crystal dimers', which exhibit peculiar and not fully understood properties. A preliminary analysis of geometry, energy and charges has been carried out to define a set of transferable fragments, which have been used as building blocks for a systematic investigation of the properties of LC dimers.

1.2 Liquid crystals: properties

The popular LC applications, like liquid crystal displays, are based on the electro-optical effect, which is the reorientation of the optical axis as a consequence of the application of an electric field. The first and still widely used device based on the electro-optical effect is the twisted nematic cell [7], whose general scheme is reported in Figure 1.2. The transmittance of the cell is determined by the competition between the reorientation of the director under the electric field, which is controlled by the dielectric anisotropy of the

LC material, and the restoring forces opposing director reorientation, which depend on the elastic moduli of the material.

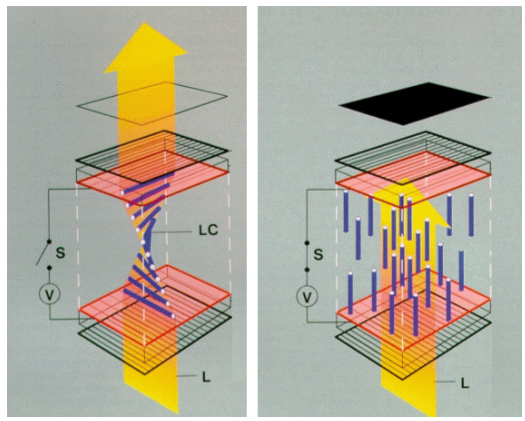

Figure 1.2: General scheme of the ON (left) and OFF (right) states of a twisted nematic cell. The labels LC and L denote the liquid crystal and the polarised light, respectively.

In this thesis we have focused our interest on the dielectric anisotropy, the elastic constants and the flexoelectric coefficients of nematics. These properties will be briefly described in the following.

The director reorientation is the most widely used effect in electro-optical devices. The relevant property is the dielectric anisotropy $\Delta\epsilon = \epsilon_{\parallel} - \epsilon_{\perp}$, defined as the difference between the permittivity parallel ($\epsilon_{\parallel}$) and perpendicular ($\epsilon_{\perp}$) to the director. This difference vanishes in the isotropic phase. Materials with non-zero dielectric anisotropy tend to reorient in presence of an applied electric field; the larger $\Delta\epsilon$, the stronger is the torque experienced by the director, therefore in most cases the LC research has been addressed to materials with large dielectric anisotropy.

Director deformations in nematics can be described in terms of three modes, called *splay*, *twist* and *bend*, which are illustrated in Figure 1.3. The elastic constants K_{11} (splay), K_{22} (twist) and K_{33} (bend) are associated to these modes; they play a crucial role in determining the performance of a twisted nematic cell [8]. The ratio K_{33}/K_{11}, for instance, affects the static and dynamic behaviour of a twisted nematic display. The optical threshold of a twisted nematic-LCD, i.e. the threshold voltage for the field-induced director reorientation, depends on both the dielectric anisotropy and the elastic con-

stants: low thresholds, therefore low-operating voltages, are attained by large dielectric anisotropy and/or small values of the elastic parameter $K = [K_{11} + (K_{33} - 2K_{22})/4]$ [8].

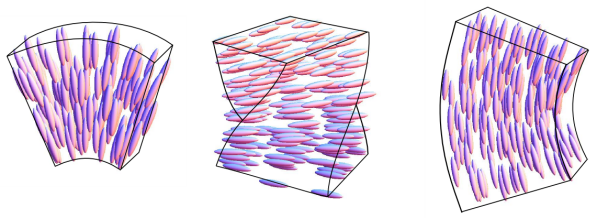

Figure 1.3: Splay, twist and bend deformations of nematics.

In this study we have also investigated the flexoelectric effect, which is the coupling between polarisation and director deformation. This phenomenon appears promising for the development of next generation electro-optical devices. At present, it is exploited in the zenithal bistable display technology [9]. Among the factors which have limited the use of this property so far, there are the difficulties in improving material characteristics. This is partly due to the strong and not easy to rationalise relation between molecular structure and flexoelectric coupling. Simple models, ignoring molecular details, have provided a general understanding of the origin of the phenomenon [10, 11], but they are scarcely useful when dealing with real molecules. In this original model, Meyer showed that flexoelectric coupling can be associated to splay and bend deformations. In addition, he suggested as molecular requirements for the flexoelectric effect (i) permanent electric dipoles and (ii) anisometry of the molecular shape. Figure 1.4 shows how splay and bend deformations can induce a flexoelectric polarisation, according to the Meyer picture.

1.3 Liquid crystal dimers

Liquid crystals can be classified as monomers, constituted by a single mesogenic core, dimers, with two mesogenic cores linked together, and polymers. This thesis focuses on LC dimers; for the sake of comparison, also the corresponding monomers are considered. Figure 1.5 shows the systems which have been investigated.

In these systems the mesogenic core is either a cyanobiphenyl or a difluorobiphenyl

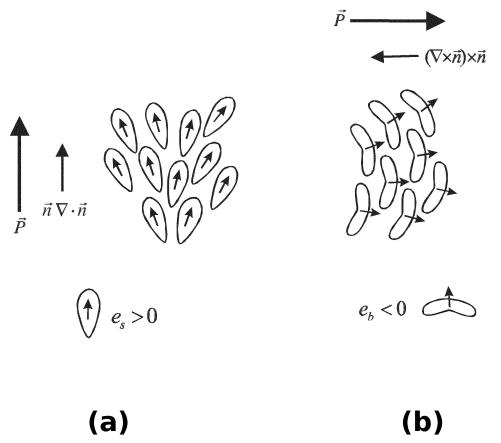

Figure 1.4: Splay and bend polarisations as a consequence of director deformations.

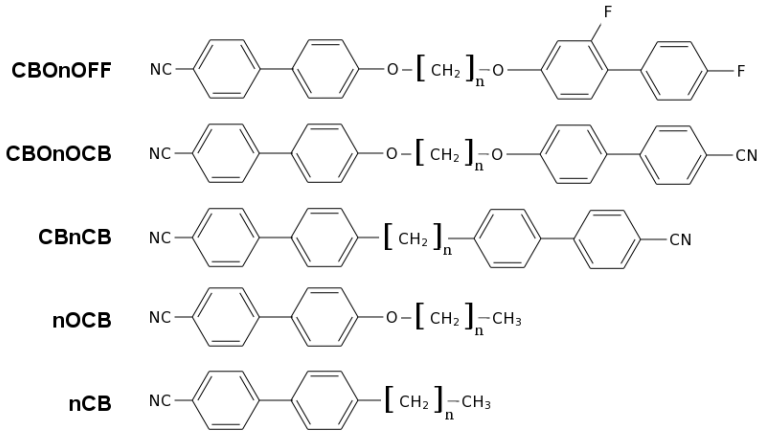

Figure 1.5: Chemical structures of the liquid crystal systems which have been studied in this thesis. CBOnOFF [α-(2',4-difluorobiphenyl-4'-yloxy)-ω-(4-cyanobiphenyl-4'-yloxy)alkanes], CBOnOCB [α,ω-bis(4-cyanobiphenyl-4'-yloxy)alkanes], CBnCB [α,ω-bis(4-cyanobiphenyl-4'-yl)alkanes], nOCB [4-cyano-4'-n-alkoxybiphenyl] and nCB [4-cyano-4'-n-alkylbiphenyl].

unit, and the flexible spacer is constituted by alkyloxy or alkyl chains. Hereafter the generic molecular structures reported in Figure 1.5 will be denoted as CBOnOFF, CBOnOCB, CBnCB, nOCB and nCB; where n is the number of methylene units in the spacer, CB indicates the cyanobiphenyl group, FF the difluorobiphenyl group and O is used for ether-linked spacer.

LC dimers display interesting properties, intermediate between those of monomers and polymers. The systems shown in Figure 1.5 appear structurally similar to each other; however, they show distinct elastic and flexoelectric behaviour [12–14]. Besides, some of them exhibit very unusual properties, as the formation of LC 'blue phases' with very wide range, upon doping with a chiral solute [15].

Table 1.1 collects the experimental nematic-isotropic transition temperatures for some of the systems under investigation. We can notice the alternation of the transition temperatures with the number of methylene groups in the spacer; this is the so called odd-even effect, which was found also for other properties of dimers [12, 14].

Table 1.1: Experimental values of the nematic-isotropic temperature temperature, T^{NI}, for 5OCB [16], 5CB and 8CB [17], CBOnOCB [18] and CBOnOFF [12], as a function of the number n of methylene groups in the alkyl chain.

nOCB		**nCB**	
	T^{NI} / K		T^{NI} / K
5OCB	34	5CB	308
		8CB	314
	CBOnOCB	**CBOnOFF**	**CBnCB**
n	T^{NI} /K	T^{NI} /K	T^{NI} / K
4	523	-	-
5	459	378	-
6	494	434	503
7	454	386	387
8	474	416	469

1.4 Outline

The thesis is organised as follows.

In chapter 2 we shall summarise the state of the art of the theoretical-computational methods employed for studying LC phases and we shall present the 'Surface Interaction' (SI) model which has been used. The molecular expressions of the investigated properties in the SI framework will be reported.

In chapter 3, molecular expressions for the elastic constants of nematics will be derived, using the SI model and the elastic continuum theory.

In chapter 4 we shall present the integrated computational procedure which has been set up, to calculate LC properties starting from the atomic coordinates of the molecular constituents. Furthermore, we shall review the quantum mechanical single molecule calculations which have been performed to define the parameters needed for the atomistic modelling of the LC dimers.

Chapters 5, 6, 7 report the numerical results. In chapter 5 the model for elastic constant described in chapter 3 is applied to typical low molar mass LCs. In chapter 6 and 7 we shall present the flexoelectric, elastic and dielectric properties of LC dimers, calculated using two different methods to treat the conformational degrees of freedom.

2

Theoretical methods

2.1 Bridging time- and length- scales

Liquid Crystals are self-organising materials characterised by the interplay of several and very different phenomena which occur over a wide range of time- and length-scales, from intra-molecular configurational changes to collective molecular motions on the director length-scale. Different theoretical and computational methodologies are available to address problems at a specific scale, e.g. accurate estimates of single molecule properties can be obtained by Quantum Mechanics *ab-initio* calculations, and on the opposite side continuum theories can be used to describe phenomena on the director length-scale.

The challenging problem is then how to transfer information between different levels of modelling and how to effectively link the different descriptions together.

In the following section an overview of the state of the art of the methodologies nowadays available is presented; then, we shall focus on the theoretical approach employed in this study. The molecular expression provided by this approach for the thermodynamic, dielectric and elastic properties of LCs, will be reported in the final section.

2.2 Theoretical methodologies: state of the art

The nematic phase is characterised by orientational order: molecules are preferentially aligned along the director. This behaviour originates from the anisotropy of the inter-

molecular interactions; their nature is complicated and is a result from different contributions, comprising electrostatic long-range interactions, induction forces and dispersion and repulsive short-range interactions. All of them contribute to the molecular ordering [19] and ultimately to the material properties of LCs.

Monte Carlo (MC) and Molecular Dynamics (MD) simulations, which belong to the so called all-atom simulation techniques, simultaneously include all these interactions, defined by the parameters collected in Force Fields. Hence, by virtue of this advantage, combined with the possibility of taking into account the full chemical detail of the system, MC and MD simulations have been, and still are, among the methodologies of choice for studying LCs. They have been proven successful, for example, to account for the molecular ordering and the nematic-isotropic transition of low molar mass liquid crystals [20]. However, to date, the state of the art of these simulations is applied to systems containing a few hundred molecules for time-scales of tens of nano-seconds, and clearly they can hardly be used to account for material properties which involve collective motions on the director scale, like elastic and dielectric properties [1]. Methodologies meant to overcome these restraints have recently been developed. In these, the molecules are mapped onto groups of atoms, the so called coarse grained particles, which interact through potentials softer than those generally involved in all-atom simulations, so allowing a simulation timestep a few order of magnitude longer. Coarse Graining can then improve the time- and length-scales covered by the simulations, although this is mostly achieved by reducing the chemical detail of the system. In the literature, examples of this kind for LC systems can be found, e.g. mixing of Lennard-Jones potentials for methylene units of alkyl chains and Gay-Berne potentials for mesogenic units [21], or, at a lower level of detail, rods and spheres mapping of molecules [1, 22].

However, these methods are yet far from being a predictive tool, useful for the synthesis and application of new materials. Firstly, because of their computational expensiveness, it is difficult to perform a sufficient number of simulations to estimate, e.g., the temperature dependence of a property. Secondly, a statistical treatment is still required to connect the microscopic information, resulting from the simulation trajectories, to bulk material properties such as the elastic constants [23].

As an alternative to MC and MD simulations, statistical theories have been developed, which use a *mean field* potential to approximate the anisotropy of the interactions

experienced by a molecule in LC phases. This may appear, and indeed is, a crude approximation of the variety of inter-molecular forces; nevertheless, mean field methods have a long history in the field of liquid crystals and have provided very important insights into the origin of orientational order and LC properties.

These mean field approaches trace back to the original Maier-Saupe theory [24, 25]. In this description the molecules are approximated by rods, ignoring in this way all the chemical and structural detail. Each molecule is viewed as moving in the average field exerted by the surrounding molecules; this is assumed to have the form

$$U(\theta) = -c\langle P_2\rangle P_2(\cos\theta) \tag{2.1}$$

where θ is the angle between the long molecular axis and the director and c is a parameter with the dimension of energy, which scales the mean field interaction. The function P_2 is the second Legendre polynomial $P_2(x) = 1.5x^2 - 0.5$, and the average value $\langle P_2\rangle$ is the molecular order parameter, which vanishes in the isotropic phase and in the nematic phase $0 < \langle P_2\rangle < 1$. The form of the Maier-Saupe mean field potential is quite general, being the simplest expression accounting for the correct molecular and phase symmetry.

Extensions to the original Maier-Saupe theory have been proposed since then, attempting to account for less than cylindrical symmetry [26] but without fully taking into account the molecular shape. This is a serious drawback, considering the importance of the molecular shape in determining LC properties: as an example, experimentally it has been found that by simply substituting the O- linkage of a CBOnOCB dimer by a methylene groups, which brings the chain perpendicular to the linked phenyl group, thus producing a change in shape, leads to a variation in the order parameter.

2.3 The Surface Interaction model

The Surface Interaction (SI) method can be seen as the simplest generalisation of the Maier-Saupe theory, to take into account the molecular shape [4–6]. It makes use of a phenomenological form for $U(\Omega)$, the mean field potential experienced by a molecule in the orientation specified by the Euler angles Ω in the nematic phases. In analogy with the Rapini-Papoular expression for the anchoring free energy of nematics [27], the orienting

potential is expressed as

$$U(\Omega) = k_B T \varepsilon \int_S P_2(\mathbf{n} \cdot \mathbf{s}) dS \tag{2.2}$$

where S is the molecular surface, $\mathbf{n}$ and $\mathbf{s}$ are unit vectors parallel to the local director axis and perpendicular to the surface element dS, respectively. T is the temperature and k_B is the Boltzmann constant. The parameter ε, with the dimensions of inverse square length, quantifies the orienting strength; it is related to the degree of order as [28]:

$$\varepsilon = -\frac{\xi^2}{v k_B T} \langle \int_S P_2(\mathbf{n} \cdot \mathbf{s}) dS \rangle \tag{2.3}$$

where v is the volume per molecule, and the angular brackets denote the orientational average.

This is defined as

$$\langle \ldots \rangle = \int f(\Omega) \ldots d\Omega \tag{2.4}$$

where $f(\Omega)$ is the orientational distribution function, which is related to the orienting potential $U(\Omega)$:

$$f(\Omega) = \frac{\exp[-U(\Omega)/k_B T]}{Q} \tag{2.5}$$

with Q being the orientational partition function

$$Q = \int \exp[-U(\Omega)/k_B T] d\Omega \tag{2.6}$$

which takes the value $Q^{iso} = 8\pi^2$ in the isotropic phase, where the orientational distribution function is simply $f^{iso} = 1/8\pi^2$.

Within the SI model, a molecule tends to align along the director axis as much surface as possible. For example, for a model ellipsoidal particle, the minimum of the mean field potential, i.e. the most stable orientation, is obtained when the long axis is parallel to the nematic director. Using a suitable definition of the molecular surface S, it is possible to take into account the geometrical details of the molecule, as shown in Figure 2.1. Thus, the mean field potential $U(\Omega)$ can be unambiguously defined for molecules of any shape, independently on their symmetry properties.

The SI model has been successfully used to connect the molecular structure to liquid crystal properties [4–6, 29]; the reason of its success can be identified in the fact that the anisotropy of short range dispersion intermolecular interactions depends on the molecular shape. Furthermore, the SI model has the great advantage to be generalisable to flexible

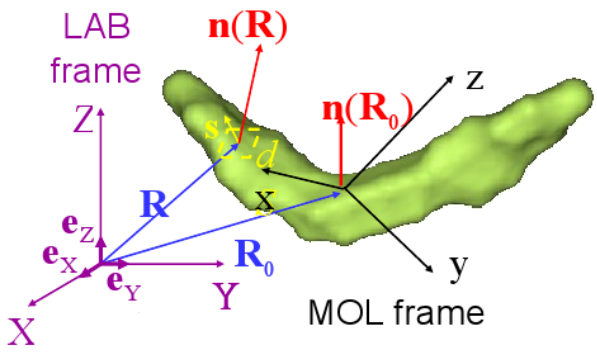

Figure 2.1: Representation of the molecular surface.

molecule in a straightforward way. This is an important feature, because flexibility is a requirement for the existence of LC phases, and cannot be neglected.

In the next section the molecular expressions for LC properties obtained in the SI framework are reported.

2.4 Molecular expressions for LC properties in the SI framework

2.4.1 The Saupe ordering matrix

The molecular order in nematics is described by the *Saupe matrix*, whose elements are defined by [30]:

$$S_{ij} = \frac{\langle 3\cos(\mathbf{e}^i \cdot \mathbf{n})\cos(\mathbf{e}^j \cdot \mathbf{n})\rangle - \delta_{ij}}{2} \tag{2.7}$$

where $\mathbf{e}^i$ and $\mathbf{e}^j$ are unit vectors parallel to the molecular axes i, j, and δ_{ij} is the Kronecker symbol. The diagonal element S_{ii} specifies the degree of orientational order of the i axis, with respect to the director. It can take all the values within the interval $-1/2 \leq S_{ii} \leq 1$, where $S_{ii} = 1$ and $S_{ii} = -1/2$ indicate perfect orientational order parallel and perpendicular to the director, respectively.

2.4.2 Properties at the Nematic-Isotropic (NI) transition

Let us consider a system with N molecules, in the volume V, at temperature T. The nematic-isotropic transition can be located using the condition that the Helmholtz free energy must be identical for the two phases coexisting phases, thus $\Delta A^{NI} = A^N - A^I = 0$. The molecular expression for the free energy change ΔA^{NI} can be obtained using the thermodynamic relation $\Delta A^{NI} = \Delta U^{NI} - T\Delta S^{NI}$, where ΔU^{NI} and ΔS^{NI} are the internal energy and entropy differences between the two phases, respectively.

Assuming that the entropy difference between the two phases derives from the orientational order in the nematic phase, the Gibbs expression can be used:

$$\Delta S = -k_B N \left[\int d\Omega f(\Omega) \ln f(\Omega) - \int d\Omega f^{iso}(\Omega) \ln f^{iso}(\Omega) \right]. \tag{2.8}$$

The internal energy difference can be approximated by the average value of the orienting mean field:

$$\Delta U = 1/2 N \langle U \rangle \tag{2.9}$$

where the factor $1/2$ is introduced to avoid double-counting of interactions.

Using Eqs. 2.8 and 2.9, we obtain

$$\frac{\Delta A}{N k_B T} = -\frac{1}{2}\langle U \rangle - \ln \frac{Q}{Q^{iso}}; \tag{2.10}$$

the value of ΔA can be calculated as a function of the parameter ε appearing in Eq. 2.2. The NI transition can be then identified with the point at which $\Delta A^{NI} = 0$.

Using Eq. 2.3, the dependence of thermodynamic properties on the orienting strength, ε, can be converted into the temperature dependence, which is more suitable for the comparison with experimental data; we can write:

$$T^* = \sqrt{\frac{\langle U \rangle}{\langle U \rangle^{NI}}} \frac{\varepsilon^{NI\,2}}{\varepsilon^2} \tag{2.11}$$

where again the index NI is used to denote values at the nematic-isotropic transition, and $T^* = T/T^{NI}$ is the reduced temperature.

2.4.3 Dielectric permittivity

The dielectric permittivity of nematics is represented by the axially symmetric tensor:

$$\epsilon = \begin{pmatrix} \epsilon_\perp & & \\ & \epsilon_\perp & \\ & & \epsilon_\parallel \end{pmatrix}$$

where $\epsilon_\parallel$ and $\epsilon_\perp$ indicate the components parallel and perpendicular to the director [30].

The average value of the permittivity tensor $\bar{\epsilon} = (2\epsilon_\perp + \epsilon_\parallel)/3$, and even more the dielectric anisotropy, $\Delta\epsilon = \epsilon_\parallel - \epsilon_\perp$, determine the response of the liquid-crystalline material to the applied electric field. The elements of the permittivity tensor are related to the molecular electric dipole μ and to the orientational order by the Maier-Meier relation [30]:

$$\epsilon_J(0) = 1 + \frac{N}{\epsilon_0 V k_B T}\langle \mu_J^2 \rangle \qquad J = \parallel, \perp \tag{2.12}$$

where μ_J^2 is the square value of the dipole moment, along the direction parallel or perpendicular to the director axis, and the angular brackets indicate the average as expressed in Eq. 2.4. Neglecting the correlations among dipoles, $\langle \mu_J^2 \rangle$ can be approximated by

$$\langle \mu_\parallel^2 \rangle = \frac{\mu^2}{3} + \frac{2}{3} Tr[\mathbf{S}(\mu \otimes \mu)] \tag{2.13}$$

$$\langle \mu_\perp^2 \rangle = \frac{\mu^2}{3} - \frac{1}{3} Tr[\mathbf{S}(\mu \otimes \mu)] \tag{2.14}$$

where the symbol $\otimes$ denotes the tensor product, Tr the trace, and $\mathbf{S}$ is the Saupe matrix defined by Eq. 2.7. Given the molecular structure and the molecular dipole, the permittivity can be evaluated by Eqs. 2.12-2.14.

2.4.4 Flexoelectric coefficients

The flexoelectric polarisation, i.e. the polarisation associated with *splay* and *bend* deformation in nematics, can be expressed as [10]:

$$\mathbf{P} = e_1 \mathbf{n}(\bigtriangledown \cdot \mathbf{n}) + e_3(\bigtriangledown \times \mathbf{n}) \times \mathbf{n} \tag{2.15}$$

where $\mathbf{P}$ is the polarisation and $\mathbf{n}(\bigtriangledown \cdot \mathbf{n})$, $(\bigtriangledown \times \mathbf{n}) \times \mathbf{n}$ represent the splay and bend deformations, respectively, and e_1, e_3 are the flexoelectric coefficients. These are characteristic materials parameters and depend on the molecular structure of the mesogen and the order of the phase.

Molecular expressions for the flexoelectric coefficients can be derived from the definition of polarisation:

$$\mathbf{P} = N\langle\mu\rangle_{1,3}/V \tag{2.16}$$

where μ indicates the molecular dipole moment. The indexes 1, 3 indicate the mean values calculated in the presence of the splay and bend deformations. Let us use Eqs. 2.2 and 2.4 and define the charge distribution of the molecule in terms of atomic charges; if we expand in power series the spatial dependence of the director field, $\mathbf{n}(\mathbf{R})$, in the presence of the deformations, and truncate this expansion at the linear term, by virtue of the different order of magnitude between the length-scale of the deformations and the molecular dimensions, we obtain:

$$e_1 = -3N\varepsilon \sum_m q_m \int_S dS \left[\langle r_Z^m r_X s_X s_Z\rangle - \frac{1}{2}\langle r_Z^m r_X^m s_X s_Z\rangle\right] \tag{2.17}$$

$$e_3 = -3N\varepsilon \sum_m q_m \int_S dS \left[\langle r_X^m r_Z s_X s_Z\rangle - \frac{1}{2}\langle r_X^m r_Z^m s_X s_Z\rangle\right] \tag{2.18}$$

where q_m and r^m indicate the atomic charges and their positions, respectively. Again S denotes the molecular surface; $\mathbf{r}$ is the vector position of points on the surface and $\mathbf{s}$ the unit vector normal to the surface at each point. X, Y, Z are the cartesian components in the laboratory coordinate system, with the Z axis parallel to the director. Notice that in Eqs. 2.17-2.18 the average values are calculated using the orientational distribution function of undeformed nematics. Eqs. 2.17-2.18 explicitly show the connection between molecular parameters (partial charges and their positions) and flexoelectric coefficients: the complicated coupling between charge distribution, order and ultimately the molecular shape, is the reason why it is so hard to find simple correlations between flexoelectric behaviour and molecular structure.

The property directly accessible to experiments is the effective flexoelectric coefficient [12, 13], defined as

$$\bar{e} = \frac{e_s - e_b}{2}. \tag{2.19}$$

2.4.5 Molecular flexibility

The expressions reported in the previous sections, which refer to rigid molecules, can be easily generalised to take into account the molecular flexibility. Let N_c be the number of

conformers; the orientational average for the j-th conformer reads:

$$\langle \cdots \rangle_j = \int \cdots f_j(\Omega) d\Omega \tag{2.20}$$

where f_j is the orientational distribution function for the conformer under examination, which can be obtained from the mean field potential U_j, calculated according to Eq. 2.2, using the molecular surface of the conformer.

Then, liquid crystal properties can be calculated as conformational-orientational averages:

$$\langle \cdots \rangle = \sum_{j=1}^{N_c} w_j \langle \cdots \rangle_j \tag{2.21}$$

where w_j is the statistical weight of the jth conformer. This is defined as:

$$w_j = \frac{\exp(-E_j/k_B T) Q_j}{Q} \tag{2.22}$$

where E_j is the potential energy of the jth conformer, with the partition functions

$$Q_j = \int \exp[-U_j(\Omega)/k_B T] d\Omega \tag{2.23}$$

and

$$Q = \sum_{j=1}^{N_c} \exp(-E_j/k_B T) Q_j \tag{2.24}$$

If the full torsional angle distribution is taken into account, Eq. 2.21 becomes:

$$\langle \cdots \rangle = \int \cdots f(\varphi, \Omega) d\varphi d\Omega \tag{2.25}$$

where $f(\varphi, \Omega)$ is the coupled distribution function for the orientation, defined by the angles Ω and the torsional angles φ.

3

Molecular expressions for the elastic constants

3.1 Introduction

In this chapter we derive molecular expressions for the bulk and surfacelike elastic constants of nematics, within the framework of the Surface Interaction model. This requires extensive use of tensor calculus; after some lengthy algebra, simple expressions are obtained, by exploiting the symmetry of the undeformed nematic phase. These expressions have been implemented in a Fortran code as a part of the computational procedure described in the next chapter.

The molecular theory for the elastic constants is presented here in the form of a paper, which has been submitted for publication.

Molecular field theory with atomistic modeling for the curvature elasticity of nematic liquid crystals

Mirko Cestari,[a] Alessandro Bosco[a,b] and Alberta Ferrarini [a]*

[a] Dipartimento di Scienze Chimiche, Università di Padova
via Marzolo 1, 35131 Padova, Italy
[b] International School for Advanced Studies (SISSA), via Beirut 2-4, Trieste

running title: **Atomistic modeling of the elastic constants of nematics**

Corresponding author: alberta.ferrarini@unipd.it

Abstract

Liquid crystals oppose elastic torques to distortions of the director. For nematics this behavior is characterized by three bulk elastic moduli (K_{11}, K_{22} and K_{33}), and two surfacelike constants (k_{13} and k_{24}). These material properties depend on the molecular structure of mesogens, but the relation between molecular features and deformations on a much longer length scale has not been fully elucidated. The prediction of elastic properties is a challenge for theoretical and computational methods: atomistic simulations require large samples and must be integrated by statistical-thermodynamics models, to connect the intermolecular correlations to the elastic response. Here we present a molecular field theory, wherein expressions for the elastic constants of nematics are derived on the basis of the orientational distribution function, which is simply parameterized according to the amount of molecular surface which can be aligned to the nematic director. A detailed account of the chemical structure is possible; moreover the conformational freedom, which is a common feature of mesogens, can be easily introduced. Given the atomic coordinates, the elastic constants can be calculated without any adjustable parameter, at a low computational cost. We report the results obtained for 4-*n*pentyl-4'-cyanobiphenyl (5CB); we show that even for 5CB, which is usually taken a prototypal rod-like molecule, the elastic moduli exhibit a strong dependence on the molecular conformation. This model is shown to provide good estimates of the magnitude and the temperature dependence of the elastic constants, if the molecular geometry is correctly taken into account.

Introduction

Liquid crystals (LCs) are characterized by curvature elasticity: they oppose a torque to distortions of the *director*, that is the average direction of molecular alignment. This is one the main properties controlling the LC behavior on the sub-micrometric length scale and plays a key role for applications. In LC cells, the director profile, which determines the optical properties, is the result of the trade-off between the deformation induced by an external electric or magnetic field and the elastic response of the LC medium [1].

The number and kind of elastic modes of a given material can be derived from symmetry considerations. The elastic behavior of nematic liquid crystals is well established since the 40's of last century: according to the Oseen-Frank theory [2,3], the bulk elasticity can be described in terms of three 'bulk' elastic constants, for *splay* (K_{11}), *twist* (K_{22}) and *bend* (K_{33}) deformations, respectively (see Figure 1), in addition to k_{13} and k_{24} , denoted as *splay-bend* and *saddle-splay*, respectively, which only contribute to the free energy density in the presence of interfaces.

[insert Figure 1 about here]

The elastic constants depend on the chemical structure of mesogens [4]. They are all positive, as required for the stability of the undeformed nematic phase, and their magnitude is of the order of some pN. For NLC formed by elongated molecules, the sequence $K_{33} > K_{11} > K_{22}$ is generally found. The elastic moduli usually increase with the degree of order, but the splay and twist constants exhibit a weak temperature dependence, whereas the bend stiffness changes more steeply. In many cases, K_{ii} approximately proportional to S_{zz}^2 is found, with S_{zz} being the major orientational order parameter. The bend elastic constant is also the most sensitive to changes in the molecular structure. We shall take as an example 4-*n*pentyl-4'-cyanobiphenyl (5CB), whose structure is displayed in Fig. 2. Its elastic constants have been measured by different technique, and some discrepancy has been found, which has been mainly ascribed to the errors affecting the different techniques or to the chemical purity of samples (see ref. [5] for a survey). As a matter of fact, the experimental determination of elastic constants is not trivial and the results are characterized by non-negligible uncertainty. Fig. 3 shows the temperature dependence of the bulk elastic constants of 5CB, as obtained in some of the reported experiments [6-9].

[insert Figure 2 about here]

[insert Figure 3 about here]

The anisotropy of elastic constants is an important material property, which exhibits a significant, yet scarcely understood, dependence on the molecular structure of the constituents [4]. The ratio K_{33}/K_{11} , which is particularly sensitive to structural changes, was proposed to be an increasing function of the length-to-width ratio. However, K_{33}/K_{11} has been shown to be strongly affected by the presence of alkyl chains: it was found to decrease with increasing chain length within homologous series [10]. The ratio K_{33}/K_{11} was also found to change under chemical modifications, which did not significantly affect the length-to-width ratio [11]. The anisotropy of elasticity can be of utmost relevance for technological applications; for instance, it determines the steepness of the voltage–transmittance curve in twisted nematic LC displays [12].

The elasticity of liquid crystals controls the mesoscale behavior of liquid crystals; it introduces anisotropy in the interactions between embedded colloidal particles [13-15] and the ratio of elastic constants affect the structure of topological defects [16] and the location of defects in confined nematics [17].

Clearly, the availability of reliable modeling methods for the elastic constants would be extremely useful for the synthetic design of LC materials with tailored elasticity. However, the prediction of collective properties, which depend on the intermolecular correlations, is not a simple task. The problem, somehow analogous, of dielectric properties, can be treated by single molecule calculations, by exploiting the dielectric continuum approximation [18]. Nothing analogous exists for the elasticity. In their pioneering work Nehring and Saupe, using a mean field approach, found $K_{ii} \propto S_{zz}^2$, where S_{zz} is the major orientational order parameter, and $K_{11} : K_{22} : K_{33}$= 5:11:5 [19]. The correct sequence, $K_{33} > K_{11} > K_{22}$, could be obtained by models of hard axially symmetric particles [20-23]; but these overestimate the K_{33} / K_{11} ratio and cannot describe the temperature dependence of the elastic constants. Better agreement with experiment could be achieved by introducing dispersion and dipole or quadrupole interactions between particles [24-26]. Qualitatively similar results, though with some differences, were obtained by Molecular Dynamics and Monte Carlo simulations of particles with hard core [27] or soft interactions [28,29]. Different routes from trajectories to elastic moduli have been proposed, some requiring theoretical models to connect the information on the local liquid structure to elastic properties [30]. The need of relatively large systems is nowadays a limit for the calculation of elastic constants from atomistic simulations [31]; the description of the temperature dependence of elastic properties would be an extremely demanding task. Good agreement with experiment was obtained by Zakharov and Maliniak for 5CB at 300 K, from Molecular Dynamics simulations with an atomistic force field [32].

Here we shall derive expressions for the elastic constants of nematics using a molecular field approach. Mean-field theories of LCs have a long and successful history, which traces back to the Maier-Saupe theory [33]. They have also contributed to shed light on the relationship between intermolecular interactions and elastic constants [19,34]. The concept of molecular surface has enabled the introduction of the molecular structure into this framework. The Surface Interaction (SI) model rests on the assumption that a molecule in the nematic phase tends to align to the director as much surface as possible [35]. In analogy with the Rapini-Papoular expression of the anchoring free energy on the surface of a particle embedded in a nematic phase [36], the simplest form consistent with the nematic symmetry, is assumed for the mean field, dU, acting on each element of the molecular surface. The orienting potential experienced by the molecule is then obtained by integrating dU over the whole surface; in this way, the orientational distribution of a molecule in the nematic phase is related to the anisometry of the molecular surface. In this work, the SI model is extended to the elastic constants of nematics. The SI approach provides good predictions of different properties of nematics: temperature dependence of orientational order and thermodynamic properties at the Nematic-Isotropic transition [35,37], helical twisting power of chiral dopants [38], flexoelectric coefficients [39]. The success of this simple model is due to the fact that the molecular surface represents a reasonable property to scale short range intermolecular interactions. This is widely recognized; indeed, the molecular surface is customarily used to parameterize non-polar interactions within implicit solvent models [40]. Our results for nematics show that it is also suitable for simple but effective modeling of the anisotropy of short-range interactions.

Some analogy between the theory for the elasticity of nematics presented here and that proposed a few years ago by Marrucci and Greco [41] can be found; both can be considered as extensions of the Maier-Saupe theory [33], based on the recognition of the importance of the geometrical features of molecules. Although the developed methodologies are quite different, in both cases the orientational mean field experienced by a molecule in the distorted environment is connected to the director orientation in the space region occupied by it. A novelty in the present work is represented by the realistic account of the molecular structure; this allows a natural inclusion of the structural differences and eliminates some arbitrariness of the molecular model.

In this work, molecular expressions for the bulk elastic constants K_{11} , K_{22} and K_{33} and the two surfacelike moduli k_{13} and k_{24} are derived, using the SI model. This can fully account for the molecular geometry and flexibility, which should not be neglected when considering liquid crystals, since this is one of the features required for the stabilization of mesophases. The elastic constants calculated for 5CB are reported. This simple example allows us to highlight one of the main results of the present method which, for the lack of suitable theoretical and computational tools, could not

be fully investigated before, i.e. the effect of the molecular flexibility on the elastic response of liquid crystals.

In the next Section, the theoretical method is outlined. To keep plain the presentation, only the main expressions will be reported; all the lengthy derivations are deferred to Appendices. In the third Section the results obtained for 5CB are presented and discussed. Conclusions and future outlooks will be summarized in the fourth Section.

Theory: elastic constants of LC by the Surface Interaction method

The elastic free energy density of nematics can be expressed as [1]:

$$f_{el} = k_2 n \cdot (\nabla \times n) + \frac{1}{2} K_{11} (\nabla \cdot n)^2 + \frac{1}{2} K_{22} \left[n \cdot (\nabla \times n) \right]^2 + \frac{1}{2} K_{33} \left| n \times (\nabla \times n) \right|^2 + \\ + k_{13} \nabla \cdot n (\nabla \cdot n) - (K_{22} + k_{24}) \nabla \cdot \left[n (\nabla \cdot n) + n \times (\nabla \times n) \right] \tag{1}$$

Here the first term accounts for the spontaneous tendency to twist of the director, which characterizes the chiral nematic (cholesteric) phase, and k_2 is generally denoted as the *chiral strength*. The three following terms represent the contributions for *splay*, *twist* and *bend* distortion modes, respectively, and K_{ii} are the corresponding elastic constants [2,3]. The two last contributions in eq. (1) are usually denoted as *splay-bend* and *saddle-splay*, respectively; these divergence terms reduce to surface integrals by the use of Gauss theorem. Their role has been a matter of extensive debate; at first they were ignored, as purely surface terms which do not contribute to determining the director configuration in bulk LCs, but then their relevance for the behavior of LCs in the presence of interfaces was recognized [42-44].

Eq. (1) is the lowest order term of the expansion of the free energy density in powers of the director distortions, which are assumed to have long wavelength. The elastic constants appearing here are material parameters which depend on the chemical composition of the system. In the following, an expression for the free energy will be derived starting from the single molecule orientational distribution function, using the SI model. Then, molecular expression for the elastic constants will be obtained as derivatives of the free energy density with respect to deformations.

The orientational distribution of molecules in the nematic phase, under the conditions of the canonical ensemble, is described by the function $p(\Omega)$:

$$p(\Omega) = \frac{\exp\left[-U(\Omega) / k_B T \right]}{Q} \tag{2}$$

where Ω are the Euler angles specifying the molecular orientation in a frame with the *Z* axis parallel to the director, and *Q* is the orientational partition function:

$$Q = \int \mathrm{d}\Omega \exp\left[-U(\Omega)/k_B T\right] \tag{3}$$

In these expressions $U(\Omega)$ is the *potential of mean torque*, for which the following form is assumed within the SI model [35]:

$$U(\Omega) = k_B T \varepsilon \int_S dS\ P_2(\mathbf{n}\cdot\mathbf{s}) \tag{4}$$

where *S* is the molecular surface, **n** and ***s*** are unit vectors, the former parallel to the director and the latter normal to the surface element d*S* and P_2 is the second Legendre polynomial. This is nothing else than the first non-vanishing term of the expansions on a suitable basis set, with the correct symmetry, of the function expressing the orientational mean field experienced by the surface element d*S*. The parameter ε, with dimension of inverse square length, specifies the orienting strength of the medium, which is an increasing function of the reduced temperature, $T^*=T/T_{\mathrm{NI}}$, with T_{NI} being the Nematic-Isotropic transition temperature. According to molecular field theories, ε is assumed to take the form [35,45]:

$$\varepsilon = -\frac{\xi^2}{v k_B T}\langle a \rangle \tag{5}$$

where *v* is the volume per molecule, ξ is a constant, *a* is the integral

$$a = \int_S dS\ P_2(\mathbf{n}\cdot\mathbf{s}) \tag{6}$$

and the angular brackets denote the orientational average:

$$\langle \cdots \rangle = \int \cdots p(\Omega)\,\mathrm{d}\Omega \tag{7}$$

The average value $\langle a \rangle$ can be seen as an order parameter, which vanishes in the isotropic phase and measures the degree of order experienced by molecules in the nematic phase.

To bridge the molecular orientational distribution function to the Helmholtz free energy, we shall start from the thermodynamic relationship:

$$f = f_{iso} + \Delta u - T\Delta s \tag{8}$$

where f_{iso} is the free energy density of the isotropic phase, and Δu, Δs are the differences of internal energy and entropy density between the nematic and the isotropic phase, respectively. These differences can be approximated as [45]:

$$\Delta u = \frac{1}{2\nu}\langle U \rangle \tag{9a}$$

$$\Delta s = -\frac{k_B}{\nu}\langle \ln p \rangle \tag{9b}$$

Using eqs. (9) with eqs. (2)-(6), eq. (8) can be rewritten as:

$$f = f_{iso} + \frac{\xi^2}{2\nu^2}\langle a \rangle^2 - \frac{k_B T}{\nu}\ln Q \tag{10}$$

This free energy density bears an intrinsic dependence on the position in deformed nematics, where the director is a function of the position, **n**=**n**(**R**). Essential for our approach is the fact that, due to the finite dimension of a molecule, the molecular surface 'feels' different director orientations, in the presence of deformations. This introduces a dependence on the deformation in the potential of mean torque, $U(\Omega)$, and then, in the orientational distribution function, $p(\Omega)$, and in the thermodynamic functions which are derived from them. It might be worth noticing the difference from other approaches, where the molecular expression of the free energy density is derived from suitable averages of the interactions between pairs of molecules [46]. In such cases, the orientational distribution function with respect to the local director is generally assumed to be the same as in the undeformed nematic phase, and no rotational entropy change is associated with deformation.

The free energy density can be expressed as $f = f\left(n_J, n_{JK}, n_{JKL}, \ldots\right)$, where n_J are components of the director, $n_{JK} = \partial n_J / \partial R_K$ are first derivatives of such components with respect to the position, $n_{JKM} = \partial^2 n_J / \partial R_K \partial R_M$ second derivatives, and so on. In the long wavelength limit, the Taylor expansion of the free energy density can be truncated at the first terms:

$$f \approx f_0 + \sum_{IJ}\left(\frac{\partial f}{\partial n_{IJ}}\right)_0 n_{IJ} + \sum_{IJK}\left(\frac{\partial f}{\partial n_{IJK}}\right)_0 n_{IJK} + \frac{1}{2}\sum_{IJKM}\left(\frac{\partial^2 f}{\partial n_{IJ}\partial n_{KM}}\right)_0 n_{IJ} n_{KM} \tag{11}$$

where the subscript 0 refers to the state of uniform director, with $n_{JK} = 0$, $n_{JKM} = 0$, and so on.

Expressions for the derivatives of the molecular form of the free energy density, eq. (10), are reported in Appendix A; by substitution of such expressions into eq. (11) we obtain:

$$
\begin{aligned}
f \approx f_0 &- \frac{\xi^2}{v^2}\langle a\rangle_0 \sum_{IJ}\left\langle \frac{\partial a}{\partial n_{IJ}}\right\rangle_0 n_{IJ} - \frac{\xi^2}{v^2}\langle a\rangle_0 \sum_{IJK}\left\langle \frac{\partial a}{\partial n_{IJK}}\right\rangle_0 n_{IJK} \\
&-\frac{1}{2}\frac{\xi^2}{v^2}\sum_{IJKM}\left\{\langle a\rangle_0\left[\left\langle \frac{\partial^2 a}{\partial n_{IJ}\partial n_{KM}}\right\rangle_0 + \frac{\xi^2}{vk_BT}\langle a\rangle_0\left(\left\langle \frac{\partial a}{\partial n_{IJ}}\frac{\partial a}{\partial n_{KM}}\right\rangle_0 - \left\langle \frac{\partial a}{\partial n_{IJ}}\right\rangle_0\left\langle \frac{\partial a}{\partial n_{KM}}\right\rangle_0\right)\right]\right. \\
&+\left[1-\frac{\xi^2}{vk_BT}\left(\left\langle a^2\right\rangle_0 - \langle a\rangle_0^{\,2}\right)\right]^{-1}\left[\left\langle \frac{\partial a}{\partial n_{IJ}}\right\rangle_0 + \frac{\xi^2}{vk_BT}\langle a\rangle_0\left(\left\langle a\frac{\partial a}{\partial n_{IJ}}\right\rangle_0 - \langle a\rangle_0\left\langle \frac{\partial a}{\partial n_{IJ}}\right\rangle_0\right)\right]\times \\
&\left.\times\left[\left\langle \frac{\partial a}{\partial n_{KM}}\right\rangle_0 + \frac{\xi^2}{vk_BT}\langle a\rangle_0\left(\left\langle a\frac{\partial a}{\partial n_{KM}}\right\rangle_0 - \langle a\rangle_0\left\langle \frac{\partial a}{\partial n_{KM}}\right\rangle_0\right)\right]\right\} n_{IJ}n_{KM}
\end{aligned}
\tag{12}
$$

where the angular brackets with zero index denote orientational averages calculated with the orientational distribution function in undistorted nematics, p_0:

$$
\langle\ldots\rangle_0 = \int \mathrm{d}\Omega\, p_0(\Omega)\ \ldots \tag{13}
$$

Using for the derivatives reported in Appendix B, eq. (12) can be rewritten as:

$$
\begin{aligned}
f \approx f_0 &+ 3\frac{k_BT\varepsilon}{v}\sum_{IJL} c_{JIL}n_L^0 n_{IJ} + \frac{3}{2}\frac{k_BT\varepsilon}{v}\sum_{IJKL} c_{KJIL}n_L^0 n_{IJK} \\
&+\frac{3}{2}\frac{k_BT\varepsilon}{v}\sum_{IJKM}\left\{\left[c_{MJKI} - 3\varepsilon\left(c_{JIL,MKN} - c_{JIL}c_{MKN}\right)n_L^0 n_N^0\right]\right. \\
&+3\left[\langle a\rangle_0 + \varepsilon\left(\left\langle a^2\right\rangle_0 - \langle a\rangle_0^{\,2}\right)\right]^{-1}\left[c_{JIL} - \varepsilon\left(b_{JIL} - \langle a\rangle_0 c_{JIL}\right)\right]\times \\
&\left.\times\left[c_{MKN} - \varepsilon\left(b_{MKN} - \langle a\rangle_0 c_{MKN}\right)\right]n_L^0 n_N^0\right\} n_{IJ}n_{KM}
\end{aligned}
\tag{14}
$$

where the elements of the tensors $\mathbf{c}^{(n)}$ (n=3,4,6) and $\mathbf{b}^{(3)}$ appear. These are defined in eqs. (B7), as integrals over the molecular surface.

To derive explicit expressions for the elastic constants, let us take a reference frame with the Z axis parallel to $\mathbf{n}^0$=$\mathbf{n}(\mathbf{R}_0)$. With this choice, $n_J^0 = \delta_{JZ}$; moreover, from the constraint $\mathbf{n}\cdot\mathbf{n} = 1$, the relationships $n_{ZJ} = 0$ and $n_{ZJK} = -n_{XJ}n_{XK} - n_{YJ}n_{YK}$ follow. Then, using eqs. (B5) for the derivatives of the function a with respect to director distortions, the density of elastic energy, f_{el}= f - f_0, reads:

$$
\begin{aligned}
f_{el} \approx\ & 3\frac{\varepsilon k_BT}{v}\sum_{K=X,Y}\sum_{J=X,Y,Z} c_{JKZ}n_{KJ} + \frac{3}{2}\frac{\varepsilon k_BT}{v}\sum_{K=X,Y}\sum_{J,M=X,Y,Z} c_{MJKZ}n_{KJM} \\
&+\frac{3}{2}\frac{\varepsilon k_BT}{v}\sum_{IJ=X,Y}\sum_{KM=X,Y,Z}\left\{\langle a\rangle_0\left[c_{KMIJ} - \delta_{IJ}c_{KMZZ} - 3\varepsilon\left(c_{KIZ,MJZ} - c_{KIZ}c_{MJZ}\right)\right]\right. \\
&\left.+3\left[\langle a\rangle_0 + \varepsilon\left(\left\langle a^2\right\rangle_0 - \langle a\rangle_0^{\,2}\right)\right]^{-1}\left[c_{KIZ} - \varepsilon\left(b_{KIZ} - \langle a\rangle_0 c_{KIZ}\right)\right]\left[c_{MJZ} - \varepsilon\left(b_{MJZ} - \langle a\rangle_0 c_{MJZ}\right)\right]\right\} n_{IK}n_{JM}
\end{aligned}
\tag{15}
$$

As a consequence of the symmetry of undeformed nematics, terms containing third-rank tensor components, c_{JKZ} and b_{JKZ}, vanish for non-chiral molecules; for chiral molecules, only those with $J\neq K\neq Z$ survive (eqs. B8).

From comparison between the molecular expression, eq. (15), and the Oseen-Frank form, eq. (1), we can write for the elastic constants (see Appendix C):

$$k_2 = 3\frac{\varepsilon k_B T}{v} c_{XYZ} \tag{16a}$$

$$k_{13} = 3\frac{\varepsilon k_B T}{v} c_{XZXZ} \tag{16b}$$

$$K_{ii} = 3\frac{\varepsilon k_B T}{v}\left\{\left[\left(c_{YYXX} - c_{YYZZ} - 2(\delta_{i1} - \delta_{i3})c_{XZXZ}\right) - 3\varepsilon\left(c_{YXZ,YXZ} - \delta_{i2}{c_{YXZ}}^2\right)\right]\right. \qquad i = 1,2,3$$
$$\left. + 3\delta_{i2}\left[\langle a\rangle_0 + \varepsilon\left(\langle a^2\rangle_0 - {\langle a\rangle_0}^2\right)\right]^{-1}\left[c_{YXZ} + 3\varepsilon\left(b_{YXZ} - \langle a\rangle_0 c_{YXZ}\right)\right]^2\right\} \tag{16c}$$

$$K_{22} + k_{24} = 3\frac{\varepsilon k_B T}{v}\left\{c_{XXXX} + c_{XXYY} - 2c_{XXZZ} - 3\varepsilon\left(c_{XXZ,XXZ} - c_{XXZ,YYZ}\right)\right\} \tag{16d}$$

It follows from eqs. (B8) that k_2 vanishes for achiral molecules. In agreement with Nehring and Saupe, we find $k_{13} \neq 0$ and $k_{24} = (K_{11} + 2k_{13} - K_{22})/2$ [19]. It has to be specified, however, that these are the bare surfacelike elastic constants; as discussed by various authors [43,47,48], they represent only one of the contributions to the effective elastic constants, which determine the behavior of nematics at interfaces.

Inclusion of molecular flexibility

The expressions reported above can be easily generalized to take into account the molecular flexibility. In general, for flexible molecules the orientational distribution function, eq. (2), should be replaced by the torsional-orientational distribution function:

$$p(\Omega,\phi) = \frac{\exp\left[-U(\Omega,\phi)/k_B T\right]}{Q} \tag{17}$$

with the partition function

$$Q = \int \mathrm{d}\Omega\, \mathrm{d}\phi \exp\left[-U(\Omega,\phi)/k_B T\right] \tag{18}$$

where ϕ collectively denote all the torsional degrees of freedom and $U(\Omega,\phi)$ is the torsional-orientational potential. The expression for the orienting strength is still given by eq. (5), with:

$$\langle a\rangle = \frac{\int \mathrm{d}\Omega\, \mathrm{d}\phi \exp\left[-U(\Omega,\phi)/k_B T\right] a(\Omega,\phi)}{Q} \tag{19}$$

If the minima of the torsional potential are separated by large enough barriers, the system can be simply treated in terms of a finite number of conformers, each corresponding to a given minimum; then, the torsional-orientational partition function, eq. (8), can be approximated as:

$$Q = \sum_m \exp\left[-V_m / k_B T\right] Q_m \tag{20}$$

where the summation is over all conformers; V_m is the torsional potential and Q_m the orientational partition function for the mth conformer:

$$Q_m = \int \mathrm{d}\Omega \exp\left[-U_m(\Omega)/k_B T\right]. \tag{21}$$

Then, the average value of any arbitrary function g can be calculated as:

$$\langle g \rangle = \sum_m w_m \overline{g_m} \tag{22}$$

with the average over single conformers:

$$\overline{g_m} = \frac{\int \mathrm{d}\Omega \exp\left[-U_m(\Omega)/k_B T\right] g_m(\Omega)}{Q_m}; \tag{23}$$

here g_m is the function evaluated for the mth conformer and w_m is the statistical weight of this conformer, defined as:

$$w_m = \frac{\exp\left[-V_m / k_B T\right] Q_m}{Q}. \tag{24}$$

In the nematic phase the statistical weights of conformers will be different from those in solution, and will depend on the degree of order. Namely, depending on their shape, conformers can be more or less accommodated in the nematic phase; in general, elongated conformers are stabilized over the bent ones.

In the presence of conformers, an additional contribution, from the torsional energy, must be included in the internal energy density, eq. (9a):

$$\Delta u = \frac{1}{2v}\langle U \rangle + \frac{1}{v}\langle \Delta V \rangle \tag{25}$$

where $\Delta V = V - \langle V \rangle_{iso}$, with $\langle V \rangle_{iso}$ being the average torsional potential in the isotropic phase. The difference in average torsional potential between the nematic and the isotropic phase derives from the change in conformational distribution between the nematic and the isotropic phase. Using eq. (25), the Helmholtz free energy, eq. (10), becomes:

$$f = f_{iso} + \frac{\xi^2}{2v^2}\langle a \rangle^2 - \frac{k_B T}{v}\ln Q + \frac{1}{v}\langle \Delta V \rangle \tag{26}$$

It is worth remarking that the averages appearing in this equation are taken not only over molecular orientations, but also over conformations.

Following the same procedure presented above for rigid mesogens, expressions for the elastic constants of flexible mesogens are obtained (see Appendix D):

$$k_2 = 3\frac{\varepsilon k_B T}{v} c_{XYZ} \tag{27a}$$

$$k_{13} = 3\frac{\varepsilon k_B T}{v} c_{XZXZ} \tag{27b}$$

$$\begin{aligned} K_{ii} = {} & 3\frac{\varepsilon k_B T}{v}\left\{\left[c_{JJXX} - c_{JJZZ} - 2(\delta_{i1} - \delta_{i3})c_{XZXZ}\right]\left(1 + \langle \Delta V' \rangle_0\right) - \left(d_{JJXX} - d_{JJZZ} - 2(\delta_{i1} - \delta_{i3})d_{XZXZ}\right)\right. \\ & \left. -3\varepsilon\left[c_{JXZ,JXZ}\left(1 + \langle \Delta V' \rangle_0\left(1 - \langle a^2 \rangle_0 / \langle a \rangle_0^{\,2}\right)\right) - d_{JXZ,JXZ}\right]\right\} \\ & +\delta_{i2} 9\frac{\varepsilon^2}{v} c_{YXZ}\left[\left(1 + \langle \Delta V' \rangle_0\left(1 - \langle a^2 \rangle_0 / \langle a \rangle_0^{\,2}\right)\right)c_{YXZ} - d_{YXZ}\right] \\ & +\delta_{i2} 9\frac{\varepsilon^2}{v}\left[\langle a \rangle_0 + \varepsilon\left(\langle a^2 \rangle_0 - \langle a \rangle_0^{\,2}\right)\right]^{-2}\left[c_{YXZ} + 3\varepsilon\left(b_{YXZ} - \langle a \rangle_0 c_{YXZ}\right)\right]^2 \times \\ & \times\left[1 + \varepsilon\left(\langle a^2 \rangle_0 - \langle a \rangle_0^{\,2} + \langle \Delta V' \rangle_0 \langle a^2 \rangle_0 - \langle \Delta V' a^2 \rangle_0 + 2\langle a \rangle_0\left(\langle \Delta V' a \rangle_0 - \langle \Delta V' \rangle_0 \langle a \rangle_0\right)\right)\right] \\ & +\delta_{i2} 3\frac{\varepsilon}{v}\left[\langle a \rangle_0 + \varepsilon\left(\langle a^2 \rangle_0 - \langle a \rangle_0^{\,2}\right)\right]^{-1}\left[c_{YXZ} + 3\varepsilon\left(b_{YXZ} - \langle a \rangle_0 c_{YXZ}\right)\right] \times \\ & \times\left\{d_{YXZ} - \langle \Delta V' \rangle_0 c_{YXZ} + 3\varepsilon\left[g_{YXZ} - \langle \Delta V' \rangle_0 b_{YXZ} + \langle a \rangle_0\left(2\langle a \rangle_0 \langle \Delta V' \rangle_0 c_{YXZ} - \langle a\, \Delta V' \rangle_0 c_{YXZ} - \langle a \rangle_0 d_{YXZ}\right)\right]\right\} \end{aligned} \tag{27c}$$

$$\begin{aligned} K_{22} + k_{24} = {} & \frac{3}{2}\frac{\varepsilon k_B T}{v}\left\{\left(c_{XXXX} + c_{XXYY} - 2c_{XXZZ}\right)\left(1 + \langle \Delta V' \rangle_0\right) - \left(d_{XXXX} + d_{XXYY} - 2d_{XXZZ}\right)\right. \\ & \left. -6\varepsilon\left[\left(c_{XXZ,XXZ} - c_{XXZ}c_{XXZ}\right)\left(1 + \langle \Delta V' \rangle_0\left(1 - \langle a^2 \rangle_0 / \langle a \rangle_0^{\,2}\right)\right) - \left(d_{XXZ,XXZ} - d_{XXZ,YYZ}\right)\right]\right\} \end{aligned} \tag{27d}$$

where $\mathbf{d}^{(n)}$ (n=3,4,6) and $\mathbf{g}^{(3)}$ are the tensors defined in eqs. (E1) and $\Delta V' = \Delta V / k_B T$. For multiple conformers with identical torsional potential, *i.e.* when $\Delta V' = 0$, eqs. (27) reduce to the form of eqs. (16), where, however, the averages have to be intended as taken over both orientations and conformers.

Computational methodology

The calculation of elastic constants requires the atomic coordinates of all conformers. For each conformer, tessellation of the molecular surface is performed [49]. Then the surface integrals, which appear in the expressions for the elastic constants, are evaluated as sums over the tesserae. The volume integrals in eqs. (B7) are conveniently transformed into surface integrals, according to the Stokes theorem, as shown in Appendix F. For a given value of the orienting strength, ε, order

parameters and orientational averages for each conformer are calculated by integrating over the orientational distribution function in undeformed nematics, eq. (13). The integrals over orientations are conveniently expressed as integrals over the Euler (β, γ) angles, by properly exploiting the axial symmetry of undeformed nematics, as shown in Appendix G. Numerical integration on the (β,γ) rectangle is carried out by the Gaussian quadrature rule [50]. Altogether, the full temperature dependence of the elastic constants of a conformer can be calculated in a few minutes on a desktop PC. Finally, the elastic constants are evaluated as sums of single conformer contributions; the computation time scales linearly with the number of conformers.

The elastic constants of 5CB

In the following we shall present the results obtained for 4-*n*pentyl-4'-cyanobiphenyl (5CB), a typical mesogen for which many experimental data are available. The structure of 5CB is shown in Fig. 2; several conformers are possible, which are obtained by rotation around the alkyl chain bonds and the phenyl-phenyl bond [51]. In our calculations we have taken the 15 lowest energy conformers, having at most a single *gauche* state in the tail; the others have been neglected, in view of the energy increase associated with the introduction of a *gauche*, which is of the order of k_BT, in the temperature range of the nematic phase. An arbitrary conformer is identified by a label, like **Ptg+t**; the first letter specifies the sign of the twist angle between phenyl rings (**M** and **P**, for angles of about +30° and about -30°, respectively), whereas the subsequent letters denote the conformational state of CH_2-CH_2 bonds, in their order, starting from the benzene ring (**t**, **g+**, **g-**, for *trans*, *gauche*+ and *gauche*-, respectively). Fig. 3 shows five of the lowest energy conformers, with their labels. Atomic coordinates of the conformers were obtained by geometry optimization at the DFT/B3LYP/6-31g** level [52]. Molecular surfaces were generated with van der Waals radii: r_C=0.185 nm, r_N=0.16 nm, r_H=0.1 nm [53] and a rolling sphere radius equal to 0.3 nm [54]; a density of points equal to 500 nm^{-2} was taken.

[insert Figure 4 about here]

In calculating the elastic constants, the volume per molecule v was taken equal to 275 $Å^3$, the value obtained from the molecular surface calculation [49]. Given the small differences between the values obtained from the DFT calculations, all conformers with a **g** bond were assumed to have the same torsional energy, 2.5 kJ mol^{-1} higher than the energy of the all-*trans* conformer [51].

Elastic constants were calculated as a function of the orienting strength, ε, or, equivalently, of the orientational order parameters. The relation with temperature was then established by comparison with the experimental temperature dependence of order parameters reported for 5CB [55]. Fig. 5 shows the principal elements of the calculated Saupe matrix [4], as a function of temperature. These are obtained by diagonalization of the average Saupe matrix, calculated from conformer contributions, all expressed in the same molecular fixed frame.

[insert Figure 5 about here]

Fig. 6 displays the elastic constants calculated for 5CB, according to eqs. (27). These can be compared with the experimental data, shown in Fig. 3: we can see that the sequence of elastic moduli is correctly predicted, as well as their temperature dependence. Fig. 6 also shows the elastic ratios, K_{22}/K_{11} and K_{33}/K_{11}, which are known to be especially sensitive to changes in the molecular structure [46]. The values obtained from our calculations are close to those derived from measurements and, in keeping with experiment, K_{22} and K_{11} are predicted to have almost the same temperature dependence, weaker than that of K_{33}. Even with the uncertainty of the experimental data, we can recognize that the calculated elastic constants, especially those for splay and twist, are lower than the measured values and the predicted K_{33}/K_{11} ratio is overestimated. These discrepancies between theory and experiment are probably due to the approximate form of the potential of mean torque; anyway, the results obtained are quite satisfactory, especially in view of the fact that no free parameter enters the calculations and presently no other methodology is available to directly connect atomic structure and elastic constants.

[insert Figure 6 about here]

In Fig. 6 we also show the elastic constants calculated by simplified expression, obtained by neglecting all the terms containing $\langle \Delta V' \rangle_0$ in eqs. (27), which derive from the change in average torsional potential between the nematic and the isotropic phase. The figure shows that this contribution is really small, therefore it could be safely neglected in calculations.

In most molecular theories the elastic constants are expressed as a function of order parameters, and contributions of different rank are distinguished; the lowest order term is proportional to the square of the second rank order parameter. In the present model, the dependence on order parameters is implicitly contained in the average values appearing in the expressions for elastic constants, eqs. (27). Fig. 7 displays the elastic constants of 5CB as a function of S_{zz}^2, the

higher principal value of the average Saupe matrix. We can see that for the splay and twist elastic moduli the relationship is close to linear in almost the whole range of order parameter; some more deviation from linearity appears for the bend stiffness. Such results are in keeping with most theories [46], and are related to the different temperature dependence of the elastic ratios, shown in Fig. 6.

[insert Figure 7 about here]

An important and still largely unexplored issue concerns the effects of the molecular flexibility on the elastic moduli of nematics. New insights can derive from our methodology, which allows us to examine the contribution of individual conformers to the elastic constants. Some results obtained for 5CB are shown in Fig. 8. We can see a strong dependence on the alkyl chain conformation, understandable because changes in chain conformation can correspond to significant changes in the whole molecular shape, as appears in Fig. 4. In general, small elastic constants are predicted for bent conformers, and much higher ones for elongated conformers. Remarkably, even negative K_{33} values are obtained for the most bent structures. It is worth stressing that this result is not in contrast with the existence of the nematic phase for 5CB; the negative contribution K_{33} has only the effect of lowering the elastic constant obtained after averaging over all the conformers. Fig. 8 shows that intermediate values of the elastic constants have been calculated for the *all-trans* conformer, the most stable and then the most important, which is slightly bent. Effects of molecular flexibility were proposed to explain the experimental dependence of elastic ratios on alkyl chain lengths in homologous series [10]. The role of flexibility was also invoked to explain the differences between the elastic constants calculated by a statistical mechanics theory for Gay-Berne particles and the results obtained from atomistic Molecular Dynamics simulations of 5CB [56]. Our calculations show that the conformers of a given molecule can give very different contributions to the elastic constants; their effect on the 'observed' elastic constants depends on their statistical weight.

[insert Figure 8 about here]

As conformers are chiral, they also give a contribution to the k_2 constant, which is related to the stabilization of a cholesteric helix in the nematic phase. Our calculations show that individual conformers would produce helical pitches in the range 0.1 μm-1 μm, i.e. comparable to the pitch measured [57] and predicted [58] for alkylcyanobiphenyl mesogens with a chiral center in the

aliphatic chain. However, for each conformer the mirror image is also present in a sample; since k_2 contributions of opposite sign are obtained for enantiomeric pairs, a vanishing k_2 value is obtained for the mixture of conformers.

Finally, Fig. 9 displays the temperature dependence of the surfacelike elastic constants, k_{13} and k_{24}. We can see that the former is negative and weakly changing with temperature, whereas the latter is positive and increases with lowering temperature; both are significantly smaller than the bulk moduli. Unfortunately we cannot evaluate the quality of our predictions by comparison with experiment, for the lack of data; only comparison with other theories and simulations is possible. Actually, only a few attempts to evaluate surfacelike elastic constants have been reported, all dealing with simple particle models. Teixeira et al [59] studied a nematic formed by Gay-Berne particles using a generalized Poniewierski-Stecki theory [22], whereas Stelzer at al [60] performed Molecular Dynamics simulations for an analogous system. In both cases k_{13} and k_{24} significantly smaller than the bulk elastic constants were obtained, in keeping with our results for 5CB. However, there is complete disagreement on the sign of the two constants. Mostly positive k_{13} and k_{24} values were predicted by Teixeira et al., whereas Stelzer and colleagues found $k_{24} >0$ and $k_{13} <0$. The discrepancies were ascribed to different approximations used for evaluating the direct correlation function, and the strong sensitivity of the surface constants to details of the latter was inferred [60]. In our calculations we have found a significant dependence of k_{13} and k_{24} on the molecular conformation. All this points to the special character of the surfacelike constants, which deserve more experimental and theoretical investigation.

[insert Figure 9 about here]

Conclusions

We have developed a molecular theory for the elasticity of nematic liquid crystals, based on the Surface Interaction model [35,37]. The relation between molecular orientation and director deformation is introduced through the assumption that the nematic director tends to lie perpendicular to each point of the molecular surface. A realistic account of the molecular structure is made possible by the use of a surface generated from atomic coordinates. The mesogen flexibility is easily introduced, through averages over molecular configurations. The elastic constants are expressed in terms of the orientational averages of tensors, defined as integrals of suitable functions over the molecular surface; they can be calculated as a function of the orientational order, without any free parameter, at low computational cost. This methodology is suitable for chiral and nonchiral

nematics. It enables us to investigate the role of molecular features and to explore how changes at the atomic level can be conveyed into changes in elastic behavior, on a quite different length scale. For this reason we think that it can shed light on the origin, still poorly understood, of the different elasticity of the nematic phase formed by mesogens with different structure. The predictive ability of this method makes it potentially useful for the synthetic design of tailored mesogens: the elastic constants can be easily calculated, once the molecular structure is known. Further investigation of different kinds of mesogens and the comparison of the theoretical results with existing data is needed to assess the quality of the predictions. Promising results have been obtained for the typical case of 5CB. Several elasticity measurements have been reported for this system, with some discrepancy. The absolute and relative magnitude of the calculated elastic constants, as well as their temperature dependence, are in keeping with experiments. The calculations show the extreme sensitivity of the elastic constants, especially that for bending, to the molecular geometry: even for 5CB, which is generally taken as a prototype of a rod-like structure, we have found remarkable differences between conformer contributions.

Within the theoretical framework presented here, also expressions for the surfacelike elastic constants of nematics are provided. The values obtained for k_{13} and k_{24} of 5CB have opposite sign, and much smaller in magnitude than those of the bulk elastic moduli. They are highly sensitive to the molecular geometry; great sensitivity to the details of the direct correlation function was evidenced by previous theories and simulations [59,60]. The absence of unambiguous experimental data makes it difficult to assess the quality of our results. Actually, as discussed by some authors [47,48], theories for the surface elasticity, as well as the interpretation of experiments, should be considered within a more framework, taking into account also the anchoring free energy. So, we think that what we have presented here should only be seen as a preliminary exploration of the problem of the surface elasticity of nematics, which deserves further investigation in the future, and we hope that our approach can provide new insights.

Developments of this work along different lines can be foreseen. In the next future, they include the investigation of a wider class of mesogens, including systems more unusual than 5CB, like cyanobiphenyl dimers [61] or bent shaped molecules [62], for whose elasticity scarce experimental information is available. Considering computational issues, the calculation of elastic constants will be introduced in a systematic procedure for generating and treating conformers of flexible molecules, with the possibility of Monte Carlo conformational sampling [63]. Moreover, it would be interesting to extend our approach to the elastic properties of other phases, e.g. biaxial nematics [64].

Acknowledgments

The starting part of this work was supported by Italian MIUR (PRIN 2005). The authors gratefully acknowledge dr. Fabio Tombolato for stimulating discussions.

Abbreviations LC: Liquid Crystals; 5CB: 4-*n*pentyl-4′-cyanobiphenyl; SI: Surface Interaction.

Appendix A

In this appendix expressions for the derivatives of the free energy density, appearing in eq. (11), are obtained. From eq. (10), we can write:

$$\frac{\partial f}{\partial n_{IJ}} = \frac{\xi^2}{v^2}\langle a\rangle \frac{\partial \langle a\rangle}{\partial n_{IJ}} - \frac{k_B T}{v}\frac{1}{Q}\frac{\partial Q}{\partial n_{IJ}} \tag{A1a}$$

$$\frac{\partial^2 f}{\partial n_{IJ}\partial n_{KM}} = \frac{\xi^2}{v^2}\langle a\rangle \frac{\partial^2 \langle a\rangle}{\partial n_{IJ}\partial n_{KM}} + \frac{\xi^2}{v^2}\frac{\partial \langle a\rangle}{\partial n_{IJ}}\frac{\partial \langle a\rangle}{n_{KM}} + \frac{k_B T}{v}\frac{1}{Q^2}\frac{\partial Q}{\partial n_{IJ}}\frac{\partial Q}{\partial n_{KM}} - \frac{k_B T}{v}\frac{1}{Q}\frac{\partial^2 Q}{\partial n_{IJ}\partial n_{KM}} \tag{A1b}$$

Considering the form of the potential of mean torque, eq. (2), the derivatives of the orientational partition function, eq. (3), are given by:

$$\frac{\partial Q}{\partial n_{IJ}} = \frac{\xi^2}{v k_B T} Q\langle a\rangle \left(\left\langle \frac{\partial a}{\partial n_{IJ}} \right\rangle + \frac{\partial \langle a\rangle}{\partial n_{IJ}} \right) \tag{A2a}$$

$$\frac{\partial^2 Q}{\partial n_{IJ}\partial n_{KM}} = Q\frac{\xi^2}{v k_B T}\left\{ \frac{\partial \langle a\rangle}{\partial n_{IJ}}\left\langle \frac{\partial a}{\partial n_{KM}} \right\rangle + \left\langle \frac{\partial a}{\partial n_{IJ}} \right\rangle \frac{\partial \langle a\rangle}{\partial n_{KM}} + \langle a\rangle \left\langle \frac{\partial^2 a}{\partial n_{IJ}\partial n_{KM}} \right\rangle + \langle a\rangle \frac{\partial^2 \langle a\rangle}{\partial n_{IJ}\partial n_{KM}} \right.$$
$$\left. \frac{\xi^2}{v k_B T}\left[\langle a\rangle^2 \left\langle \frac{\partial a}{\partial n_{IJ}}\frac{\partial a}{\partial n_{KM}} \right\rangle + \langle a^2\rangle \frac{\partial \langle a\rangle}{\partial n_{IJ}}\frac{\partial \langle a\rangle}{\partial n_{KM}} + \langle a\rangle \frac{\partial \langle a\rangle}{\partial n_{IJ}}\left\langle a\frac{\partial a}{\partial n_{KM}} \right\rangle + \langle a\rangle \left\langle a\frac{\partial a}{\partial n_{IJ}} \right\rangle \frac{\partial \langle a\rangle}{\partial n_{KM}} \right] \right\} \tag{A2b}$$

By substitution of eqs. (A2a-b) into eqs. (A1a-b) we obtain:

$$\frac{\partial f}{\partial n_{IJ}} = -\frac{\xi^2}{v^2}\langle a\rangle \left\langle \frac{\partial a}{\partial n_{IJ}} \right\rangle \tag{A3a}$$

$$\frac{\partial^2 f}{\partial n_{IJ}\partial n_{KM}} = -\frac{\xi^2}{v^2}\langle a\rangle \left\{ \left\langle \frac{\partial^2 a}{\partial n_{IJ}\partial n_{KM}} \right\rangle + \frac{\xi^2}{v k_B T}\langle a\rangle \left[\left\langle \frac{\partial a}{\partial n_{IJ}}\frac{\partial a}{n_{KM}} \right\rangle - \left\langle \frac{\partial a}{\partial n_{IJ}} \right\rangle \left\langle \frac{\partial a}{n_{KM}} \right\rangle \right] \right\}$$
$$- \frac{\xi^2}{v^2}\frac{\partial \langle a\rangle}{\partial n_{IJ}} \left\{ \left\langle \frac{\partial a}{\partial n_{KM}} \right\rangle + \frac{\xi^2}{v k_B T}\langle a\rangle \left[\left\langle a\frac{\partial a}{n_{KM}} \right\rangle - \langle a\rangle \left\langle \frac{\partial a}{n_{KM}} \right\rangle \right] \right.$$
$$\left. - \frac{\xi^2}{v^2}\frac{\partial \langle a\rangle}{\partial n_{KM}} \left\{ \left\langle \frac{\partial a}{\partial n_{IJ}} \right\rangle + \frac{\xi^2}{v k_B T}\langle a\rangle \left[\left\langle a\frac{\partial a}{n_{IJ}} \right\rangle - \langle a\rangle \left\langle \frac{\partial a}{n_{IJ}} \right\rangle \right] \right\} \right.$$
$$+ \frac{\xi^2}{v^2}\frac{\partial \langle a\rangle}{\partial n_{IJ}}\frac{\partial \langle a\rangle}{n_{KM}} \left[1 - \frac{\xi^2}{v k_B T}\left(\langle a^2\rangle - \langle a\rangle^2 \right) \right] \tag{A3b}$$

For the first derivative of the average value $\langle a\rangle$, we can write:

$$\frac{\partial \langle a\rangle}{\partial n_{IJ}} = \left[1 - \frac{\xi^2}{v k_B T}\left(\langle a^2\rangle - \langle a\rangle^2 \right) \right]^{-1} \left[\left\langle \frac{\partial a}{\partial n_{IJ}} \right\rangle + \frac{\xi^2}{v k_B T}\langle a\rangle \left(\langle a\rangle \left\langle \frac{\partial a}{\partial n_{IJ}} \right\rangle - \left\langle a\frac{\partial a}{\partial n_{IJ}} \right\rangle \right) \right] \tag{A4}$$

which substituted into eq. (A.3b) leads to:

$$\frac{\partial^2 f}{\partial n_{IJ}\partial n_{KM}} = -\frac{\xi^2}{v^2}\langle a\rangle\left\{\left\langle \frac{\partial^2 a}{\partial n_{IJ}\partial n_{KM}}\right\rangle + \frac{\xi^2}{vk_BT}\langle a\rangle\left[\left\langle \frac{\partial a}{\partial n_{IJ}}\frac{\partial a}{n_{KM}}\right\rangle - \left\langle \frac{\partial a}{\partial n_{IJ}}\right\rangle\left\langle \frac{\partial a}{n_{KM}}\right\rangle\right]\right\} \tag{A5}$$
$$-\frac{\xi^2}{v^2}\left[1-\frac{\xi^2}{vk_BT}\left(\left\langle a^2\right\rangle - \langle a\rangle^2\right)\right]^{-1}\left\{\left\langle \frac{\partial a}{\partial n_{IJ}}\right\rangle + \frac{\xi^2}{vk_BT}\langle a\rangle\left[\left\langle a\frac{\partial a}{n_{IJ}}\right\rangle - \langle a\rangle\left\langle \frac{\partial a}{n_{IJ}}\right\rangle\right]\right\}\times$$
$$\times\left\{\left\langle \frac{\partial a}{\partial n_{KM}}\right\rangle + \frac{\xi^2}{vk_BT}\langle a\rangle\left[\left\langle a\frac{\partial a}{n_{KM}}\right\rangle - \langle a\rangle\left\langle \frac{\partial a}{n_{KM}}\right\rangle\right]\right\}$$

An expression analogous in form to eq. (A3a) is obtained for the derivative of the free energy density with respect to $n_{JKM} = \partial^2 n_J / \partial R_K \partial R_M$.

Appendix B

Here we shall make explicit the position dependence of the function $P_2(\mathbf{n}\cdot\mathbf{s})$, appearing in the expression for the potential of mean torque, eq. (4), in the presence of director distortions. Let us assume that the origin of the molecular frame is located at the point $\mathbf{R}_0$ in the sample; if $\mathbf{n}^0 = \mathbf{n}(\mathbf{R}=\mathbf{R}_0)$ is the director in this point, the function $P_2(\mathbf{n}\cdot\mathbf{s})$ at any arbitrary position on the molecular surface, $\mathbf{R} = \mathbf{R}_0 + \mathbf{r}$, can be expressed by the Taylor expansion in powers of the displacement **r**:

$$P_2(\mathbf{n}\cdot\mathbf{s}) \approx P_2(\mathbf{n}^0\cdot\mathbf{s}) + 3\sum_{IJK} r_K s_J s_I n_I^0 n_{JK} + \frac{3}{2}\sum_{IJKM} r_M r_K s_I s_J n_I^0 n_{JKM} + \frac{3}{2}\sum_{IJKM} r_M r_K s_I s_J n_{IM} n_{JK} + \ldots \tag{B1}$$

For small displacements on the length scale of the deformation, this expansion can be truncated at the first terms.

Using eq. (B1), the function *a* defined in eq. (6) can be approximated as:

$$a \approx a_0 + 3\sum_{IJK} T_{KJI} n_I^0 n_{JK} + \frac{3}{2}\sum_{IJKM} T_{MKJI} n_I^0 n_{JKM} + \frac{3}{2}\sum_{IJKM} T_{MKJI} n_{IM} n_{JK} \tag{B2}$$

where $T_{IJKM\ldots}$ are elements of the *n*th rank $\mathbf{T}^{(n)}$ tensors:

$$T_{IJ} = \int_S s_I s_J dS \tag{B3a}$$
$$T_{IJK} = \int_S r_I s_J s_K dS \tag{B3b}$$
$$T_{IJKM} = \int_S r_I r_J s_K s_M dS \tag{B3c}$$

From the definition, the following symmetry relations are derived:

$$T_{IJ} = T_{JI} \tag{B4a}$$

$$T_{IJK} = T_{IKJ} \tag{B4b}$$

$$T_{IJKM} = T_{JIKM} = T_{IJMK} = T_{JIKM} \tag{B4c}$$

The derivatives of the function *a* appearing in eq. (12) can then be expressed as:

$$\frac{\partial a}{\partial n_{JK}} = 3\sum_{I} T_{KJI} n_I^0 + 3\sum_{IM} T_{MKJI} n_{IM} \tag{B5a}$$

$$\frac{\partial a}{\partial n_{JKM}} = \frac{3}{2}\sum_{I} T_{MKJI} n_I^0 \tag{B5b}$$

$$\frac{\partial^2 a}{\partial n_{JK}\partial n_{IM}} = 3T_{MKJI} \tag{B5c}$$

The $\mathbf{T}^{(n)}$ tensors defined in eqs. (B3) depend on the location of the origin of the molecular frame. Under a shift of the origin, $O' \to O$, the coordinates of points in the molecular surface transform as $\mathbf{r}=\mathbf{r}'-\mathbf{r_0}$, where the vector $\mathbf{r}_0$ specifies the position of the new origin in the original frame. It follows that for the $\mathbf{T}^{(n)}$ tensors we can write:

$$T'_{IJ} = T_{IJ} \tag{B6a}$$

$$T'_{IJK} = T_{IJK} - r_{0,I} T_{JK} \tag{B6b}$$

$$T'_{IJKM} = T_{IJKM} + r_{0,I} r_{0,J} T_{KM} - r_{0,I} T_{JKM} - r_{0,J} T_{IKM} \tag{B6c}$$

where $r_{0,I}$ and $r_{0,J}$ are Cartesian components of the vector $\mathbf{r}_0$.

The expression for the free energy density, eq. (12), contains averages of the derivatives of the function *a*, eqs. (B5), taken over the orientational distribution function in undeformed nematics, p_0, introduced in eq. (13). After further averaging over all positions of the origin within the molecular volume, as appropriate in a fluid without positional order, we can define the following tensors:

$$c_{IJK} = \langle T_{IJK} \rangle_0 - \frac{1}{v}\left\langle \left(\int_v d\mathbf{r}\; r_{0,I} \right) T_{JK} \right\rangle_0 \tag{B7a}$$

$$b_{IJK} = \langle a T_{IJK} \rangle_0 - \frac{1}{v}\left\langle \left(\int_v d\mathbf{r}\; r_{0,I} \right) a T_{JK} \right\rangle_0 \tag{B7b}$$

$$c_{IJKM} = \langle T_{IJKM} \rangle_0 + \frac{1}{v}\left\langle \left(\int_v d\mathbf{r}\; r_{0,I} r_{0,J} \right) T_{KM} \right\rangle_0 - \frac{1}{v}\left\langle \left(\int_v d\mathbf{r}\; r_{0,I} \right) T_{JKM} \right\rangle_0 - \frac{1}{v}\left\langle \left(\int_v d\mathbf{r}\; r_{0,J} \right) T_{IKM} \right\rangle_0 \tag{B7c}$$

$$c_{IJK,LMN} = \langle T_{IJK} T_{LMN} \rangle_0 + \frac{1}{v}\left\langle \left(\int_v d\mathbf{r}\; r_{0,I} r_{0,L} \right) T_{JK} T_{MN} \right\rangle_0 \tag{B7d}$$

$$- \frac{1}{v}\left\langle \left(\int_v d\mathbf{r}\; r_{0,I} \right) T_{JK} T_{LMN} \right\rangle_0 - \frac{1}{v}\left\langle \left(\int_v d\mathbf{r}\; r_{0,L} \right) T_{IJK} T_{MN} \right\rangle_0$$

where *v* is the molecular volume.

Some relationships, which exist between the components of the $\mathbf{c}^{(n)}$ tensors, by virtue of the uniaxial symmetry of the undistorted nematic phase, are exploited in deriving the expressions for the elastic constants. In a laboratory frame with the *Z* axis parallel to the director, after averaging

over the distribution function for undeformed nematics, p_0, the number of independent components of the $\mathbf{c}^{(n)}$ tensors is strongly reduced. In particular, for the relevant elements of the third-rank tensor we can write:

$$\langle T_{IJZ} \rangle_0 = \varepsilon_{IJZ} \langle T_{IJZ} \rangle_0 \quad (= 0 \quad \text{for achiral molecules}) \tag{B8a}$$

$$\langle aT_{IJZ} \rangle_0 = \varepsilon_{IJZ} \langle aT_{IJZ} \rangle_0 \quad (=0 \quad \text{for achiral molecules}) \tag{B8b}$$

where ε_{IJZ} is the Levi-Civita symbol [65].

The components of the fourth rank tensors obey the following relationships:

$$\langle T_{XXXX} \rangle_0 = \langle T_{YYYY} \rangle_0 \tag{B9a}$$

$$\langle T_{XXZZ} \rangle_0 = \langle T_{YYZZ} \rangle_0 \tag{B9b}$$

$$\langle T_{XXYY} \rangle_0 = \langle T_{YYXX} \rangle_0 \tag{B9c}$$

$$\langle T_{ZZXX} \rangle_0 = \langle T_{ZZYY} \rangle_0 \tag{B9d}$$

$$\langle T_{XZXZ} \rangle_0 = \langle T_{YZYZ} \rangle_0 \tag{B9e}$$

$$\langle T_{XZYX} \rangle_0 = \langle T_{YZXY} \rangle_0 = 0 \tag{B9f}$$

$$\langle T_{YXYZ} \rangle_0 = \langle T_{XYXZ} \rangle_0 = 0 \tag{B9g}$$

$$\langle T_{XXYZ} \rangle_0 = \langle T_{YYXZ} \rangle_0 = \langle T_{XXXZ} \rangle_0 = \langle T_{YYYZ} \rangle_0 = \langle T_{YYXZ} \rangle_0 = \langle T_{YXXZ} \rangle_0 = \langle T_{XYYZ} \rangle_0 = 0 \tag{B9h}$$

$$\langle T_{YZXZ} \rangle_0 = \langle T_{YZYZ} \rangle_0 = \langle T_{ZYXZ} \rangle_0 = \langle T_{ZYYZ} \rangle_0 = 0 \tag{B9i}$$

$$\langle T_{XYXX} \rangle_0 = \langle T_{XYYY} \rangle_0 = \langle T_{XYZZ} \rangle_0 = 0 \tag{B9l}$$

$$\langle T_{XXXY} \rangle_0 = \langle T_{YYXY} \rangle_0 = \langle T_{ZZXY} \rangle_0 = 0 \tag{B9m}$$

$$\langle T_{XXXX} \rangle_0 = \langle T_{XXYY} \rangle_0 + 2\langle T_{XYXY} \rangle_0 \tag{B9n}$$

and for the components of the sixth rank tensors we have:

$$\langle T_{XXZ} T_{XXZ} \rangle_0 = \langle T_{YYZ} T_{YYZ} \rangle_0 \tag{B10a}$$

$$\langle T_{XYZ} T_{XYZ} \rangle_0 = \langle T_{YXZ} T_{YXZ} \rangle_0 \tag{B10b}$$

$$\langle T_{ZXZ} T_{ZXZ} \rangle_0 = \langle T_{ZYZ} T_{ZYZ} \rangle_0 \tag{B10c}$$

$$\langle T_{XXZ} T_{XXZ} \rangle_0 = \langle T_{XXZ} T_{YYZ} \rangle_0 + \langle T_{XYZ} T_{XYZ} \rangle_0 + \langle T_{XYZ} T_{YXZ} \rangle_0 \tag{B10d}$$

Analogous symmetry relations can be written for the tensors defined in eqs. (B7).

Appendix C

For the comparison with eq.(1), it is convenient to collect the terms in eq. (15) as shown in the following.

$$
\begin{aligned}
f_{el} &= 3\frac{\varepsilon k_B T}{v} c_{XYZ}\left(n_{YX}-n_{XY}\right)+3\frac{\varepsilon k_B T}{v} c_{XZXZ}\left(n_{XXZ}+n_{YYZ}\right) \\
&+\frac{3}{2}\frac{\varepsilon k_B T}{v}\left[c_{XXXX}-c_{XXZZ}-3\varepsilon c_{YXZ,YXZ}\right]\left(n_{XX}{}^2+n_{YY}{}^2\right) \\
&+\frac{3}{2}\frac{\varepsilon k_B T}{v}\left\{c_{YYXX}-c_{YYZZ}-3\varepsilon\left(c_{YXZ,YXZ}-c_{YXZ}c_{YXZ}\right)\right. \\
&\left.+3\left[\langle a\rangle_0+\varepsilon\left(\langle a^2\rangle_0-\langle a\rangle_0{}^2\right)\right]^{-1}\left[c_{YXZ}-\varepsilon\left(b_{YXZ}-\langle a\rangle_0 c_{YXZ}\right)\right]\left[c_{YXZ}-\varepsilon\left(b_{YXZ}-\langle a\rangle_0 c_{YXZ}\right)\right]\right\}\left(n_{XY}{}^2+n_{YX}{}^2\right) \\
&+\frac{3}{2}\frac{\varepsilon k_B T}{v}\left[c_{ZZXX}-c_{ZZZZ}-3\varepsilon c_{ZXZ,ZXZ}\right]\left(n_{XZ}{}^2+n_{YZ}{}^2\right) \\
&+3\frac{\varepsilon k_B T}{v}\left\{c_{YXYX}-3\varepsilon c_{XXZ,YYZ}\right\}n_{XX}n_{YY} \\
&+3\frac{\varepsilon k_B T}{v}\left\{c_{YXYX}-3\varepsilon\left(c_{YXZ,XYZ}-c_{YXZ}c_{XYZ}\right)\right. \\
&\left.+3\left[\langle a\rangle_0+\varepsilon\left(\langle a^2\rangle_0-\langle a\rangle_0{}^2\right)\right]^{-1}\left[c_{YXZ}-\varepsilon\left(b_{YXZ}-\langle a\rangle_0 c_{YXZ}\right)\right]\left[c_{XYZ}-\varepsilon\left(b_{XYZ}-\langle a\rangle_0 c_{XYZ}\right)\right]\right\}n_{XY}n_{YX}
\end{aligned}
\tag{C1}
$$

In the first line, the relationship $n_{KJM}= n_{KMJ}$ has been used.

After some algebra, this can be rewritten as:

$$
\begin{aligned}
f_{el} &= 3\frac{\varepsilon k_B T}{v} c_{XYZ}\left(n_{YX}-n_{XY}\right) \\
&+3\frac{\varepsilon k_B T}{v} c_{XZXZ}\left[\left(n_{XX}+n_{YY}\right)^2-\left(n_{XZ}{}^2+n_{YZ}{}^2\right)+\left(n_{XXZ}+n_{YYZ}\right)\right] \\
&+\frac{3}{2}\frac{\varepsilon k_B T}{v}\left[c_{XXXX}-c_{XXZZ}-2c_{XZXZ}-3\varepsilon c_{XXZ,XXZ}\right]\left(n_{XX}+n_{YY}\right)^2 \\
&+\frac{3}{2}\frac{\varepsilon k_B T}{v}\left\{c_{YYXX}-c_{YYZZ}-3\varepsilon\left(c_{YXZ,YXZ}-c_{YXZ}{}^2\right)\right. \\
&\left.+3\left[\langle a\rangle_0+\varepsilon\left(\langle a^2\rangle_0-\langle a\rangle_0{}^2\right)\right]^{-1}\left[c_{YXZ}-\varepsilon\left(b_{YXZ}-\langle a\rangle_0 c_{YXZ}\right)\right]\left[c_{YXZ}-\varepsilon\left(b_{YXZ}-\langle a\rangle_0 c_{YXZ}\right)\right]\right\}\left(n_{XY}-n_{YX}\right)^2 \\
&+\frac{3}{2}\frac{\varepsilon k_B T}{v}\left[c_{ZZXX}-c_{ZZZZ}+2c_{XZXZ}-3\varepsilon c_{ZXZ,ZXZ}\right]\left(n_{XZ}{}^2+n_{YZ}{}^2\right) \\
&+\frac{3}{2}\frac{\varepsilon k_B T}{v}\left\{-c_{XXXX}+2c_{XXZZ}-c_{XXYY}+6\varepsilon\left(c_{XXZ,XXZ}-c_{XXZ,YYZ}\right)\right\}\left(n_{XX}n_{YY}-n_{XY}n_{YX}\right)
\end{aligned}
\tag{C2}
$$

Appendix D

In this appendix we shall obtain expressions for the derivatives of the free energy density suitable for flexible mesogens, eq. (26), with respect to director deformations. We can write:

$$\frac{\partial f}{\partial n_{IJ}} = \frac{\xi^2}{v^2}\langle a\rangle \frac{\partial \langle a\rangle}{\partial n_{IJ}} - \frac{k_B T}{v}\frac{1}{Q}\frac{\partial Q}{\partial n_{IJ}} + \frac{1}{v}\frac{\partial \langle V\rangle}{\partial n_{IJ}} \tag{D1a}$$

$$\frac{\partial^2 f}{\partial n_{IJ}\partial n_{KM}} = \frac{\xi^2}{v^2}\langle a\rangle \frac{\partial^2 \langle a\rangle}{\partial n_{IJ}\partial n_{KM}} + \frac{\xi^2}{v^2}\frac{\partial \langle a\rangle}{\partial n_{IJ}}\frac{\partial \langle a\rangle}{n_{KM}} + \frac{k_B T}{v}\frac{1}{Q^2}\frac{\partial Q}{\partial n_{IJ}}\frac{\partial Q}{\partial n_{KM}} - \frac{k_B T}{v}\frac{1}{Q}\frac{\partial^2 Q}{\partial n_{IJ}\partial n_{KM}} + \frac{1}{v}\frac{\partial^2 \langle V\rangle}{\partial n_{IJ}\partial n_{KM}} \tag{D1b}$$

These expressions differ from eqs. (A1a-b) for the presence of terms containing the torsional potential *V*.

It is convenient to exploit the following relationships, which can be derived from the definition of orientation-conformational averages, eq. (22), and that of conformer weight, eq. (24):

$$\frac{\partial \langle V\rangle}{\partial n_{IJ}} = \frac{1}{Q}\sum_m \exp(-V_m / k_B T)\frac{\partial Q_m}{\partial n_{IJ}}\left(V_m - \langle V\rangle\right) \tag{D2a}$$

$$\begin{aligned}\frac{\partial^2 \langle V\rangle}{\partial n_{IJ}\partial n_{KM}} &= \frac{1}{Q}\sum_m \exp(-V_m / k_B T)\frac{\partial^2 Q_m}{\partial n_{IJ}\partial n_{KM}}\left(V_m - \langle V\rangle\right) \\ &- \frac{1}{Q^2}\sum_{m,n}\exp\left[-(V_m + V_n)/k_B T\right]\frac{\partial Q_m}{\partial n_{IJ}}\frac{\partial Q_n}{\partial n_{KM}}\left(V_m + V_n - 2\langle V\rangle\right)\end{aligned} \tag{D2b}$$

where summations are extended to all conformers.

The derivatives of the orientational partition functions for individual conformers, defined in eq. (21), are given by:

$$\frac{\partial Q_m}{\partial n_{IJ}} = \frac{\xi^2}{v k_B T} Q_m \left(\langle a\rangle \overline{\frac{\partial a_m}{\partial n_{IJ}}} + \overline{a}_m \frac{\partial \langle a\rangle}{\partial n_{IJ}} \right) \tag{D3a}$$

$$\begin{aligned}\frac{\partial^2 Q_m}{\partial n_{IJ}\partial n_{KM}} = \frac{\xi^2}{v k_B T} Q_m \Bigg\{ &\frac{\partial \langle a\rangle}{\partial n_{IJ}}\overline{\frac{\partial a_m}{\partial n_{KM}}} + \overline{\frac{\partial a_m}{\partial n_{IJ}}}\frac{\partial \langle a\rangle}{\partial n_{KM}} + \langle a\rangle\left[\overline{\frac{\partial^2 a_m}{\partial n_{IJ}\partial n_{KM}}} + \frac{\partial^2 \langle a\rangle}{\partial n_{IJ}\partial n_{KM}}\right] \\ &+ \frac{\xi^2}{v k_B T}\left[\langle a\rangle^2 \overline{\frac{\partial a_m}{\partial n_{IJ}}\frac{\partial a_m}{\partial n_{KM}}} + \overline{a_m}^2 \frac{\partial \langle a\rangle}{\partial n_{IJ}}\frac{\partial \langle a\rangle}{\partial n_{KM}} + \langle a\rangle \frac{\partial \langle a\rangle}{\partial n_{IJ}}\overline{a_m \frac{\partial a_m}{\partial n_{KM}}} + \langle a\rangle \overline{a_m \frac{\partial a_m}{\partial n_{IJ}}}\frac{\partial \langle a\rangle}{\partial n_{KM}}\right]\Bigg\}\end{aligned} \tag{D3b}$$

with the the upper bar indicating the orientational average, as in eq. (23).

For the derivatives of the average torsional potential we can write:

$$\frac{\partial\langle V\rangle}{\partial n_{IJ}} = \frac{\xi^2}{\nu k_B T}\frac{1}{Q}\sum_m \exp(-V_m/k_B T)Q_m\left(\langle a\rangle\overline{\frac{\partial a_m}{\partial n_{IJ}}} + \overline{a_m}\frac{\partial\langle a\rangle}{\partial n_{IJ}}\right)\left(V_m - \langle V\rangle\right) = \tag{D4a}$$
$$= \frac{\xi^2}{\nu k_B T}\left[\langle a\rangle\left(\left\langle V\frac{\partial a}{\partial n_{IJ}}\right\rangle - \langle V\rangle\left\langle\frac{\partial a}{\partial n_{IJ}}\right\rangle\right) + \frac{\partial\langle a\rangle}{\partial n_{IJ}}\left(\langle Va\rangle - \langle a\rangle\langle V\rangle\right)\right]$$

$$\frac{\partial^2\langle V\rangle}{\partial n_{IJ}\partial n_{KM}} = \frac{\xi^2}{\nu k_B T}\left\{\frac{\partial\langle a\rangle}{\partial n_{IJ}}\left\langle V\frac{\partial a}{\partial n_{KM}}\right\rangle + \frac{\partial\langle a\rangle}{\partial n_{KM}}\left\langle V\frac{\partial a}{\partial n_{IJ}}\right\rangle + \langle a\rangle\left\langle V\frac{\partial^2 a}{\partial n_{IJ}\partial n_{KM}}\right\rangle\right. \tag{D4b}$$
$$\left. + \frac{\xi^2}{\nu k_B T}\left[\langle a\rangle^2\left\langle V\frac{\partial a}{\partial n_{IJ}}\frac{\partial a}{\partial n_{KM}}\right\rangle + \langle Va^2\rangle\frac{\partial\langle a\rangle}{\partial n_{IJ}}\frac{\partial\langle a\rangle}{\partial n_{KM}} + \langle a\rangle\frac{\partial\langle a\rangle}{\partial n_{IJ}}\left\langle Va\frac{\partial a}{\partial n_{KM}}\right\rangle + \langle a\rangle\frac{\partial\langle a\rangle}{\partial n_{KM}}\left\langle Va\frac{\partial a}{\partial n_{IJ}}\right\rangle\right]\right\}$$
$$- \frac{\xi^2}{\nu k_B T}\langle V\rangle\left\{\frac{\partial\langle a\rangle}{\partial n_{IJ}}\left\langle\frac{\partial a}{\partial n_{KM}}\right\rangle + \frac{\partial\langle a\rangle}{\partial n_{KM}}\left\langle\frac{\partial a}{\partial n_{IJ}}\right\rangle + \langle a\rangle\left\langle\frac{\partial^2 a}{\partial n_{IJ}\partial n_{KM}}\right\rangle\right.$$
$$\left. + \frac{\xi^2}{\nu k_B T}\left[\langle a\rangle^2\left\langle\frac{\partial a}{\partial n_{IJ}}\frac{\partial a}{\partial n_{KM}}\right\rangle + \langle a^2\rangle\frac{\partial\langle a\rangle}{\partial n_{IJ}}\frac{\partial\langle a\rangle}{\partial n_{KM}} + \langle a\rangle\frac{\partial\langle a\rangle}{\partial n_{IJ}}\left\langle a\frac{\partial a}{\partial n_{KM}}\right\rangle + \langle a\rangle\frac{\partial\langle a\rangle}{\partial n_{KM}}\left\langle a\frac{\partial a}{\partial n_{IJ}}\right\rangle\right]\right\}$$
$$- \left(\frac{\xi^2}{\nu k_B T}\right)^2\langle a\rangle\left(\langle a\rangle\left\langle V\frac{\partial a}{\partial n_{IJ}}\right\rangle + \langle Va\rangle\frac{\partial\langle a\rangle}{\partial n_{IJ}}\right)\left(\left\langle\frac{\partial a}{\partial n_{KM}}\right\rangle + \frac{\partial\langle a\rangle}{\partial n_{KM}}\right)$$
$$- \left(\frac{\xi^2}{\nu k_B T}\right)^2\langle a\rangle\left(\langle a\rangle\left\langle V\frac{\partial a}{\partial n_{KM}}\right\rangle + \langle Va\rangle\frac{\partial\langle a\rangle}{\partial n_{KM}}\right)\left(\left\langle\frac{\partial a}{\partial n_{IJ}}\right\rangle + \frac{\partial\langle a\rangle}{\partial n_{IJ}}\right)$$
$$+ 2\left(\frac{\xi^2}{\nu k_B T}\right)^2\langle V\rangle\langle a\rangle^2\left(\left\langle\frac{\partial a}{\partial n_{KM}}\right\rangle + \frac{\partial\langle a\rangle}{\partial n_{KM}}\right)\left(\left\langle\frac{\partial a}{\partial n_{IJ}}\right\rangle + \frac{\partial\langle a\rangle}{\partial n_{IJ}}\right)$$

By substitution of eqs. (D3) and (D4) into eqs. (D1), using eq. (A4), we obtain:

$$\frac{\partial f}{\partial n_{IJ}} = -\frac{\xi^2}{\nu^2}\langle a\rangle\left\langle\frac{\partial a}{\partial n_{IJ}}\right\rangle + \frac{\xi^2}{\nu^2 k_B T}\left\{\langle a\rangle\left(\left\langle V\frac{\partial a}{\partial n_{IJ}}\right\rangle - \langle V\rangle\left\langle\frac{\partial a}{\partial n_{IJ}}\right\rangle\right) + \right. \tag{D5a}$$
$$\left.\left[1 - \frac{\xi^2}{\nu k_B T}\left(\langle a^2\rangle - \langle a\rangle^2\right)\right]^{-1}\left[\left\langle\frac{\partial a}{\partial n_{IJ}}\right\rangle - \frac{\xi^2}{\nu k_B T}\langle a\rangle\left(\langle a\rangle\left\langle\frac{\partial a}{\partial n_{IJ}}\right\rangle - \left\langle a\frac{\partial a}{\partial n_{IJ}}\right\rangle\right)\right]\left(\langle Va\rangle - \langle a\rangle\langle V\rangle\right)\right\}$$

$$\frac{\partial^2 f}{\partial n_{IJ}\partial n_{KM}} = \frac{\xi^2}{v^2}\frac{\partial\langle a\rangle}{\partial n_{IJ}}\frac{\partial\langle a\rangle}{n_{KM}}\left\{1-\frac{\xi^2}{vk_BT}\left(\langle a^2\rangle-\langle a\rangle^2\right)\right\} \tag{D5b}$$
$$-\frac{\xi^2}{v^2}\left[1-\frac{\xi^2}{vk_BT}\left(\langle a^2\rangle-\langle a\rangle^2\right)\right]^{-1}\left[\left\langle\frac{\partial a}{\partial n_{IJ}}\right\rangle-\frac{\xi^2}{vk_BT}\langle a\rangle\left(\langle a\rangle\left\langle\frac{\partial a}{\partial n_{IJ}}\right\rangle-\left\langle a\frac{\partial a}{\partial n_{IJ}}\right\rangle\right)\right]$$
$$\left[\left\langle\frac{\partial a}{\partial n_{KM}}\right\rangle-\frac{\xi^2}{vk_BT}\langle a\rangle\left(\langle a\rangle\left\langle\frac{\partial a}{\partial n_{KM}}\right\rangle-\left\langle a\frac{\partial a}{\partial n_{KM}}\right\rangle\right)\right]$$

$$-\frac{1}{v}\left(\frac{\xi^2}{vk_BT}\right)^2\left[1-\frac{\xi^2}{vk_BT}\left(\langle a^2\rangle-\langle a\rangle^2\right)\right]^{-2}\left[\left\langle\frac{\partial a}{\partial n_{IJ}}\right\rangle-\frac{\xi^2}{vk_BT}\langle a\rangle\left(\langle a\rangle\left\langle\frac{\partial a}{\partial n_{IJ}}\right\rangle-\left\langle a\frac{\partial a}{\partial n_{IJ}}\right\rangle\right)\right]$$
$$\left[\left\langle\frac{\partial a}{\partial n_{KM}}\right\rangle-\frac{\xi^2}{vk_BT}\langle a\rangle\left(\langle a\rangle\left\langle\frac{\partial a}{\partial n_{KM}}\right\rangle-\left\langle a\frac{\partial a}{\partial n_{KM}}\right\rangle\right)\right]\left[\left(\langle V\rangle\langle a^2\rangle-\langle Va^2\rangle\right)+2\langle a\rangle\left(\langle Va\rangle-\langle V\rangle\langle a\rangle\right)\right]$$

$$+\frac{\xi^2}{v^2k_BT}\left[1-\frac{\xi^2}{vk_BT}\left(\langle a^2\rangle-\langle a\rangle^2\right)\right]^{-1}\left[\left\langle\frac{\partial a}{\partial n_{IJ}}\right\rangle-\frac{\xi^2}{vk_BT}\langle a\rangle\left(\langle a\rangle\left\langle\frac{\partial a}{\partial n_{IJ}}\right\rangle-\left\langle a\frac{\partial a}{\partial n_{IJ}}\right\rangle\right)\right]\times$$
$$\times\left\{\left[\left\langle V\frac{\partial a}{\partial n_{KM}}\right\rangle-\langle V\rangle\left\langle\frac{\partial a}{\partial n_{KM}}\right\rangle+\frac{\xi^2}{vk_BT}\langle a\rangle\left[\left\langle Va\frac{\partial a}{\partial n_{KM}}\right\rangle-\langle V\rangle\left\langle a\frac{\partial a}{\partial n_{KM}}\right\rangle\right.\right.\right.$$
$$\left.\left.\left.+\langle a\rangle\left(2\langle a\rangle\langle V\rangle\left\langle\frac{\partial a}{\partial n_{KM}}\right\rangle-\langle Va\rangle\left\langle\frac{\partial a}{\partial n_{KM}}\right\rangle-\langle a\rangle\left\langle V\frac{\partial a}{\partial n_{KM}}\right\rangle\right)\right]\right\}$$

$$+\frac{\xi^2}{v^2k_BT}\left[1-\frac{\xi^2}{vk_BT}\left(\langle a^2\rangle-\langle a\rangle^2\right)\right]^{-1}\left[\left\langle\frac{\partial a}{\partial n_{KM}}\right\rangle-\frac{\xi^2}{vk_BT}\langle a\rangle\left(\langle a\rangle\left\langle\frac{\partial a}{\partial n_{KM}}\right\rangle-\left\langle a\frac{\partial a}{\partial n_{KM}}\right\rangle\right)\right]\times$$
$$\times\left\{\left[\left\langle V\frac{\partial a}{\partial n_{IJ}}\right\rangle-\langle V\rangle\left\langle\frac{\partial a}{\partial n_{IJ}}\right\rangle+\frac{\xi^2}{vk_BT}\langle a\rangle\left[\left\langle Va\frac{\partial a}{\partial n_{IJ}}\right\rangle-\langle V\rangle\left\langle a\frac{\partial a}{\partial n_{IJ}}\right\rangle\right.\right.\right.$$
$$\left.\left.\left.+\langle a\rangle\left(2\langle a\rangle\langle V\rangle\left\langle\frac{\partial a}{\partial n_{IJ}}\right\rangle-\langle Va\rangle\left\langle\frac{\partial a}{\partial n_{IJ}}\right\rangle-\langle a\rangle\left\langle V\frac{\partial a}{\partial n_{IJ}}\right\rangle\right)\right]\right\}$$

$$-\frac{\xi^2}{v^2}\langle a\rangle\left\{\left\langle\frac{\partial^2 a}{\partial n_{IJ}\partial n_{KM}}\right\rangle+\frac{\xi^2}{vk_BT}\langle a\rangle\left[\left\langle\frac{\partial a}{\partial n_{IJ}}\frac{\partial a}{n_{KM}}\right\rangle-\left\langle\frac{\partial a}{\partial n_{IJ}}\right\rangle\left\langle\frac{\partial a}{n_{KM}}\right\rangle\right]\right\}$$
$$+\frac{\xi^2}{v^2k_BT}\left\{\langle a\rangle\left\langle V\frac{\partial^2 a}{\partial n_{IJ}\partial n_{KM}}\right\rangle-\langle a\rangle\langle V\rangle\left\langle\frac{\partial^2 a}{\partial n_{IJ}\partial n_{KM}}\right\rangle\right.$$
$$+\frac{\xi^2}{vk_BT}\left[\left(\langle a\rangle^2\left\langle V\frac{\partial a}{\partial n_{IJ}}\frac{\partial a}{\partial n_{KM}}\right\rangle-\langle a^2\rangle\langle V\rangle\left\langle\frac{\partial a}{\partial n_{IJ}}\frac{\partial a}{\partial n_{KM}}\right\rangle\right)\right.$$
$$\left.\left.+\langle a\rangle^2\left(2\langle V\rangle\left\langle\frac{\partial a}{\partial n_{IJ}}\right\rangle\left\langle\frac{\partial a}{\partial n_{KM}}\right\rangle-\left\langle V\frac{\partial a}{\partial n_{IJ}}\right\rangle\left\langle\frac{\partial a}{\partial n_{KM}}\right\rangle-\left\langle\frac{\partial a}{\partial n_{IJ}}\right\rangle\left\langle V\frac{\partial a}{\partial n_{KM}}\right\rangle\right)\right]\right\}$$

An expression analogous in form to eq. (D5a) is obtained for the derivative of the free energy density with respect to $n_{JKM} = \partial^2 n_J / \partial R_K \partial R_M$.

Appendix E

If the mesogen flexibility is taken into account, in addition to those defined by eqs. (B7), some other tensors appear in the molecular expressions for the elastic constants. Their components are defined as:

$$d_{IJK} = \langle \Delta V' T_{IJK} \rangle_0 - \frac{1}{v} \left\langle \left(\int_v d\mathbf{r}\, r_I \right) \Delta V' T_{JK} \right\rangle_0 \tag{E1a}$$

$$g_{IJK} = \langle \Delta V' a T_{IJK} \rangle_0 - \frac{1}{v} \left\langle \left(\int_v d\mathbf{r}\, r_I \right) \Delta V' a T_{JK} \right\rangle_0 \tag{E1b}$$

$$\begin{aligned} d_{IJKM} = {} & \langle \Delta V' T_{IJKM} \rangle_0 + \frac{1}{v} \left\langle \left(\int_v d\mathbf{r}\, r_I r_J \right) \Delta V' T_{KM} \right\rangle_0 \\ & - \frac{1}{v} \left\langle \left(\int_v d\mathbf{r}\, r_I \right) \Delta V' T_{JKM} \right\rangle_0 - \frac{1}{v} \left\langle \left(\int_v d\mathbf{r}\, r_J \right) \Delta V' T_{IKM} \right\rangle_0 \end{aligned} \tag{E1c}$$

$$\begin{aligned} g_{IJK,LMN} = {} & \langle \Delta V' T_{IJK} T_{LMN} \rangle_0 + \frac{1}{v} \left\langle \left(\int_v d\mathbf{r}\, r_I r_L \right) \Delta V' T_{JK} T_{MN} \right\rangle_0 \\ & - \frac{1}{v} \left\langle \left(\int_v d\mathbf{r}\, r_I \right) \Delta V' T_{JK} T_{LMN} \right\rangle_0 - \frac{1}{v} \left\langle \left(\int_v d\mathbf{r}\, r_L \right) \Delta V' T_{IJK} T_{MN} \right\rangle_0 \end{aligned} \tag{E1d}$$

where the angular brackets denote orientational-conformational averages, defined by eq. (19) or eq.(22), according to whether the full torsional potential or only its minima are considered. The index 0 is used for averages performed over the orientational distribution in the undistorted nematic phase.

Appendix F

For computational purposes it is convenient to transform the volume integrals in eqs. (B7) into integrals over the molecular surface, according to the Stokes theorem [65]. For example we can write:

$$\int_v d\mathbf{r}\, r_I = \begin{cases} \int_v dS\, r_I s_K & I \neq K \\ (1/2) \int_v dS\, r_I^2 s_K & I = K \end{cases} \tag{F1a}$$

$$\int_v d\mathbf{r}\, r_I r_J = \begin{cases} \int_v dS\ r_I r_J s_K & I \neq K, I \neq K \\ (1/2) \int_v dS\, r_I^2 r_J s_K & I \neq J, I = K \text{ or } J = K \\ (1/3) \int_v dS\, r_I^3 s_K & I = J = K \end{cases} \tag{F1b}$$

So, if we introduce the tensors

$$G_{IJK} = \int_S dS\, r_I r_J s_K \tag{F2a}$$

$$G_{IJKM} = \int_S dS\, r_I r_J r_K s_M \tag{F2b}$$

the average tensor components c_{IJL} and b_{IJL} appearing in the expressions for elastic constants, and defined by eqs. (B7), can be expressed in a compact form as:

$$c_{IJL} = \langle T_{IJL} \rangle_0 - \begin{cases} \langle G_{IK} T_{JL} \rangle_0 & I \neq K \\ (1/2) \langle G_{IIK} T_{JL} \rangle_0 & I = K \end{cases} \tag{F3a}$$

$$b_{IJL} = \langle T_{IJL} \rangle_0 - \begin{cases} \langle a G_{IK} T_{JL} \rangle_0 & I \neq K \\ (1/2) \langle a G_{IIK} T_{JL} \rangle_0 & I = K \end{cases} \tag{F3b}$$

$$c_{IJLM} = \langle T_{IJLM} \rangle_0 + \begin{cases} \langle G_{IJK} T_{LM} \rangle_0 - \langle G_{IK} T_{JLM} \rangle_0 - \langle G_{JK} T_{ILM} \rangle_0 & I \neq K, J \neq K \\ (1/2) \langle G_{IIJK} T_{LM} \rangle_0 - (1/2) \langle G_{IIK} T_{JLM} \rangle_0 - \langle G_{JK} T_{ILM} \rangle_0 & I \neq J, I = K \\ (1/2) \langle G_{IIJK} T_{LM} \rangle_0 - \langle G_{IK} T_{JLM} \rangle_0 - (1/2) \langle G_{JJK} T_{ILM} \rangle_0 & I \neq J,\ J = K \\ (1/3) \langle G_{IIIK} T_{LM} \rangle_0 - \langle G_{JJK} T_{ILM} \rangle_0 & I = J = K \end{cases} \tag{F3c}$$

$$c_{IJL,KMN} = \langle T_{IJL} T_{KMN} \rangle_0 + \begin{cases} \langle G_{IJKK} T_{JL} T_{MN} \rangle_0 - \langle G_{IK} T_{JLM} \rangle_0 - \langle G_{JK} T_{ILM} \rangle_0 & I \neq K, J \neq K \\ (1/2) \langle G_{IIJK} T_{LM} \rangle_0 - (1/2) \langle G_{IIK} T_{JLM} \rangle_0 - \langle G_{JK} T_{ILM} \rangle_0 & I \neq J, I = K \\ (1/2) \langle G_{IIJK} T_{LM} \rangle_0 - \langle G_{IK} T_{JLM} \rangle - (1/2) \langle G_{JJK} T_{ILM} \rangle_0 & I \neq J,\ J = K \\ (1/3) \langle G_{IIIK} T_{LM} \rangle_0 - \langle G_{JJK} T_{ILM} \rangle_0 & I = J = K \end{cases} \tag{F3d}$$

Appendix G

The tensor components defined in Appendix B depend on the three Euler angles (α,β,γ); however, exploitation of the axial symmetry of undeformed nematic phase allows us to calculate their average values in the undeformed nematic phase, defined by eq. (13), as double integrals over the (β,γ) Euler angles. For example, we can calculate $\langle T_{XZXZ} \rangle_0$ and $\langle T_{ZXZ} T_{ZXZ} \rangle_0$ as:

$$\langle T_{XZXZ} \rangle_0 = \pi \left(\langle \langle T_{XZXZ} \rangle \rangle_0 + \langle \langle T_{YZYZ} \rangle \rangle_0 \right) \tag{G1a}$$

$$\langle T_{ZXZ} T_{ZXZ} \rangle_0 = \pi \left(\langle \langle T_{ZXZ} T_{ZXZ} \rangle \rangle_0 + \langle \langle T_{ZYZ} T_{ZYZ} \rangle \rangle_0 \right) \tag{G1b}$$

where

$$\langle \langle \cdots \rangle \rangle_0 = \int \sin\beta \, \mathrm{d}\beta \int d\gamma \cdots p_0(\beta, \gamma) \quad . \tag{G2}$$

with p_0 being the orientational partition function in undeformed nematics.

The integrals $\langle T_{XXXX} \rangle_0$, $\langle T_{XXYY} \rangle_0$ and $\langle T_{XYXY} \rangle_0$ can be obtained by solving the set of algebraic equations:

$$\begin{cases} \langle T_{XXXX} \rangle_0 + \langle T_{YYYY} \rangle_0 = \pi \left(\langle \langle T_{XXXX} \rangle \rangle_0 + \langle \langle T_{YYYY} \rangle \rangle_0 + \langle \langle T_{XXYY} \rangle \rangle_0 + \langle \langle T_{YYXX} \rangle \rangle_0 \right) \\ \langle T_{XXYY} \rangle_0 - \langle T_{YYXX} \rangle_0 = \pi \left(\langle \langle T_{XXYY} \rangle \rangle_0 + \langle \langle T_{YYXX} \rangle \rangle_0 - 2 \langle \langle T_{XYXY} \rangle \rangle_0 \right) \end{cases} \tag{G3}$$

together with eq. (B9m).

Expressions analogous to eqs. (G1a-b) or (G3) can be used for all average tensor components appearing in the expressions for the elastic constants.

References

[1] P.G. de Gennes, *The Physics of Liquid Crystals* (Clarendon, Oxford, 1974).

[2] C.W. Oseen, Trans. Faraday Soc. **29**, 883 (1933).

[3] F.C. Frank, Discuss. Faraday Soc. **25**, 19 (1958).

[4] G. Vertogen, W.H. de Jeu, *Thermotropic Liquid Crystals*: *Fundamentals* (Springer, Berlin, 1988).

[5] A. Bogi, S. Faetti, Liq. Cryst. **28**, 729 (2001).

[6] N.V. Madhusudana, R. Pratibha, Mol. Cryst. Liq. Cryst. **89**, 249 (1982).

[7] M.J. Bradshav, E.P. Raynes, J.D. Bunning, T.E. Faber, J. Phys. (France) **46**, 1513 (1985).

[8] G.-P. Chen, H. Takezoe, A. Fukuda, Liq. Cryst. **5**, 341 (1989).

[9] H.J. Coles, in *The Optics of Thermotropic Liquid Crystals*, eds. S. Elston, R. Sambles (Taylor & Francis, London, 1998).

[10] W.H. de Jeu, W.A.P. Claassen, J. Chem. Phys. **67**, 3705 (1977).

[11] M. Schadt, P.R. Gerber, Z. Naturforsch. **37a**, 165 (1982).

[12] D.-K. Yang, S.-T. Wu, *Fundamentals of Liquid Crystal Devices* (John Wiley & Sons, Chichester, 2006).

[13] M. Ravnik, M. Škarabot,2 S. Žumer, U. Tkalec, I. Poberaj, D. Babič, N. Osterman, I. Muševič, Phys. Rev. Lett. **99,** 247801 (2007).

[14] K. Takahashi, M. Ichikawa, Y. Kimura, Phys. Rev. E **77**, 020703 (2008).

[15] C. Lapointe, N. Cappallo, D. H. Reich, and R. L. Leheny, J. Appl. Phys. **97**, 10Q304 (2005).

[16] S.D. Hudson, E.L. Thomas, Phys. Rev. Lett. **62,** 1993 (1989).

[17] H. Shin, M.J. Bowick, X. Xing, Phys. Rev. Lett. **101,** 037802 (2008).

[18] A. Ferrarini, in *Continuum Solvation Models in Chemical Physics. From Theory to Applications*, eds. B. Mennucci, R. Cammi (Wiley, Chichester, 2007).

[19] J. Nehring, A. Saupe, J. Chem. Phys. ***5*4**, 337 (1971); *ibidem* **56**, 5527 (1972).

[20] J.P. Straley, Phys. Rev. A **8**, 2181 (1973).

[21] R.G. Priest, Phys. Rev. A **7,** 720 (1973).

[22] A. Poniewierski, J. Stecki, Mol. Phys. **38,** 1931 (1979).

[23] J. Stecki, A. Poniewierski, Mol. Phys. **41,** 1451 (1980).

[24] A.M. Somoza, P. Tarazona, Mol. Phys. **72**, 991 (1991).

[25] W.M. Gelbart, A. Ben Shaul, J. Chem. Phys. **77,** 916 (1982).

[26] A. Srivastava and S. Singh, J. Phys.: Condens. Matter **16**, 7169 (2004).

[27] M.P. Allen, D. Frenkel, Phys. Rev. A **37**, 1813 (1998); **42**, 3641 (1990).

[28] M.P. Allen, M.A. Warren, M.R. Wilson, A. Sauron, W. Smith, J. Chem. Phys. **105**, 2850 (1996).

[29] N.H. Puong, G. Germano, F. Schmid, J. Chem. Phys. 115, 7227 (2001).

[30] M.P. Allen, A.J. Masters, J. Mat. Chem. **11**, 2678 (2001).

[31] M.R. Wilson, Int. Rev. Phys. Chem. **24**, 421 (2005).

[32] W. Maier, A. Saupe, Z. Naturforsch. A **14A**, 882 (1959); **15A**, 287 (1960).

[33] G. Barbero, L.R. Evangelista, Phys. Rev. E **56**, 6189 (1997); L.R. Evangelista, I. Hibler, H. Mukai, Phys. Rev. E **58**, 3245 (1998).

[34] A.V. Zakharov and A. Maliniak, Eur. Phys. J. E **4**, 85 (2001).

[35] A. Ferrarini, G.J. Moro, P.L. Nordio, G.R. Luckhurst, Mol. Phys. **77**, 1 (1992).

[36] A. Rapini, M. Papoular, J. Phys. (Paris) Colloq. **30 C4**, 54 (1969).

[37] A. Ferrarini, G.R. Luckhurst, P.L. Nordio, S.J. Roskilly, J. Chem. Phys. **100**, 1460 (1994).

[38] A. Ferrarini, G.J. Moro, P.L. Nordio, Phys. Rev. E **53**, 681 (1996); A. Ferrarini, G.J. Moro, P.L. Nordio, Mol. Phys. **87**, 485 (1996).

[39] A. Ferrarini, Phys. Rev. E **64**, 021710 (2000).

[40] A.R. Leach, *Molecular Modelling: Principles and Applications* (Dorset Press, Dorchester, 2001).

[41] G. Marrucci, F. Greco, Molec. Cryst. Liq. Cryst. **206**, 17 (1991).

[42] C. Oldano, G. Barbero, Phys. Lett. **110A**, 213 (1985).

[43] S. Faetti, M. Riccardi, J. Phys. II (France) **5**, 1165 (1995).

[44] O.D. Lavrentovich, V.M. Pergamenschik, Int. J. Mod. Phys. B **9**, 2389 (1995).

[45] G.R. Luckhurst, G.W. Gray, *The Molecular Physics of Liquid Crystals* (Academic, London, 1979).

[46] S. Singh, Phys. Rep. **277**, 283 (1996).

[47] H. Yokoyama, Phys. Rev.E **55**, 2938 (1997).

[48] V.M. Pergamenschik, S. Zumer, Phys. Rev. E **59**, R2531 (1999).

[49] M.F. Sanner, J.C. Spehner, A.J. Olson, Biopolymers **38**, 305 (1996).

[50] W.H. Press, B.P. Flannery, S.A. Teukolsky, W.T. Vetterling, *Numerical Recipes* (Cambridge University Press, Cambridge, 1992).

[51] C.J. Adam, S.J. Clark, M.R. Wilson, G.J. Ackland, J. Crain, Molec. Phys. **93**, 947 (1998).

[52] M.J. Frisch et al , Gaussian 03, Revision C.02 (Gaussian Inc., Wallingford CT, 2004).

[53] D.R. Lide (Ed.), *Handbook of Chemistry and Physics* (CRC; Boca Raton, 1996).

[54] A . Ferrarini, F. Janssen, G.J. Moro, P.L. Nordio, Liq. Cryst. **26**, 201 (1999).

[55] L.G.P. Dalmolen, SJ. Picken, A.F. de Jong, W.H. de Jeu, J. Phys. (France) **46**, 1443 (1985).

[56] A.V. Zakharov, M.N. Tsvetkova, V.G. Korsakov, Phys. Sol. St. **44**, 1795 (2002).

[57] G.W. Gray, D.G. McDonnell, Mol. Cryst. Liq. Cryst. **37**, 189 (1976); G.W. Gray, D.G. McDonnell, Mol. Cryst. Liq. Cryst. Lett. **34**, 211 (1977).

[58] S.M. Todd, A. Ferrarini, G.J. Moro, Phys. Chem. Chem. Phys. **3**, 5535 (2001).

[59] P.I.C. Teixeira, V.M. Pergamenshchik, T.J. Sluckin, Mol. Phys. **80**, 1339 (1993).

[60] J. Stelzer, H.-R. Trebin, L. Longa, J. Chem. Phys. **103**, 3098 (1995); *ibidem* **107**, 1295 (1997).

[61] N.V. Tsvetkov, V.V. Zuev, I.V. Ksenofontov, V.N. Tsvetkov, Mol. Cryst. Liq. Cryst. **331**, 1901 (1999)

[62] D. Wiant, J.T. Gleeson, N. Eber, K. Fodor-Csorba, A. Jakli, T. Toth-Katona, Phys. Rev. E **72,** 041712 (2005).

[63] M. Cestari, PhD thesis (Università di Padova, 2009).

[64] Y. Singh, K. Rajesh, V.J. Menon, S. Singh, Phys. Rev. E **49**, 501 (1994); L. Longa, J. Stelzer, D. Dunmur, J. Chem. Phys. **109**, 1555 (1998); A. Kapanowski, Phys. Rev. E **77,** 052702 (2008).

[65] G.B. Arfken, H.J. Weber, *Mathematical Methods for Physicists* (Academic Press, London, 2001).

Captions to the Figures

Figure 1 Splay, twist and bending deformations of nematics.

Figure 2 Chemical structure of 4-*n*pentyl-4'-cyanobiphenyl (5CB).

Figure 3 Temperature dependence of the bulk elastic constants of 5CB, as obtained from different experiments: full simbols [7,9], open symbols [8], dashed line [6].

Figure 4 Conformers of 5CB considered for the calculations of elastic constants. The labels **P** and **M** are used for positive (~ +30°) and negative (~ -30°) biphenyl twist angles, respectively. The symbols **t** (*trans*) and **g** (*gauche*) denote the conformational state of CH_2-CH_2 bonds. Each conformer is identified by a sequence of symbols, listed in order, starting from the CH_2-CH_2 bond closer to the benzene ring.

Figure 5 Temperature dependence of the principal values of the average Saupe matrix calculated for 5CB.

Figure 6 Left: bulk elastic constants calculated for 5CB, as a function of temperature; the dashed lines show the results obtained by neglecting the change in average torsional potential from the nematic to the isotropic phase. Right: elastic ratios, from calculations (line) and from experiment (triangles [6], circles [8]).

Figure 7 Bulk elastic constants calculated for 5CB, as a function of S_{zz}^2, the square of the major eigenvalue of the average Saupe matrix. Dashed lines are introduced to highlight deviations from linearity.

Figure 8 Contribution of selected conformers to the elastic constants of 5CB. Conformer labels are reported in Figure 4. For comparison, also the values obtained after averaging over conformers are shown (dashed line).

Figure 9 Surfacelike elastic constants calculated for 5CB, as a function of temperature.

Figure 1

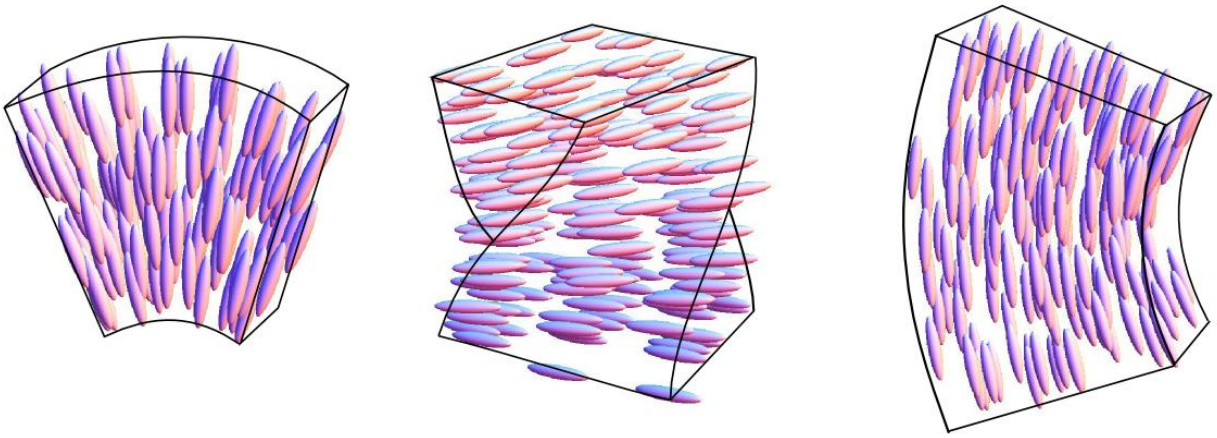

Figure 2

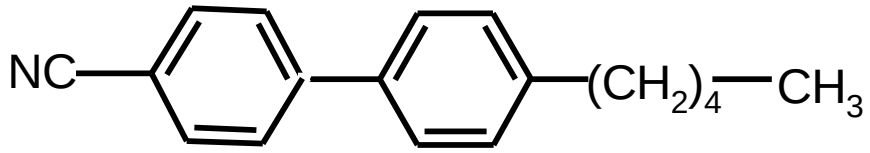

Crystal (275.5 K) Nematic (308 K) Isotropic

Figure 3

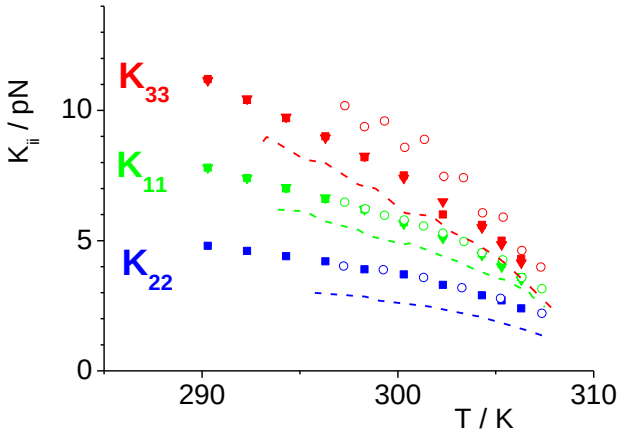

Figure 4

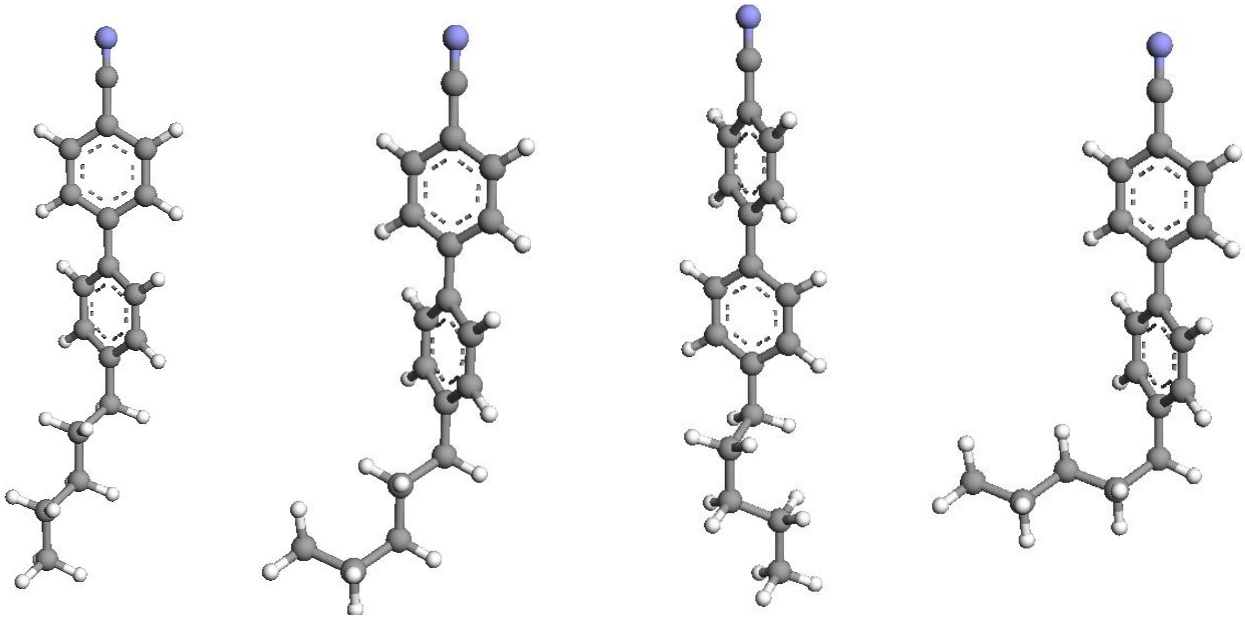

Pttt Pttg$_+$ Ptg$_+$t Pg$_+$tt

Figure 5

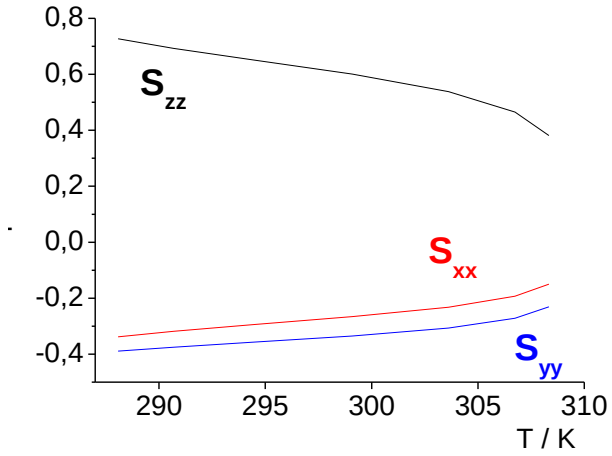

Figure 6

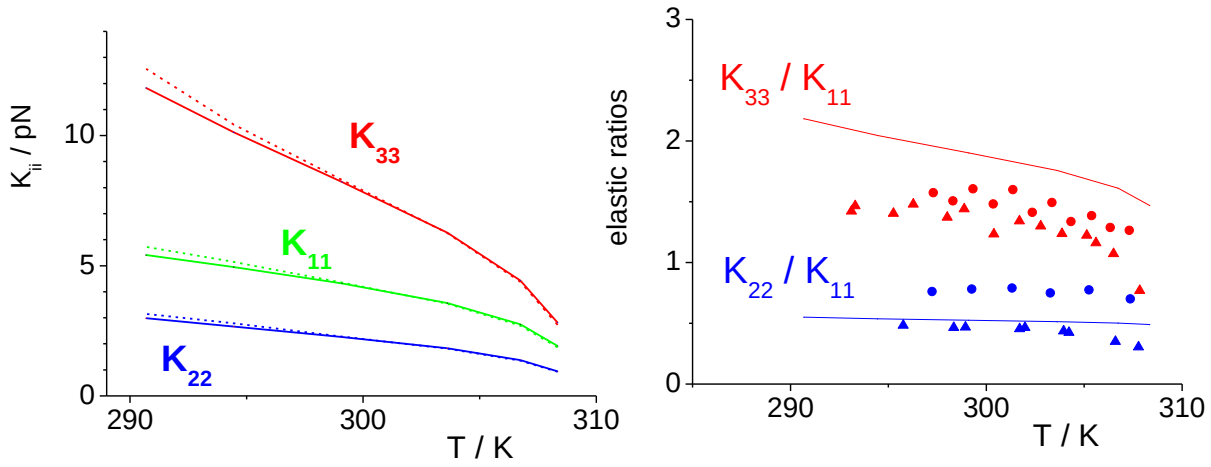
K_ii / pN
10
5
0
290
300
310
T / K
K33
K11
K22
elastic ratios
3
2
1
0
290
300
310
T / K
K33 / K11
K22 / K11

Figure 7

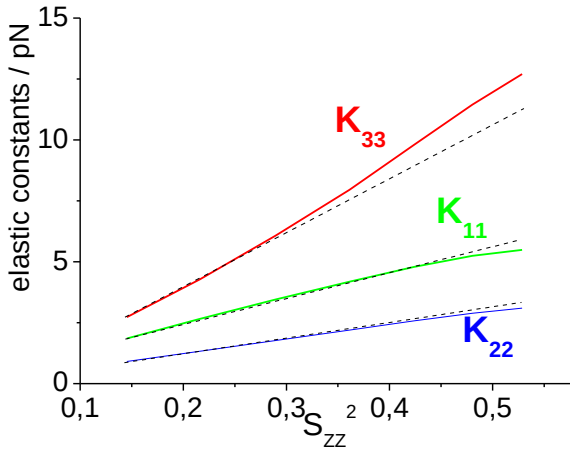

Figure 8

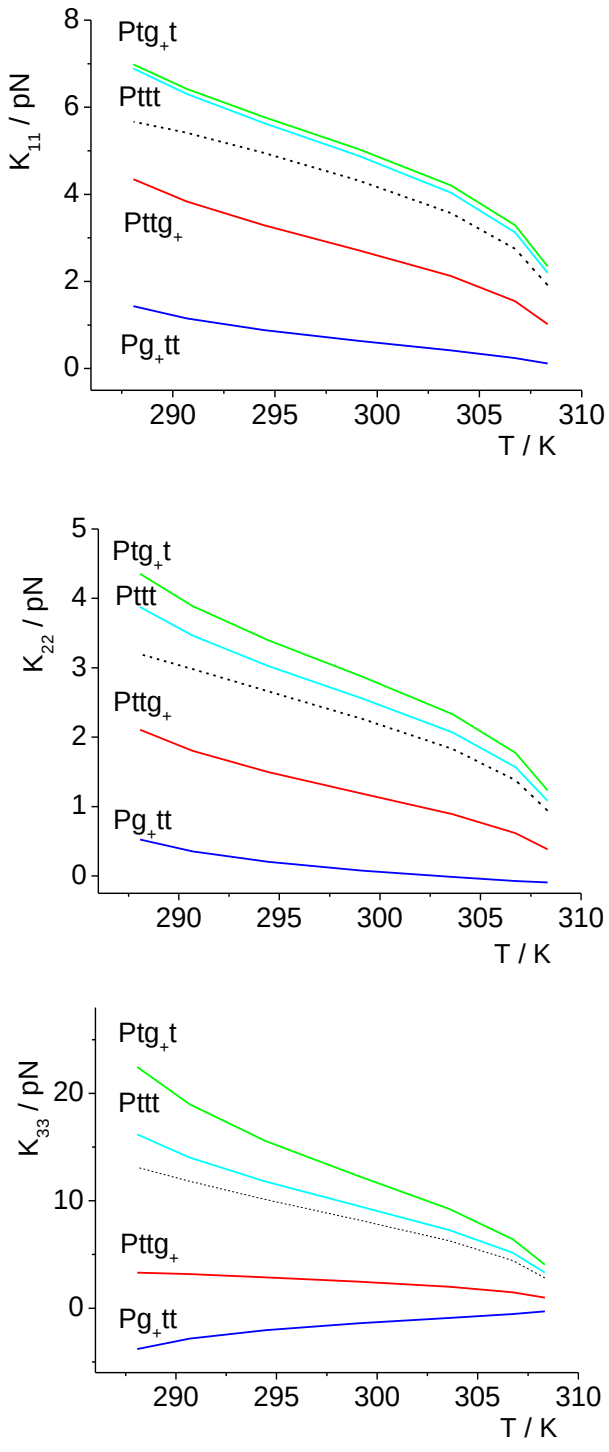
8
6
4
2
0
K11 / pN
Ptg+t
Pttt
Pttg+
Pg+tt
290
295
300
305
310
T / K
5
4
3
2
1
0
K22 / pN
Ptg+t
Pttt
Pttg+
Pg+tt
290
295
300
305
310
T / K
20
10
0
K33 / pN
Ptg+t
Pttt
Pttg+
Pg+tt
290
295
300
305
310
T / K

Figure 9

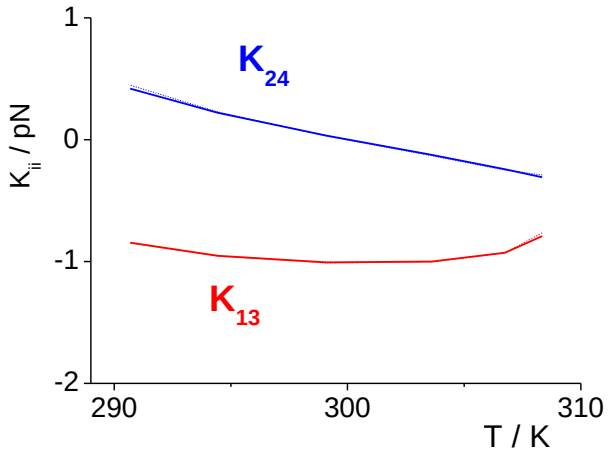

4

Computational methodology and parametrisation for selected systems

4.1 Introduction

An integrated computational procedure has been set up, for the calculation of properties of nematics starting from the molecular structure of the constituents, according to the theory presented in chapter 2 and 3. This methodology was employed to investigate the class of systems shown in Fig. 1.5. To this purpose, a preliminary analysis of selected subsystems was performed, aimed at the definition of (i) a set of transferable charges, energy and geometry parameters for the systems under investigation; (ii) a small number of molecular fragments to be used as building blocks to generate the coordinates of mesogens. An important feature of the present methodology is the account of the molecular flexibility; this is introduced either in terms of stable conformers, according to the Rotational Isomeric State (RIS) approximation [31], or by Monte Carlo sampling of the torsional angles.

This chapter begins with a summary of the results obtained from the study of selected subsystem; this is followed by the definition of the molecular fragments along with the parametrisation of angles, dihedrals, torsional energies and atomic charges. Then, the methods used to treat the conformational degrees of freedom of mesogens are presented. Finally, the computational methodology is outlined and some of its features are discussed.

4.2 Single molecule properties

Transferable geometric and energetic parameters and charges were derived from quantum mechanics (QM) calculations for selected subsystems. Unless differently stated, the DFT method was used, at the B3LYP/6-31g** level [32].

4.2.1 Torsional potentials for CBOnOCB and CBOnOFF

Torsional potentials were calculated for the twist angle between the aromatic rings, for the dihedrals of the alkyl chain and for the bonds connecting aromatic rings and alkyl chains.

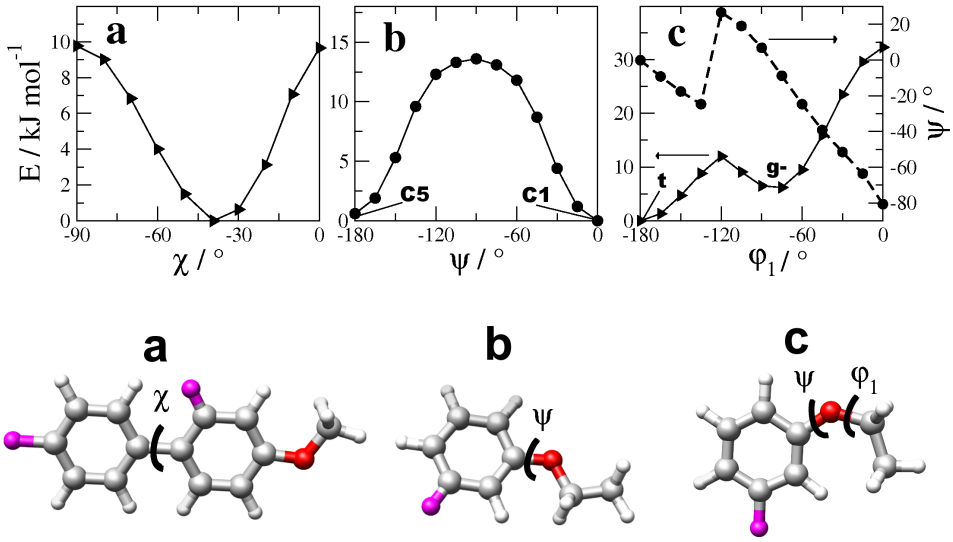

Figure 4.1: Torsional potentials, calculated at the DFT/BY3LYP/6-31g** level, for the dihedral angles indicated in the structures shown below. In each plot, the value of the potential energy at the absolute minimum is taken equal to zero; because of the local symmetry, only the potential energy over a restricted range is shown. The value of 0° corresponds to the planar geometry in case (**a**), to the O-CH_2 bond on the phenyl plane, on the same side of the F atom in (**b**), and to the CH_2-CH_3 bond on the same side of the bond between oxygen and aromatic ring in (**c**). The dashed line in (**c**) shows the values of the ψ torsional angle. In the molecular structures shown at the bottom, the colours gray, white, purple and red are used for C, H, F and O atoms, respectively.

Figure 4.1 reports the torsional profiles obtained for the angle between the phenyl rings (χ) and for rotations around the phenyl-O and O-CH_2 bonds (ψ and φ_1, respectively), in the model systems shown in the same figure. The torsional profiles were obtained by relaxed scans, i.e. at each point only the selected dihedral angle is fixed, while all the other degrees of freedom are allowed to relax.

The torsional profile for the angle between the phenyl rings in 2,4'-fluoro-4-methoxybiphenyl, reported in Figure 4.1a, has four equivalent minima, two of them at about $\pm 40°$ and the other two symmetrically located at about $\pm 140°$. These minima are separated by barriers of approximately 9 kJ/mol, at 0°, 180° and $\pm 90°$. These results are in keeping with those obtained experimentally for biphenyl by electron diffraction [33–35] and Raman spectroscopy [36]; they agree also well with those obtained for biphenyl by QM calculations at different levels [37–39]. Thus, we can infer that presence of the fluorine substituents has scarce influence on the twist angle between the aromatic rings.

Figure 4.1b shows the torsional potential calculated for the phenyl-O bond of 3-fluoro-1-ethoxybenzene. We can see the presence of two almost equivalent minima at 0° (OCH_2 on the same side of the F atom) and 180° (OCH_2 on the opposite side of the F atom); henceforth the two minima will be denoted as $c1$ and $c5$, respectively. The minima are separated by barriers of nearly 14 kJ/mol at $\pm 90°$. The torsional profile is similar to that reported in ref. [40] for 1-ethoxybenzene; this indicates that also the rotation around the phenyl-O bond is scarcely affected by the fluorine substituent in the aromatic ring.

Figure 4.1c shows the torsional potential calculated for the PhO-CH_2 bond in 1-ethoxy-3-fluorobenzene. In the same plot, for each value of the φ_1 dihedral, also the corresponding ψ value is reported. The torsional potential has the absolute minimum at 0° and two relative minima at $\pm 82°$. The latter are separated by an high energy barrier, whereas much lower barriers are found between the absolute and the relative minima. The analogy with the torsional potential for the CH_2-CH_2 bonds in hydrocarbons can be noticed [31]; however, the energy difference between the minima is significantly higher here. As for hydrocarbons, we shall denote the absolute minimum as *trans* (0°, t) and the relative minima as *gauche*$^{\pm}$ ($\pm 82°$, $g^{\pm}$), [31]. The figure shows that the φ_1 and ψ dihedrals are correlated; in all the minima ψ takes a value close to 0°. The results shown for 1-ethoxy-3-fluorobenzene are in general agreement with those obtained by calculations for 1-ethoxybenzene [40] and for 1,3-dimethoxypropane [41].

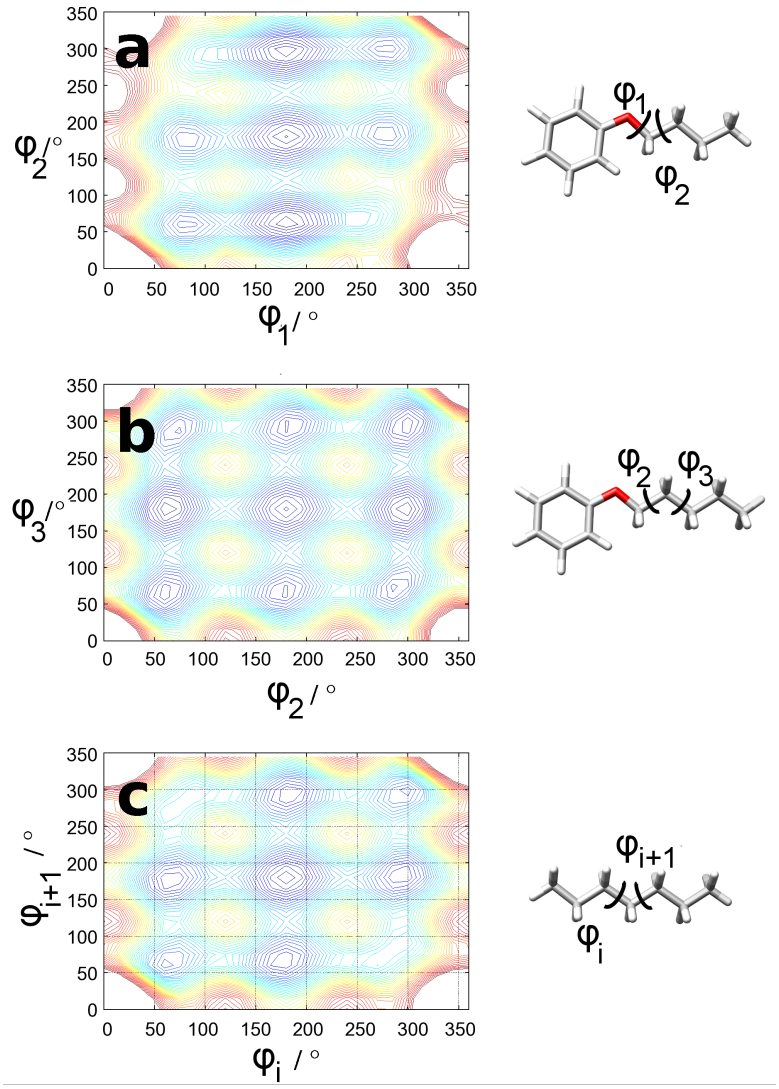

Figure 4.2: Torsional potentials calculated for pairs of adjacent dihedral angles. On the right side the rotating bonds are shown by black arrows on the molecular structures; the colours gray, white, purple and red refer to C, H, F and O atoms, respectively.

To characterise the flexibility of the spacer in the CBOnOCB and CBOnOFF systems, we have calculated the torsional potentials for the CH_2-CH_2 and the O-CH_2 bonds. To analyse also possible correlation between adjacent bonds, we have calculated potential energy surfaces as a function of pairs of dihedral angles (φ_1, φ_2), (φ_2, φ_3) and $(\varphi_i, \varphi_{i+1})$, with $3 \leq i \leq n-2$; these are shown in Figure 4.2. Again, relaxed scans were carried out. The potential energy surfaces show some common features, first of all the presence of three minima, corresponding to the *trans* (t), *gauche*$^+$ (g^+) and *gauche*$^-$ (g^-) states, for each single bond. There are also some differences between the three cases; the most relevant is probably the stabilisation of the *gauche* over the *trans* state for the O-CH_2 bond. This is in keeping with the results obtained for 1,3-dimethoxypropane [41, 42]. We can also find some differences in the position of the wells of the torsional potential between the three cases shown in Figure 4.2. The minima are located at 180° and ±66° for the CH_2-CH_2 bond (Figure 4.2c and 4.2b), at 180° and ±82° for the O-CH_2 bond (Figure 4.2a). The shift of the *gauche* minimum in the latter case is due to steric clashes between the hydrogen atoms of the first methylene group in the spacer and the aromatic ring. The value of ±66° for the dihedral in the *gauche* state of the CH_2-CH_2 bond is in agreement with that obtained by QM calculations at an analogous level (DFT/B3LYP/6-311++g**) [43].

In the potential energy surface for pairs of bonds we can find nine minima, corresponding to the states tt, tg^+, tg^-, g^+g^+, g^+t, g^+g^-, g^-g^-, g^-t, g^-g^+, with the symbols in each label indicating the state of the adjacent bonds, in their order. The all-*trans* state (tt) is the absolute minimum. For all systems, the correlations between adjacent dihedral angles become non-negligible in the g^-g^+ and g^+g^- states (the well known $g^{\pm}g^{\mp}$ effect in alkyl chains [31]): in these regions, as a consequence of steric clashes between groups at the (i, i+4) positions, the potential energy surface become significantly different from the simple combination of single bond contributions. For the cases, denoted by (a) and (b) in Figure 4.2, a single conformational minimum is found in the $g^{\pm}g^{\mp}$ states, with the dihedral values (±100°, ∓60°) in the former and (±75°, ∓75°) in the latter. For pairs of CH_2-CH_2 bonds (case (c) in Figure 4.2) two equivalent minima can be identified, with the dihedral values (±60°, ∓90°) and (±90°, ∓60°), respectively; in the following the same label, $g^{\pm}g^{\mp}$, will be used for both. The same result was found by previous QM calculations for alkyl chains [43–45].

Table 4.1: Energy increase, with respect to the all *trans* configuration, upon introduction of one or more *gauche* states. Calculations were performed for the CBO8OFF dimer; the geometry of the conformers was obtained at the DFT/B3LYP/6-31g** level. The label n indicates the number of methylene groups in the spacer. The labels g_i ($3 \leq$ i $\leq$ n-2) are used for CH2-CH2 bonds with neighbouring CH_2 groups; g_1, g_{n+1} for O-CH_2 bonds, and g_2, g_n for CH_2-CH_2 bonds with an oxygen atom on one side.

	Energy / kJ mol^{-1} (DFT/B3LYP/6-31g**)	Energy / kJ mol^{-1} (MP2/6-31g**)
single *gauche*		
g_i ($3 \leq$ i $\leq$ n-2)	3.52	2.18
g_1 , g_{n+1}	5.44	3.47
g_2 , g_n	-1.17	-2.85
pairs of adjacent *gauche*$^{\pm}$ *gauche*$^{\mp}$ and *gauche*$^{\pm}$*gauche*$^{\pm}$		
$g_i^{\pm}\ g_{i+1}^{\mp}$ ($3 \leq$ i $\leq$ n-2)	5.94	6.03
$g_2^{\pm}\ g_3^{\mp}$, $g_{n-1}^{\pm}\ g_n^{\mp}$	1.88	1.34
$g_1^{\pm}\ g_2^{\mp}$, $g_n^{\pm}\ g_{n+1}^{\mp}$	7.03	6.74
$g_i^{\pm}\ g_{i+1}^{\pm}$ ($3 \leq$ i $\leq$ n-2)	-0.08	-0.75
$g_2^{\pm}\ g_3^{\pm}$, $g_{n-1}^{\pm}\ g_n^{\pm}$	-0.42	-1.17
$g_1^{\pm}\ g_2^{\pm}$, $g_n^{\pm}\ g_{n+1}^{\pm}$	0.42	0.29
c1-c5	0.67	0.63

It has been pointed out [43,46] that DFT calculations tend to overestimate the energy increase upon introduction of *gauche* states in alkyl chains. To check this issue, for selected conformers of the system shown in Figure 4.3 we have carried out further single point energy calculations at the MP2/6-31g** level, using the same coordinates obtained from DFT geometry optimisation. The results reported in Table 4.1 confirm the previous findings: taking as reference the all-*trans* state, in all cases a lower energy increase is predicted by the MP2 calculations. The strongest effects are found for conformers with a single *gauche*; the MP2 energy difference for the CH_2-CH_2 bond (with neighbouring CH_2 groups) falls within the range of recent experimental results (0.47-0.71 kcal mol^{-1}) [47–49] and is in line with other QM calculations reported in the literature [43–46, 50]. Table 1 also shows that, in general, the energies of conformers with more than a single *gauche* are less affected by the level of the calculation. The values obtained for pairs of adjacent CH_2-CH_2 bonds (Figure 4.2c) are in agreement with those reported by Pastor and co-workers [44, 45].

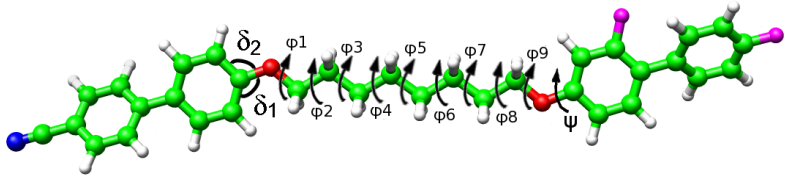

Figure 4.3: Labelling of dihedral angles in CBOnOFF dimers. The same labels are used for CBOnOCB dimers.

4.2.2 Torsional potentials for CBnCB

The only difference in the chemical structure of the CBnCB and the CBOnOCB dimers is the nature of the groups connecting aromatic rings and alkyl spacer (see Figure 1.5). The simple replacement of methylenes by oxygen atoms has a sizable effect in the shape of the dimers; in fact, the all-*trans* alkyl chain lies perpendicular to the phenyl plane in the CBnCB dimers and on the same plane of the phenyl ring in CBOnOCB dimers. Figure 4.4 shows the torsional potentials calculated for the Ph-CH_2 and PhCH_2-CH_2 bonds in the model systems which are also shown in the figure.

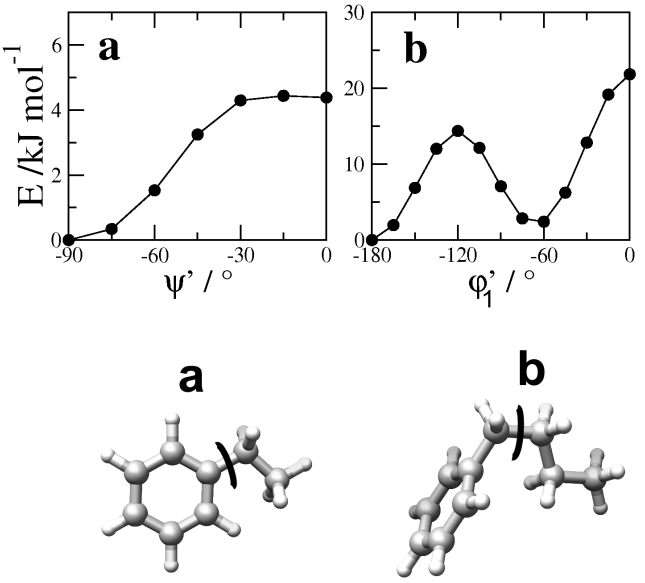

Figure 4.4: Torsional potentials calculated at the DFT/BY3LYP/6-31g** level for the dihedral angles indicated in the structures shown below. In each plot, the value of the potential energy at the absolute minimum is taken equal to zero; because of the local symmetry, only the potential energy over a restricted range is shown. The value of 0° corresponds to the CH_2-CH_3 bond in the phenyl plane in (**a**); to the CH_2-CH_2 bond in the same plane and on the same side of the phenyl-CH_2 bond in case (**b**). In the molecular structures shown at the bottom, the colours gray and white are used for C and H atoms, respectively.

The torsional potential for the Ph-CH_2 bond (in figure denoted by ψ') has two minima, as the torsional potential of the Ph-O bond, reported in Figure 4.1. However the two profiles differ in the position of the minima, which are located at $\pm 90°$ in the former case and at 0°, 180° in the latter. Moreover, the height of the barriers for the Ph-CH_2 bond is about one third of that for the Ph-O bond. This means that the rotation is much less hindered in the former case, and we will show in the following that this can be important for modelling of the systems under investigation. Figure 4.4b reports the torsional potential for the first CH_2-CH_2 bond of an alkyl chain attached to a benzene ring; this is very similar to the torsional profile for the central bond of butane.

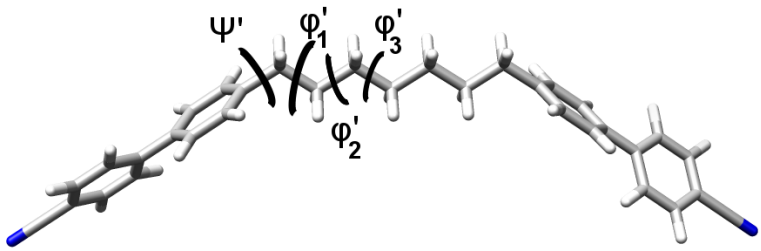

Figure 4.5: Labelling of dihedral angles in CBnCB dimers.

4.2.3 Bond angles

Because of their effects on the overall geometry, the bond angles in the spacer can be particularly important for the LC behaviour of the dimers under investigation [51]. We have obtained values of 119°, 107° and 113° for the $C_{ar}OC$, OCC and CCC bond angles, respectively, in keeping with the available X-ray data for CBO8OCB [52]. Moreover, our calculations have shown that the two $C_{ar}C_{ar}O$ bond angles of a given aromatic ring are different: the values 125° and 115° have been obtained for the angles denoted in Figure 4.3 as δ_1 and δ_2, respectively. This difference, due to steric clash between spatially close hydrogen atoms belonging to the chain and to the ring, is in very good agreement with X-ray data for CBO8OCB [52] and electron diffraction results for anisole [35]. For the CB7CB system, the values 125° and 113° have been obtained for $C_{ar}C_{ar}C$ and CCC bond angles, respectively.

Table 4.2: Dipole moments calculated at the DFT/B3LYP/6-31g** level for selected LC monomers and dimers. For monomers the dipole shows a scarce dependence on conformation; the reported values have been obtained for the all-*trans* chain. For dimers, the sequence of labels indicates in order the state of subsequent rotating bonds; so, e.g. the sequence $c1tg^+g^-g^+tt$ represents the conformer of CBO5OFF having the ψ angle in the $c1$ state, the next φ_1 bond in the *trans* state, and so on.

Monomers					
molecule		μ/D			
5OCB - $c1$		7.04 (exp. 4.9 [53])			
5OFF - $c1$		3.39			
5OFF - $c5$		3.97			
Dimers					
CBO8OCB		**CBO8OFF**			
conformer	μ/D	conformer	μ/D	conformer	μ/D
$ttttttttt$	0.29	$c1ttttttttt$	3.72	$c5ttttttttt$	3.76
$g^+tttttttt$	6.34	$c1g^+tttttttt$	5.84	$c5g^+tttttttt$	4.71
$tg^+tttttttt$	4.78	$c1tg^+tttttttt$	4.83	$c5tg^+tttttttt$	6.22
$ttg^+ttttttt$	7.04	$c1ttg^+ttttttt$	6.44	$c5ttg^+ttttttt$	4.88
$tttg^+ttttt$	4.32	$c1tttg^+ttttt$	4.46	$c5tttg^+ttttt$	5.88
$ttttg^+tttt$	7.15	$c1ttttg^+tttt$	6.47	$c5ttttg^+tttt$	5.45
		$c1tttttg^+ttt$	4.42	$c5tttttg^+ttt$	6.26
		$c1ttttttg^+tt$	6.49	$c5ttttttg^+tt$	5.07
		$c1tttttttg^+t$	4.50	$c5tttttttg^+t$	6.00
		$c1ttttttttg^+$	6.03	$c5ttttttttg^+$	4.77

4.2.4 Atomic charges

The accuracy of the predicted of dielectric and flexoelectric properties of LCs also depends on the use of reliable atomic charges. The dipole moments calculated for mesogens using the sets of charges available in common force fields are generally far from the experimental values; for instance, the atomic charges from the OPLS force field yield a net dipole moment of 3.35 D for the 5OCB mesogen, to be compared with an experimental value of 4.9 D [53]. For these reasons, in atomistic Molecular Dynamics simulations of LCs, atomic charges obtained from ab initio calculations are generally used [54–56].

We have calculated atomic charges for some conformers of our dimers and of the corresponding monomers, using the Merz-Kollman-Singh scheme [57, 58], as implemented in the Gaussian03 suite of programs [32]. Charges estimated at the DFT/B3LYP/6-31g** level were compared with those obtained with different choices of the basis set; only small effects were found, in agreement with the results reported for water [59].

Table 4.2 shows the dipole moments calculated at the DFT/B3LYP/6-31g** level for a few systems. We can see that the change in molecular structure, from nOCB to nOFF, yields a strong reduction of the net dipole moment of monomers; on the contrary, rotations around the phenyl-O bond or around chain bonds have only a small effect on the dipole. Comparison with the measured value, which is available for 5OCB [53], shows that the calculated dipole is overestimated; analogous discrepancies between calculated and measured dipoles are generally found. However, slightly too high effective dipoles can be suitable for calculations in which the molecular polarizability is neglected.

As a consequence of the change of the angle between the mesogenic groups, which bear the largest charges, the dipole moment of dimers is strongly affected by the introduction of *gauche* states in the spacer. The results reported in Table 4.2, show that a shift in position of a single *gauche* state in the CBO8OCB molecule can yield a variation of about 2 D in the the overall dipole moment. The same decrease is shown by the CBO8OFF dimer, whose dipole is also affected by a rotation of 180° around the Ph-O bond (states denoted as $c1$ and $c5$, see Figure 4.1).

4.3 Definition of transferable fragments

The information on geometry and charges, obtained from single molecule calculations, was exploited for the definition of transferable fragments, to be used as building blocks for generating conformers of the LC monomers and dimers under investigations. The molecular fragments are shown in Figure 4.6. Bond lengths and bond angles were assigned the values obtained by geometry optimisation, as reported previously. Each fragment is characterised by a set of atomic charges, which are also shown in Figure 4.6, and is globally neutral.

The definition of the charges of a fragment require some care. The first reason is the uncertainty affecting charges obtained according to the MKS scheme [57, 58]. We performed calculations for the *trans* conformer and for all the conformers with a single *gauche* in the chain for CBO8OFF and CB8CB. For different conformers of a given compound, slightly different charges were obtained. The charges of the biphenyl fragments were then obtained by averaging over all the conformers. Such charges were then slightly adjusted, to comply with symmetry requirements, if any, and to guarantee electroneutrality of the fragment. This was done by uniformly distributing the small net charge of the original set, of the order of 0.001 e, over all the atoms in the fragment. Due to non-equivalence of atomic charges obtained when the ψ bond is in the $c1$ or in the $c5$ state, two kinds of fragments are defined for the FFO moiety; both are shown in Figure 4.6. Table 4.3 shows that they have a non-negligible difference in the total dipole moment, which in both cases is lower than the value calculated for the CBO fragment.

Table 4.3: Values of the dipole moment of the fragments shown in Figure 4.6.

	FFO - $c1$	**FFO - $c5$**	**CBO**	**CB**
μ / D	3.05	4.03	6.55	5.34

The MKS charges on the carbon and hydrogen atoms in the flexible spacer exhibit fluctuate about values, which anyway are small; for instance, the partial charges on alkyl carbons can range from 0.12 e to 0. To check the sensitivity of LC properties to the value of these charges, we calculated the flexoelectric coefficients of some conformers of CBO5OFF with two different sets of charges for the C and H atoms of the methylene

groups: (0.00 e / 0.00 e) and (-0.6 e/ 0.3 e). We verified that the flexoelectric coefficients were scarcely affected by these charges; therefore we have assigned to C and H the value -0.12 e / +0.06 e in methylene and -0.18 e / +0.06 e in methyl. These are the same charges assumed for the C and H atoms of methylene and methyl groups in the OPLSA force field [60].

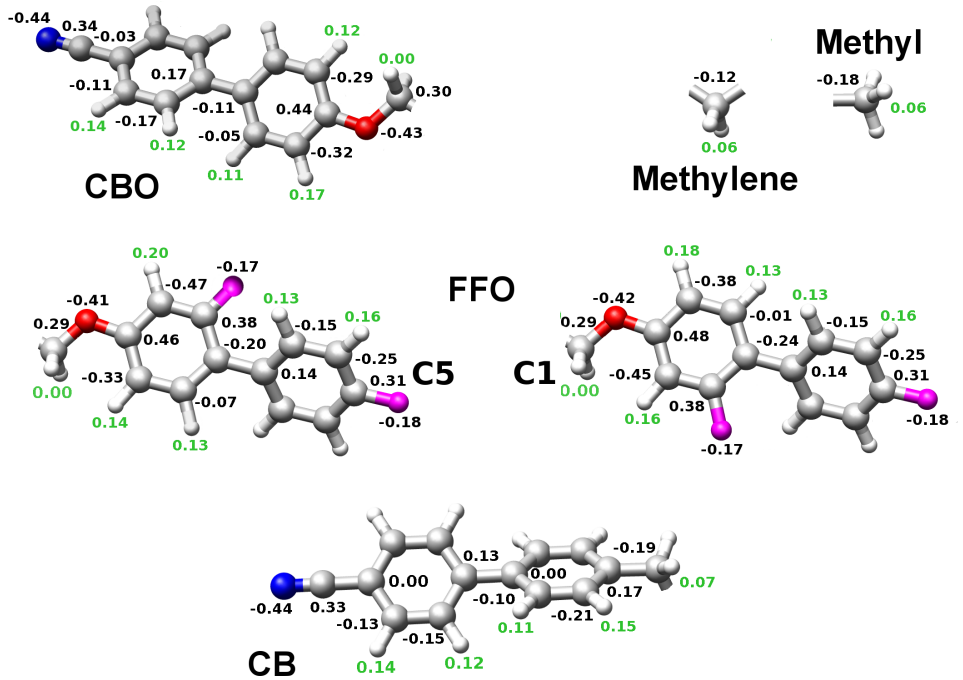

Figure 4.6: Definition of the molecular fragments used to build conformers of monomers and dimers, with their atomic charges. The colours blue, gray, white, purple and red refer to N, C, H, F and O atoms, respectively.

4.4 Rotational Isomeric State approximation (RIS)

The analysis of torsional potentials has shown that in most cases well-defined energy minima are present, separated from each other by energy barriers higher than a few k_BT units at 300-400 K. Under these conditions, fluctuations around the torsional minima can be neglected and the system can be described in terms of a finite number of conformers,

with geometry corresponding to the minima of the torsional potential.

Any arbitrary conformer is identified by a label given by a sequence of symbols, indicating in order the state of subsequent rotating bonds; so, e.g. the sequence $c1tg^+g^-g^+tt$ represents the conformer of CBO5OFF having the ψ dihedral angle in the $c1$ state, the next φ_1 bond in the *trans* state, and so on. This is the so called Rotational Isomeric State (RIS) approximation [31]. In the following, the parameters characterising geometry and energy of the RIS conformers are summarised.

4.4.1 Geometry

Table 4.4 shows the values of the torsional angles used to define the RIS conformers; these were obtained from the analysis of the torsional potentials presented at the beginning of this chapter. Because of the non-negligible geometry effects, special care must be paid in the presence of adjacent g^+g^- pairs. For the $g_i^{\pm}g_{i+1}^{\mp}$ pairs ($3 \leq i \leq n$-2), both conformations with dihedral angles ($\pm 66°$,$\mp 90°$) and ($\pm 90°$,$\mp 66°$) (labelled by "A" and "B", respectively, in Table 4.4) must be considered. For the $g_1^{\pm}g_2^{\mp}$ and $g_{n-i}^{\pm}g_n^{\mp}$ pairs in CBOnOCB or CBOnOFF, the dihedral angle of the adjacent ψ angle was taken equal to 10°. Analogously, when the φ_1' torsional angle is in the *gauche*+ or *gauche*- states in CBnCB, ψ' must be changed to 75° or to 105°, respectively.

4.4.2 Energy

According to the RIS approximation [31], the torsional energy of the j-*th* conformer, E_j, can be approximated as:

$$E_j = \sum^{N_g} E_{tg_i} \tag{4.1}$$

where N_g is the total number of *gauche* states in the alkyl chain and E_{tg_i} is the *gauche-trans* energy difference at the i chain position.

To improve this approximation of the potential energy, two terms are added to Eq. 4.1: $E_{g^{\pm}g^{\mp}}$, accounting for the so-called pentane effect, and $E_{g^{\pm}g^{\pm}}$ [44, 45]. Hence, Eq. 4.1 reads:

$$E_j = \sum^{N_g} E_{tg_i} + \sum^{N_{g^{\pm}g^{\mp}}} E_{g_i^{\pm}g_{i+1}^{\mp}} + \sum^{N_{g^{\pm}g^{\pm}}} E_{g_i^{\pm}g_{i+1}^{\pm}} \tag{4.2}$$

where, again, the index i indicates the position in the spacer chain of a single *gauche*

Table 4.4: Values of the torsional angles used in the RIS model for the flexible spacer linking the biphenyl groups in dimers. The label n indicates the number of methylene groups in the chain. The labels i and $i+1$ indicate the bond position in the chain, as shown in Figure 4.3 for CBOnOFF and CBOnOCB and in Figure 4.5 for CBnCB.

CBOnOCB and CBOnOFF		
	$\varphi_i/^\circ$	
t_i	180	
single *gauche*		
g_1 , g_{n+1}	± 82	
g_i ($2 \leq$ i $\leq$ n)	± 66	
pairs of adjacent *gauche*$^\pm$ *gauche*$^\mp$	$\varphi_i/^\circ$	$\varphi_{i+1}/^\circ$
$g_1^\pm\ g_2^\mp$	$\pm$ 108	$\mp$ 66 ($\psi = 10$)*
$g_{n-1}^\pm\ g_n^\mp$	$\pm$ 66	$\mp$ 108 ($\psi = 10$)*
$g_2^\pm\ g_3^\mp$	$\pm$ 75	$\mp$ 75
$g_{n-2}^\pm\ g_{n-1}^\mp$	$\pm$ 75	$\mp$ 75
$g_i^\pm\ g_{i+1}^\pm$ (A), ($3 \leq$ i $\leq$ n-2)	$\pm$ 66	$\mp$ 90
$g_i^\pm\ g_{i+1}^\mp$ (B), ($3 \leq$ i $\leq$ n-2)	$\pm$ 90	$\mp$ 66

CBnCB		
	$\varphi_i/^\circ$	
t_i	180	
single *gauche*		
g_1 , g_{n-1}	66 ($\psi' = 75$), -66 ($\psi' = 105$)*	
g_i ($2 \leq$ i $\leq$ n-2)	± 66	
pairs of adjacent *gauche*$^\pm$ *gauche*$^\mp$	$\varphi_i/^\circ$	$\varphi_{i+1}/^\circ$
$g_1^\pm\ g_2^\mp$	$\pm$ 75	$\mp$ 75 ($\psi' = 90 \mp 15$)*
$g_{n-2}^\pm\ g_{n-1}^\mp$	$\pm$ 75	$\mp$ 75 ($\psi' = 90 \mp 15$)*
$g_i^\pm\ g_{i+1}^\pm$ (A), ($2 \leq$ i $\leq$ n-3)	$\pm$ 66	$\mp$ 90
$g_i^\pm\ g_{i+1}^\mp$ (B), ($2 \leq$ i $\leq$ n-3)	$\pm$ 90	$\mp$ 66

* in brackets the value of the adjacent ψ or ψ' is reported.

state and of pairs of adjacent *gauche*, $g^{\pm}g^{\mp}$ and $g^{\pm}g^{\pm}$. The symbols $N_{g^{\pm}g^{\mp}}$ and $N_{g^{\pm}g^{\pm}}$ indicate the numbers of adjacent *gauche* states present in the chain.

The energetic parameters E_{tg_i}, $E_{g_i^{\pm}g_{i+1}^{\mp}}$ and $E_{g_i^{\pm}g_{i+1}^{\pm}}$ employed in our calculations are collected in Table 4.1. They are obtained by averaging the QM energies of conformers of CBO8OFF, differing for the position of the *gauche* states in the spacer. For example, the value E_{tg_i} was obtained by averaging the energies of the conformers $c1g^{+}ttttttt$, $c1tg^{+}ttttttt$, $c1ttg^{+}ttttttt$, and so on. The other parameters were estimated in analogous way.

In the calculation of LC properties, the molecular flexibility is taken into account by averages over molecular conformations, expressed in the form of Eq. 2.21. The potential energy defined by Eq. 4.2 is then used to calculate the statistical weight w_j. In the presence of $g_i^{\pm}g_{i+1}^{\mp}$ pairs ($3 \leq i \leq n$-2), a factor equal to 1/2 is introduced, to take into account the splitting of the minima in the torsional potential (see Figure 4.2c).

4.4.3 The cut-off distance

According to the RIS approximation, every φ or φ' dihedral angle in the alkyl spacer can exist in one of the three states: *trans*, and *gauche*$^{\pm}$, whereas two states are assumed for the ψ and ψ' dihedrals, as the large barrier reported in Figure 4.1b suggests.

In our calculations, only conformers with a maximum number of five *gauche* states in the flexible chain were retained. This can be justified on the basis of the energy increase associated with the introduction of *gauche* states.

The number of conformers is further reduced by eliminating those with atom clashes or with pair of atoms closer than a cut-off distance. A reasonable guess of this distance for a pair of atoms i and j could be the sum of their van der Waals radii, however since the RIS approximation for its nature is not sufficiently flexible, this is not a good choice. The number of accepted conformers varies as a function of the cut-off distance, which can be expressed as d=x(ri+rj) where ri and rj are the van der Waals radii of the atoms i and j, and x is a parameter ranging from 0 to 1. The plots in Figure 4.7 show the number of accepted conformers versus the parameter x for CBO5OCB and CB7CB. As the value of x increases, the number of accepted conformers decreases, and only the all-*trans* conformer is retained when x is larger than 0.92 for the CBO5OCB dimer.

The plots in Figure 4.7 suggest the presence of some common patterns. Considering

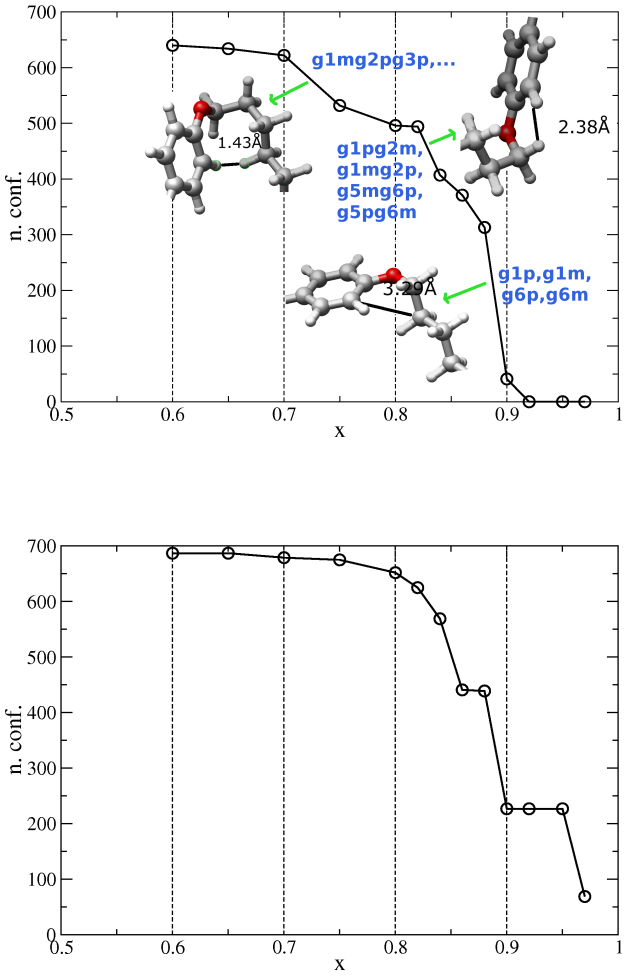

Figure 4.7: Number of accepted conformers as a function of the parameter x (see text) for CBO5OCB (top) and for CB7CB (bottom).

CBO5OCB for example, in the range between x= 0.88 and x= 0.90 about 250 conformers are excluded and all of them are characterised by the φ_1 angle in a $g^{\pm}$ state. After having checked the stability of molecular geometries by DFT/B3LYP/6-31g** optimisations, we have taken x= 0.82 for CBOnOCB and CBOnOFF dimers, and x= 0.80 for CBnCB dimers.

4.5 Monte Carlo sampling of conformations

When the energy barriers between the conformational minima are not much higher than k_BT, the torsional probability is broadly distributed around the minima and fluctuations cannot be neglected. Under these conditions, the system can no longer be described in terms of conformers, with geometry corresponding to the minima of the torsional potential. This means that statistical averages must be calculated as integrals over the full distribution function, as in Eq. 2.25. We have used Monte Carlo sampling of the conformational space to calculate this kind of integrals.

In the following sections the implementation of the MC sampling procedure is briefly exposed.

4.5.1 Scheme of the Monte Carlo sampling procedure

The Metropolis algorithm [61] has been used to sample the canonical distribution of torsional angles. Each step of the Monte Carlo procedure is constituted by:

1. generation of a trial molecular conformation;
2. check of atom distances with the method described in Sec. 4.4.3; if no atom clashes are present:
   (a) calculation of the torsional potential energy for the new conformation;
   (b) acceptance of the new conformation according to the Metropolis criterion;

At each step, a new conformation is generated, changing a random number of torsional angles of torsional angles, by a random angles within the interval $[-\delta, +\delta]$. The efficiency of the sampling is improved by introducing jumps of $\pm 120^\circ$ with frequency F [62, 63].

The parameters δ and F are chosen to guarantee a Metropolis acceptance around 50% (we have used $F = 0.20$ and $\delta = 30°$).

The same procedure (see Sec. 4.4.3) to avoid atom clashes has been adopted in the MC procedure. Here, for pair of atoms closer than the cut-off distance we have an infinite potential, thus for the Metropolis criterion the conformer is not accepted.

Fitting of the QM torsional potentials

The torsional potentials used in the MC calculations were obtained by fitting the torsional profiles obtained at DFT/B3LYP/6-31g** level. Neglecting correlations, independent single bond torsional potentials have been assumed. For CBOnOCB dimers we fit the torsional potentials denoted as ψ, φ_1 and φ_2 in Figures 4.1 and 4.3. For the CB7CB dimer we fit the torsional potentials for the angles involving the aromatic carbon, denoted by ψ' and φ'_1 in Figure 4.4. The following form was used to fit the QM torsional potential for an arbitrary (θ) dihedral

$$E_{\text{tors}}(\theta) = V_0 + \sum_j \frac{V_j}{2} \left[1 + \cos\left(j\theta + \gamma_j\right)\right] \tag{4.3}$$

where the integer j and the phase γ_j are fixed, whereas the coefficients V_j are fitting parameters. These were obtained by non-linear fitting, using the LevenbergMarquardt algorithm as implemented in the GRACE program [64]. By suitable choice of the γ_j values this expression becomes the same employed for the torsional parameters of the OPLSA [60] and AMBER [65] force fields. Analogous expressions were used in recent papers by Wilson and coworkers [66] and Cacelli *et al* [67] to interpolate QM potential energy curves obtained for 1,2-dimethoxyethane and 5CB, respectively.

Figure 4.8 shows the fitting curves obtained in this way; the corresponding V_j and γ_j parameters are collected in Table 4.5.

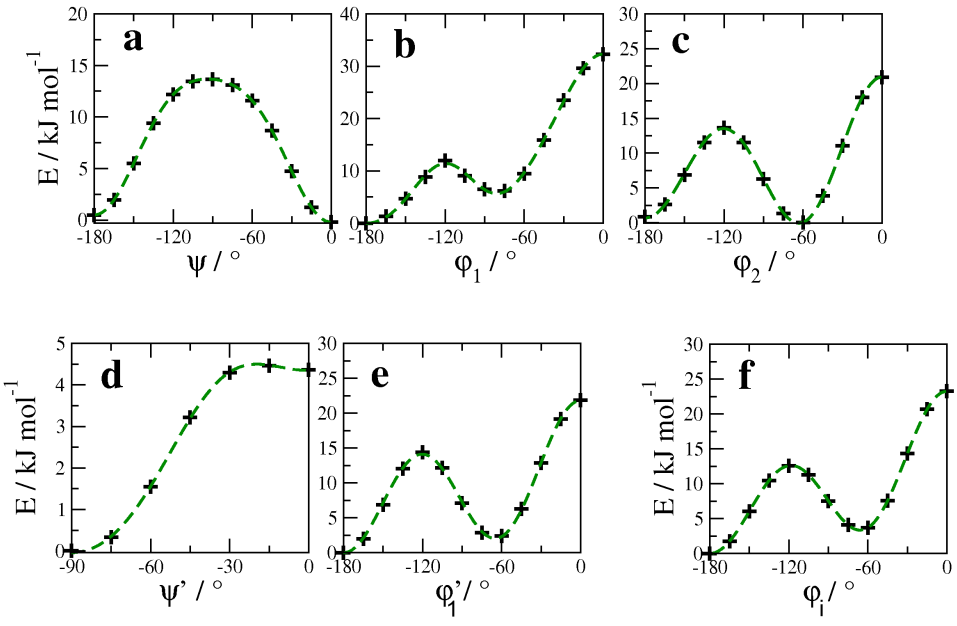

Figure 4.8: Fitting curves (green dashed lines) of the QM torsional potentials (+). Plots (**a**, **b**, **c**) refer to the ψ, φ_1 and φ_2 torsional angles of the CBOnOCB systems (see Figures 4.1 and 4.3); (**d**, **e**) refer to the ψ' and φ' angles (see Figure 4.5) of the CBnCB system. φ_i in plot (**f**) represents the torsional angle for an arbitrary C-C bond of an alkyl chain (see text).

Table 4.5: Parameters V_j and γ_j, used to calculate the torsional potentials shown in Figure 4.8 according to Eq. 4.3.

	CBOnOCB					
V_j	$\gamma_j/°$	ψ / kJ mol^{-1}	$\gamma/°$	φ_1 / kJ mol^{-1}	$\gamma/°$	φ_2 / kJ mol^{-1}
V_0	-	0.50	-	-	-	0.68
V_1	0	-0.88	0	20.96	0	4.53
V_2	180	13.51	180	-8.80	180	-4.49
V_3	0	0.18	0	11.93	0	15.73
V_4	180	2.13	180	1.30	180	-0.87
V_5			0	-0.59		
V_6			180	-0.95		
	CB7CB				**chain**	
V_n	$\gamma/°$	ψ' / kJ mol^{-1}	$\gamma/°$	φ_1' / kJ mol^{-1}	$\gamma/°$	φ_i / kJ mol^{-1}
V_0	-	1.00	-	-	-	-
V_1	-	-	0	6.66	0	9.57
V_2	0	4.76	180	-3.64	180	-4.08
V_3	-	-	0	15.15	0	13.68
V_4	0	-1.04	180	0.04	180	-0.56
V_5	-	-				
V_6	0	-0.37				

4.6 Computational scheme

The computational procedure for the calculation of LC properties, starting from the molecular structure, accomplishes four main tasks:

- (i) generation of molecular structures as assembly of molecular fragments;
- (ii) generation of molecular surface for each molecular conformation;
- (iii) calculation of the contribution of each molecular conformation to the orientational-conformational partition function and to average LC properties;
- (iii) calculation of average LC properties, by summing over all conformations.

All these points are carried out using third-party software (the MSMS code [68] for generating Connolly molecular surfaces) home-made Fortran codes for the calculation of LC properties and two Python scripts, the first (PSI) for with I/O file generation, and the second (PSII) for data analysis. A cartoon of the computational scheme is sketched in Figure 4.9.

From a *pdb* file containing the starting atomic coordinates of a molecule, the PSI script generates different conformations and saves the corresponding coordinates in single *pdb* files. In our calculations, the all-*trans* conformation, as obtained by geometry optimisation at the DFT/B3LYP/6-31g** level, was taken as the starting molecular structure. Molecular conformations are then generated according to the RIS approximation, or by Monte Carlo-Metropolis sampling of the torsional angle distribution, as discussed in in Sections 4.4 and 4.5. The coordinates of each conformation are saved in a *pdb* file; then the input files for MSMS are prepared and the molecular surfaces are generated. Then, a main Fortran Code for the calculation of LC properties is run and the output files are archived. The computation time scales linearly with the number of conformers; typically the calculation of a whole temperature dependence for a given conformer takes about 100 seconds of CPU time on a PentiumIV 2Ghz desktop computer.

The PSII script analyses the output files and collects the useful data exploiting the powerful regular expressions libraries provided by Python. Then the data analysis is performed, making use of the Numerical Python (NumPy) module.

An important feature of this procedure is its flexibility. A change of the molecular system just requires the modification of the first *pdb* file, that originates all the subsequent

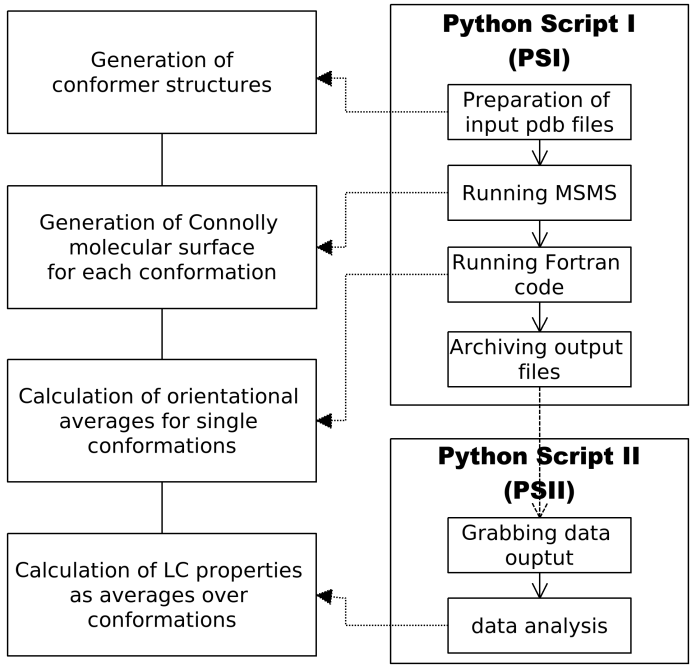

Figure 4.9: Scheme of the computational methodology set up in this study.

molecular conformations. Calculation of different LC properties can be easily introduced, by changing the Fortran code and, accordingly, the analysis program (PSII). The separation of simulation and analysis in two distinct Python scripts, PSI and PSII respectively, allows to perform a preliminary analysis of the results while the calculations are running. The use of Python and Fortran languages has the clear advantage of exploiting the peculiar features of both, i.e. flexibility and high performance calculation. The procedure relies on Fortran codes for the parts involving intensive computation and on high level Python scripting to control the whole scheme. By virtue of the clean syntax and the high modularity, Python allows fast code development. It is particularly recommended when gluing different applications is required [69], that is when the central tasks are running programs, grabbing output data and directing them to other programs, as in our case [69].

4.7 Molecular surface

To calculate the integrals over the molecular surface, Eqs. 2.2, 2.17, 2.18, a numerical description of this surface in terms of position vectors $\mathbf{r}$, surface elements dS and surface normal vectors $\mathbf{s}$ is required.

The definition of molecular surface is not unique; one of the most popular is the surface obtained as the contour of the volume not accessible to solvent molecules. This solvent-excluded surface (SES) is generated by rolling a probe sphere, representative of an external group of atoms, over the surface constituted by van der Waals spheres centered at the atomic positions.

In our computational procedure, molecular surfaces are generated with the program MSMS v2.5 [68]. This uses triangulation of the surface, once the positions and the van der Waals radii of the atoms, the radius of the probe sphere, and density of the vertices are provided. We take the radius of the probe sphere equal to 3 Å, [70] the density of vertices equal to 5 vertices/Å^2; standard values are employed for the van der Waals radii [71]: 1.5 Å for O and N, 1.85 Å for C and 1.0 Å for H atoms.

5

Results

Elastic constants of typical mesogens

5.1 Introduction

In this chapter the elastic behaviour of three typical liquid crystals mesogens (PAA, 5CB, 8CB) is investigated, using the molecular field theory presented in Chapter 3. Application to standard systems, for which many experimental data are available, allows us to assess the quality of the theoretical predictions.

The study of the elasticity of PAA, 5CB and 8CB is presented in the form of a paper, which has been submitted for publication.

Curvature elasticity of nematic liquid crystals: simply a matter of molecular shape ? Insigths from atomistic modeling

Mirko Cestari and Alberta Ferrarini *

Dipartimento di Scienze Chimiche, Università di Padova
via Marzolo 1, 35131 Padova, Italy

Corresponding author: alberta.ferrarini@unipd.it

Summary

The elastic moduli of low molar mass thermotropic liquid crystals (LCs) exhibit an intriguing dependence on the molecular structure of the constituents, which can be very important for applications. We have recently developed a molecular field theory, wherein the elastic constants of nematics are expressed in terms of the anisometry of the molecular surface. This theory, combined with molecular geometry optimization, allows us to connect mesoscale deformations in liquid crystals to atomic scale details. Here we investigate typical mesogenic systems, *i.e.* *para*-azoxyanisole (PAA) and 4-*n*-alkyl,-4'-cyanobiphenyls (*n*CBs), whose elastic properties exhibit clear differences. We show that these can be traced back to the differences in molecular shape. Our calculations also highlight the importance of the flexibility of mesogens, which was generally ignored by previous theories: in view of their different shape, conformers are shown to give different contributions to the elastic constants. The key role of deviations from a rod-like shape, which is generally assumed by models of mesogens, emerges from our calculations. The bend elastic constant is shown to be particularly sensitive; for a given compound, rod-like conformers give a high contribution to the bending stiffness, whereas the contribution of bent conformers is low or even negative. The possible implications of these findings are discussed, with special reference to the behavior of bent-core mesogens. Finally, we predict the temperature dependence of the surfacelike elastic constants, whose experimental determination is still controversial; we find that these are generally smaller than the bulk moduli and even more sensitive to changes in molecular shape.

Introduction

Liquid crystals (LCs) are anisotropic, as a consequence of the anisotropy in the orientational distribution of molecules. The average molecular orientation is specified by the unit vector **n**, denoted as the *director*. Restoring forces oppose distortions of the director; this property plays an essential role in most, if not all, LC applications.[1] The elasticity of nematics is described by the Oseen -Frank theory;[2,3] the elastic energy density is expressed as

$$f_{el} = k_2 \mathbf{n}\cdot(\nabla\times\mathbf{n}) + \frac{1}{2}K_{11}(\nabla\cdot\mathbf{n})^2 + \frac{1}{2}K_{22}\left[\mathbf{n}\cdot(\nabla\times\mathbf{n})\right]^2 + \frac{1}{2}K_{33}\left|\mathbf{n}\times(\nabla\times\mathbf{n})\right|^2 + \\ + k_{13}\nabla\cdot\mathbf{n}(\nabla\cdot\mathbf{n}) - (K_{22}+k_{24})\nabla\cdot\left[\mathbf{n}(\nabla\cdot\mathbf{n}) + \mathbf{n}\times(\nabla\times\mathbf{n})\right] \quad (1)$$

The first term accounts for the spontaneous tendency of the director to twist inchiral nematics (cholesterics), and vanishes for achiral nematics. The three subsequent terms correspond to the *splay*, *twist* and *bend* distortion modes, respectively, and K_{ii} are the corresponding bulk elastic constants. The fourth and fifth contributions are usually denoted as *splay-bend* and *saddle-splay*, respectively. These pure divergence terms can be expressed as surface integrals, using the Gauss theorem. Their role has been widely debated; they were at first ignored, as purely surface terms which do not contribute to the response of bulk LCs, but then their importance for the behavior of LCs in the proximity of interfaces was proposed.[4-6] However, the surfacelike contributions elude direct experimental determination; therefore uncertainty on their role and their magnitude remains.

The splay, twist and bend elastic constants have values of the order of some pN and the relationships $K_{22} < K_{11} < K_{33}$ are generally found for low molar mass thermotropic nematics formed by elongated molecules, as those used in the most common applications. As a first approximation, for the splay and twist elastic constants $K_{ii} \sim S_{zz}^2$ is found, where S_{zz} is the major orientational order parameter; a different dependence on the order parameter is often exhibited by the bend elastic constant. The ratios K_{22}/K_{11} and K_{33}/K_{11}, which define the anisotropy of elasticity, show a significant dependence on the molecular structure of the LC constituents. This is interesting both for fundamental reasons and for application purposes: for instance, such ratios govern the steepness of the transmission/voltage curve in twisted nematic cells.[7,8] Recently, Monte Carlo simulations showed that the splay to bend modulus governs the defect location in spherical nematics,[9] a result which appears rich of implications for the design of organized assemblies of LC colloids.[10]

In general, the ratio K_{33}/K_{11} increases with the length-to-width ratio of rather rigid mesogens; in the presence of alkyl chains, this ratio was found to decrease with increasing chain length.[11,12] This has been know for more than three decades and possible explanations have been proposed,[13] without reaching a definite conclusion. The elasticity of nematics has been studied by theories and

simulations; a comprehensive review can be found in ref. [14]. It was early suggested that wedged and bent molecular shapes could reduce the splay and bend elastic constants of nematics,[15] but subsequent theories and simulations rather dealt with more manageable systems of axially symmetric particles: rods, spherocylinders and ellipsoids. Hard particle models have confirmed the importance of the length-to-width ratio; however they predict too high K_{33} values, beside being unsuitable to account for the temperature dependence of the elastic constants.[16-18] The introduction of the biaxiality of orientational order was found to have a small effect on the calculated elastic constants.[19] A more complex picture was obtained by generalized van der Waals theories, taking into account also attractive intermolecular interactions,[20] or by theories based on the density functional formalism, including dispersion and electric quadrupole interactions between molecules;[21,22] the elastic constants were found to be sensitive to the form of the intermolecular potential. In particular, this was shown to affect the relative magnitude of the bend to splay moduli. Actually, more realistic representations of molecules are needed to assess the prediction of these models, by closer comparison with experimental data. However atomistic simulations, which appear the appropriate techniques to investigate the effects of changes in the molecular structure, are extremely demanding, because large samples and long trajectories are needed for the prediction of elastic constants.[23,24] Zakharov and Maliniak calculated the bulk elastic constants of 4-*n*-pentyl-4′-cyanobiphenyl (5CB), a typical mesogen, at a single temperature of 300 K, using a statistical mechanics approach to connect the outcome of atomistic Molecular Dynamics simulations to the elastic properties.[25] They showed the dependence of the results on the assumptions of the statistical mechanics theory and, for some choice, they obtained values of the elastic constants in agreement with experiment.

Recently, we have developed a molecular field theory with atomistic modeling for the elastic constants of nematics.[26] The method rests on the so-called Surface Interaction (SI) model: the orienting molecular field in the nematic phase is parameterized according to the anisometry of the molecular shape. It is assumed that each element of the molecular surface tends to align to the nematic director, so that the probability distribution of molecular orientations can be related to the amount of surface aligned to the director. For the simple case of an elongated cylindrical particle, the resulting molecular field has the Maier-Saupe form[27] and the preferred orientation would be that with the symmetry axis parallel to the director. As a matter of fact, the SI method can be seen as an extension of the Maier-Saupe theory, which allows the introduction of molecular features into the orienting molecular field. This simple approach has been shown to the able to account for the dependence on the molecular structure of the order and thermodynamic properties of nematics,[28,29] of the orientational order of solutes in nematic solvents,[30] of the helical twisting power of chiral

dopants in nematics,[31] as well as of flexoelectric coefficients of nematics.[32,33] Valuable features of this approach are the possibility of introducing the molecular flexibility which, like the anisometry, is a common feature of mesogens, and the low computational cost. Indeed, this model is intended to account for the anisotropy of the short-range intermolecular interactions, which depend on the molecular shape. This determines not only steric repulsions, but also dispersion attractions between molecules; indeed, it is just the latter contribution which is responsible for the temperature dependence of the properties of thermotropic LCs.[34] The success of the SI approach can be ascribed to the major role played by the anisotropy of short-range intermolecular interactions for the order and stability of LC phases.

In ref. [26] molecular expression for the elastic constants in the framework of the SI model were derived and the theory was applied to 4-*n*-pentyl-4'-cyanobiphenyls (5CB). The good accord between calculations and experimental data gives us confidence that the developed methodology can be sensitive enough to give new insights into the relationship between chemical structure of mesogens and elastic moduli of their nematic phase. Therefore, in the present work the SI theory has been used to investigate the elasticity of some typical mesogens, *para*-azoxyanisole (PAA) and 4-*n*-alkyl-4'-cyanobiphenyls (*n*CBs), whose structures are shown in Fig. 1. Several measurements of elastic constants have been performed for PAA and for *n*CBs. Despite the structural similarity, significant differences were found between them; in particular, these systems exhibit different elastic anisotropy. For these reasons, they seem appropriate benchmarks for our methodology. Despite the speculations on the origin of the experimental differences, no definite explanation has been provided, so far. We can now try to shed light on this issue, hoping that our theoretical-computational methodology can provide new insights.

In the next Section, a short outline of the theory will be presented. Then the results obtained for PAA and nCBs will be reported and discussed. The final section contains the conclusions of this study, in relation with existing theories, and some more general considerations on the implications of the results of this study.

Elastic constants of LC by the Surface Interaction (SI) method

Our recent theoretical model provides molecular expressions for the elastic constants of nematics.[26] The starting point is the Helmholtz free energy density in the presence of director distortions, which is derived from the single molecule orientational distribution function, $p(\Omega)$, where Ω are the Euler angles specifying the molecular orientation in a laboratory frame:

$$p(\Omega) = \frac{\exp\left[-U(\Omega)/k_B T\right]}{Q}. \tag{2}$$

Here Q is the orientational partition function:

$$Q = \int \mathrm{d}\Omega \exp\left[-U(\Omega)/k_B T\right] \tag{3}$$

and $U(\Omega)$ is the *potential of mean torque*, experienced by molecules in the nematic phase. For the latter, the SI model is used;[26] in the following, we shall only outline the main points.

The following form is assumed for the potential of mean torque:[28]

$$U(\Omega) = k_B T \varepsilon \int_S dS\ P_2(\mathbf{n}\cdot\mathbf{s}) \tag{4}$$

where S is the molecular surface, $\boldsymbol{s}$ and $\mathbf{n}$ are unit vectors normal to the surface element dS e parallel to the director, respectively, and P_2 is the second Legendre polynomial. The parameter ε, with dimension of inverse square length, specifies the orienting strength of the medium, which is an increasing function of the reduced temperature, $T^*=T/T_{\mathrm{NI}}$, where T_{NI} is the Nematic-Isotropic transition temperature.

In the case of flexible molecules, which can exist in different conformational states, the orientational distribution function, eq. (2), should be replaced by the conformational-orientational distribution function:

$$p_m(\Omega) = \frac{\exp\left[-V_m/k_B T\right]\exp\left[-U_m(\Omega)/k_B T\right]}{Q}\ , \tag{5}$$

where the index denotes the mth conformer, characterized by the conformational energy V_m and the orienting potential U_m. Then, the conformational-orientational partition function reads:

$$Q = \sum_m \exp\left[-V_m/k_B T\right] Q_m\,, \tag{6}$$

where the sum is over all molecular conformers and Q_{m} is the orientational partition function for the mth conformer:

$$Q_m = \int \mathrm{d}\Omega \exp\left[-U_m(\Omega)/k_B T\right]. \tag{7}$$

The average value of any arbitrary function g can be expressed as:

$$\langle g \rangle = \sum_m w_m \overline{g_m}\,, \tag{8}$$

where w_m is the statistical weight of the mth conformer:

$$w_m = \frac{\exp\left[-\mathrm{V}_m/k_B T\right] Q_m}{Q}. \tag{9}$$

and $\overline{g_m}$ the orientational average of the function for the mth conformer, g_m :

$$\overline{g_m} = \frac{\int d\Omega \exp\left[-U_m(\Omega)/k_B T\right] g_m(\Omega)}{Q_m}; \tag{10}$$

In the nematic phase the statistical weights of conformers will be different from those in solution, and will depend on the degree of order. Namely, depending on their shape, conformers can be more or less well accommodated in the nematic phase; in general, elongated conformers are stabilized over the bent ones.

According to molecular field theories, the orienting strength ε appearing in eq. (4) is assumed to take the form:[28,29,35]

$$\varepsilon = -\frac{\xi^2}{v k_B T}\langle a \rangle \tag{11}$$

where v is the volume per molecule, ξ is a constant and $\langle a \rangle$ is the average value of the surface integral appearing in eq. (4). For the mth conformer we can write:

$$a_m = \int_{S_m} dS\, P_2(\mathbf{n}\cdot\mathbf{s}), \tag{12}$$

with S_m being the molecular surface of the conformer. The average value $\langle a \rangle$ can be seen as an order parameter, which vanishes in the isotropic phase and measures the degree of molecular order in the nematic phase.

The density of Helmholtz free energy in the nematic phase can be expressed as:

$$f = f_{iso} + \Delta u - T\Delta s \tag{13}$$

where f_{iso} is the free energy density of the isotropic phase, and Δu, Δs are the differences of internal energy and entropy density between the nematic and the isotropic phase, respectively. These differences can be expressed in terms of the potential of mean torque and of the orientational distribution function in the nematic phase, as:[29,35]

$$\Delta u = \frac{1}{2v}\langle U \rangle + \frac{1}{v}\langle \Delta V \rangle \tag{14a}$$

$$\Delta s = -\frac{k_B}{v}\langle \ln p \rangle \tag{14b}$$

where $\Delta V = V - \langle V \rangle_{iso}$, with $\langle V \rangle_{iso}$ being the average torsional potential in the isotropic phase. Then, the Helmholtz free energy density takes the form:

$$f = f_{iso} + \frac{\xi^2}{2v^2}\langle a \rangle^2 - \frac{k_B T}{v}\ln Q + \frac{1}{v}\langle \Delta V \rangle \tag{15}$$

The key point, for the derivation of expressions for the elastic constants, is the recognition that the free energy defined by eq. (15) is an implicit function of director distortions. These affect the

potential of mean torque, eq. (4), since, in their presence, the vector **n** becomes a function of the position on the molecular surface. For small deformations, characterized by a length scale much longer than the molecular dimensions, the Taylor expansion of the free energy density with respect to deformations can be truncated at the quadratic contributions and the elastic constants are identified with the coefficients of these terms. The following molecular expressions are obtained for the elastic constants appearing in the Oseen-Frank elastic energy density, eq. (1): [36]

$$k_2 = 3\frac{\varepsilon k_B T}{v} c_{XYZ} \tag{16a}$$

$$k_{13} = 3\frac{\varepsilon k_B T}{v} c_{XZXZ} \tag{16b}$$

$$K_{ii} = 3\frac{\varepsilon k_B T}{v}\left\{\left[\left(c_{JJXX} - c_{JJZZ} - 2(\delta_{i1} - \delta_{i3})c_{XZXZ}\right) - 3\varepsilon\left(c_{JXZ,JXZ} - \delta_{i2}{c_{YXZ}}^2\right)\right] + \right.$$
$$\left. + 3\delta_{i2}\left[\langle a\rangle_0 + \varepsilon\left(\langle a^2\rangle_0 - {\langle a\rangle_0}^2\right)\right]^{-1}\left[c_{YXZ} + 3\varepsilon\left(b_{YXZ} - \langle a\rangle_0 c_{YXZ}\right)\right]^2\right\} \tag{16c}$$
$$J = X \quad \text{for} \quad i = 1, \quad J = Y \quad \text{for} \quad i = 2, \quad J = Z \quad \text{for} \quad i = 3$$

$$K_{22} + k_{24} = 3\frac{\varepsilon k_B T}{v}\left\{c_{XXXX} + c_{XXYY} - 2c_{XXZZ} - 3\varepsilon\left(c_{XXZ,XXZ} - c_{XXZ,YYZ}\right)\right\} \tag{16d}$$

The terms c_{JKL}, c_{JKLM}, $c_{JKL,JKL}$, b_{JKL}, appearing in these expressions, are the average values, calculated over the orientational distribution for undeformed nematics, of elements of Cartesian tensors, defined as integrals over the molecular surface; their forms are reported in ref. [26]. The indices X,Y,Z refer to the axes of a laboratory frame.

Results and Discussion

The systems under investigation are *para*-azoxyanisole (PAA) and 4-*n*-alkyl-4'-cyanobiphenyls (*n*CBs), whose chemical structures are shown in Fig. 1. These compounds have some differences which, though small, have clear effects on the elasticity of the nematic phases. PAA is relatively rigid; for it the four conformers shown in Fig. 2 can be identified. They differ only in the orientation of the methyl substituents and have very similar overall shape. By virtue of the flexibility of the biphenyl moiety, and especially that of the alkyl chains, *n*CBs have a higher number of conformers and display a corresponding variety of overall shapes. Fig. 3 and Fig. 4 show some of the lowest energy conformers of 5CB and 8CB, which have at most a single *gauche* in the alkyl chain.[37] An arbitrary conformer is identified by a label; the first letter specifies the sign of the twist angle between phenyl rings (**P** and **P**, for twist angles of about +30° and about -30°, respectively),

whereas the subsequent letters denote the conformational state of CH_2-CH_2 bonds, in their order, starting from the benzene ring (**t**, **g+**, **g-**, for *trans*, *gauche*+ and *gauche*-, respectively).

Atomic coordinates and energy of the conformers were obtained by geometry optimization at the DFT/B3LYP/6-31g** level.[38] The energy of the four conformers of PAA are very close to each other, therefore we have taken them identical in our calculations. Fo r *n*CBs, the all-*trans* conformer is the most stable, and the energy increases with the number of *gauche* states in the alkyl chain. Given the *gauche–trans* energy difference,[39] we have retained only conformers with at most a single *gauche* state. For 5CB, 14 conformers of this kind can be found, whereas for 8CB this number rises to 26. Individual conformers can be chiral, but they can be grouped in pairs of enantiomers, so that the ensemble of conformers is globally achiral; therefore the chiral strength k_2 in eq. (1) vanishes. In our calculations we have neglected the small energy differences, obtained from the DFT calculations, between conformers having *g* states at different chain positions, and we have assumed that all of them are 2.5 kJ mol^{-1} higher in energy than the all-*trans* conformer. Molecular surfaces were generated with the Sanner code,[40] giving the van der Waals radii the values r_C = 0.185 nm, r_O = 0.15 nm, r_N = 0.16 nm, r_H = 0.1 nm [41], with a rolling sphere radius equal to 0.3 nm;[30] a density of points equal to 500 nm^{-2} was taken. Elastic constants were calculated as a function of the orienting strength, ε. The volume per molecule, *v*, was given the value 0.256 nm^3 for PAA, 0.275 nm^3 for 5CB and 0.321 nm^3 for 8CB, as obtained from the molecular surface calculation.[40]

Fig. 5 displays the temperature dependence of the principal values of the molecular Saupe matrix, obtained for the three systems under investigation. For each ε value, the molecular Saupe matrix, $\boldsymbol{S}$,[13] was calculated, by averaging the individual Saupe matrices of conformers, all expressed in the same molecular fixed frame, according to eq. (8). From comparison between the ε dependence of the major order parameter, S_{zz}, and the experimental temperature dependence reported in the literature ([42] for PAA, [43] for 5CB and 8CB), the relationship between orienting strength ε and temperature was derived. In Fig. 5 also the $(S_{xx}-S_{yy})/S_{zz}$ ratio is shown; it ranges between 0 and 1, and quantifies the biaxiality of molecular order. We can see that the biaxiality is rather low for the two CB derivatives, but is significantly higher for PAA, in agreement with the shape of this mesogen.

[insert Figure 5 about here]

In Fig. 6 the temperature dependence of the elastic constants calculated for PAA, 5CB and 8CB is shown; for comparison, experimental data from the literature are also reported. As

mentioned in the Introduction, clear differences between the three cases appear, despite the small structural diversity. All the three elastic constants decrease on going from PAA to 8CB, through 5CB, but the effect is small for K_{22}, slightly larger for K_{11}, and significantly larger for K_{33}. We can see that the experimental trends are reflected by the calculated elastic constants: these exhibit the correct temperature dependence (they increase with lowering temperature), the correct sequence, $K_{22} < K_{11} < K_{33}$, and the magnitude of elastic moduli is rather well predicted. These general features, however, are not extremely critical, and could be predicted also by other molecular theories for the elasticity of liquid crystals.[14] The really interesting issue of the present methodology is its ability to account for the changes of elastic moduli induced by modifications in the molecular structure. This is also shown in Fig. 7, where the calculated K_{22}/K_{11} and K_{33}/K_{11} ratios are compared with the corresponding experimental values; as mentioned in the Introduction, the anisotropy of elasticity is particularly sensitive to changes in the molecular structure. We can see in Fig. 7 that for all the systems under investigation, in keeping with experiment, the calculated K_{22}/K_{11} ratio is weakly dependent on temperature and scarcely affected by structural changes, whilst higher variability is exhibited by K_{33}/K_{11}. This ratio is close to one and almost temperature independent for 8CB; it becomes higher and increases with lowering temperature for 5CB; the effect is even more pronounced for PAA. All these feature are clearly recognizable in the calculated elastic constants; some discrepancies between calculated and experimental data probably reflect the intrinsic limits of the model, which rests on a phenomenological, though sensible, representation of the orientational distribution function.

[insert Figure 6 about here]

[insert Figure 7 about here]

The temperature dependence of the elastic constants mainly derives from the change of orientational order; experiments have shown that K_{11} and K_{22} are approximately proportional to the square of the main order parameter, S_{zz}^2, whereas this is not always true for K_{33}.[12] This behavior was also found theoretically.[14] In our model the dependence of the elastic constants on the degree of order is implicit in the average values appearing in eqs. (16); they do not simply depend on S_{zz}, but also on the biaxiality of order, as well as on higher rank order parameters. The results we have obtained for the splay and twist elastic constants of PAA, 5CB and 8CB, shown in Fig. 8, are in general agreement with the relation $K_{ii} \approx \text{const} \cdot S_{zz}^2$, with higher slope for splay, as in experiment.

Significant deviations from linearity appear for the bend elastic constants and are particularly pronounced in the case of PAA.

[insert Figure 8 about here]

We can now try to understand the origin of the differences between PAA, 5CB and 8CB. In the literature, a role of the molecular biaxiality[19] and flexibility[11,25] has been proposed, as well as effects of dispersion and electrostatic interactions between molecules.[20-22] The agreement between our results and experimental data suggest that probably the latter do not need to be invoked. Flexibility is certainly an important difference between the three mesogens under investigation, which can affect our results. PAA has limited conformational freedom; the four conformers shown in Fig. 2 are very similar, roughly linear in shape and they do give similar contributions to the elastic constants. A wider variety of shapes is possible for 5CB and even more for 8CB, as a consequence of the rotational freedom of the alkyl chain. Fig. 9 shows individual contributions to the elastic constants of 8CB from the seven conformers shown in Fig. 4; each curve in the plots is obtained by restricting to a single conformer the summations in eqs. (16). We can see a strong dependence on shape of the elastic constants. The conformers can be grouped in two classes, according to the position of the *gauche* state in the chain: the elastic constants calculated for conformers with a *gauche* at an even chain bond are not too far from those obtained for the all-*trans* structure. On the contrary, large differences, along with an unexpected dependence on order, are found for the elastic moduli of conformers with a *gauche* at an odd chain bond. We can see in Fig. 4 that the structures belonging to the former group are more elongated and similar to the all-*trans*, which explains the similar results obtained for them. The other structures have the common feature of being more or less V-shaped. Thus, the results presented in Fig. 9 suggest a correlation between the degree of molecular bending and the deviations from the all-*trans* behavior: the most dramatic effects are exhibited by the **Mg-ttttt** conformer, which has the alkyl chain almost perpendicular to the cyanobiphenyl core. Differences between conformers are found for all the elastic costants, but they are particularly pronounced for the bending stiffness: for the bent conformers, even negative K_{33} values are predicted, which would promote spontaneous bending of the director. The effect of the molecular bending could be ascribed to the weak and highly biaxial order which characterizes bent conformers,[51] but this is not the case. To highlight this point, we have also reported in Fig. 9 the elastic constants calculated for the **C** conformer of PAA, whose orientational order is characterized by a biaxiality similar to that of the **Mtt g-ttt** conformer of 8CB. We can see that the elastic constants calculated for the two structures are quite different; actually, the results obtained

for the PAA conformer are close to those reported for the elongated conformers of 8CB, though these are characterized by a significantly lower biaxiality. We conclude that the biaxiality of order does not strongly affect the elastic behavior of nematics; the same conclusion was reached for hard ellipsoids by the classical density functional theory .[19] On the contrary, we suggest that a major role is played by the molecular bending, which has the general effect of reducing the elastic moduli. Comparing Fig. 9 and Fig. 8, we can provide an explanation for the decrease of the elastic constants on going from of PAA to 5CB and then to 8CB: the relatively high stiffness of PAA is due to its low flexibility and shape linearity. For the single all-*trans* conformer of 5CB and 8CB, lower K_{22} and K_{33} values would be predicted, as a consequence of their slightly bent shape. A further reduction of the elastic constants derives from the contribution of other conformers; though higher in energy than the all-*trans*, these are quite numerous and some of them give very low, or even negative, contributions to the elastic constants.

[insert Figure 9 about here]

Finally, Fig. 10 shows the temperature dependence of the surfacelike elastic moduli of the systems under investigation. We can see a much stronger dependence on molecular structure than for bulk elastic constants. The magnitude of k_{13} and k_{24} never exceeds a few pN, but positive and negative values are predicted for PAA and the *n*CB derivatives, respectively. Unfortunately, no experimental estimates of these surfacelike elastic constants are available and probably, if suitable experiments were performed, the measured quantities would not simply be the bare k_{13} and k_{24} constants defined by eqs. (16).[52,53] Neither comparison with other models can be useful, since few and different results have been reported. Positive k_{13} , much smaller than the bulk elastic constants and higher than k_{24}, was obtained for a Gay-Berne model using the classical density functional theory.[54] For the same model, positive k_{24} along with very small and negative k_{13} was obtained from Molecular Dynamics simulations.[55] So, we are not presently able to evaluate the real significance of our predictions; we can only infer an extreme sensitivity of the surfacelike elastic constants upon the details of intermolecular interactions, as was already noticed in ref. [55].

[insert Figure 10 about here]

Conclusions

Using our recently developed molecular field model, based on an atomistic representation of mesogen structure within a molecular field approach, we have calculated the bulk and surfacelike elastic constants of PAA, 5CB and 8CB. These have been chosen as representative cases because of their different elasticity, despite the structural similarity. The results can be summarized as follows.

- Magnitude, order ($K_{22} < K_{11} < K_{33}$) and temperature dependence of the elastic constants are correctly estimated. Actually, these general features can also be predicted by other theories. The main distinguishing peculiarity of our approach is its ability to account for the molecular structure: here, we have shown that the experimental differences between the investigated systems, including the anisotropy of elasticity, are well predicted. The only specific feature of a given compound required to this purpose is the molecular shape. The accord between our results and experimental data gives us confidence that indeed this is the main factor behind the different elastic properties of low molar mass nematics. Given the essential role played by the molecular shape, the method rests on the availability of molecular structures. To this purpose, the molecular field theory can be fruitfully integrated with quantum mechanical molecular structure calculations. Remarkably, our predictions are comparable to those obtained by MD simulations,[25] at an extremely lower computational cost: the full temperature dependence of the elastic constants for systems like those under investigation takes a few hours on a modern desktop PC, and takes some hours. No free parameter enters the calculations and the method has predictive ability.
- The elastic constants calculated for splay and twist distortions are rather similar in magnitude for PAA, 5CB and 8CB and are proportional to the square of the major orientational order parameter. A less simple behavior is obtained for the bend stiffness, which can have a much stronger dependence on temperature and on the structure of the mesogen. All these results are in keeping with experimental findings for PAA, 5CB and 8CB. From experiment, the value of K_{33} is generally found to lower with increasing the length of alkyl chains in homologous series of mesogens. The opposite trend was predicted for hard uniaxial particles: the bend modulus should steadily increase with the length-to-width ratio.[14] As an explanation for this discrepancy, the increase of flexibility with chain length was invoked;[11] however this hypothesis could not be assessed, because of the difficulties related to the introduction of molecular flexibility into molecular models. The observed deviations from the predictions for hard particles were also ascribed to the

additional presence of other intermolecular forces, with a different dependence on the molecular structure, i.e. dispersion or electrostatic interactions between molecular dipoles and quadrupoles.[10-22] Using an atomistic representation of the molecular structure, we can now provide another explanation.

- Our approach can take into account the molecular flexibility; we find that this plays an essential role and should not be neglected by molecular models for the elasticity of nematics. The extreme sensitivity of the elastic moduli to conformational changes is related to the corresponding changes in molecular shape. The importance of the molecular flexibility of mesogens for the elasticity of nematics was also singled out by Zakharov et al, when comparing atomistic Molecular Dynamics simulations and statistical mechanics theories for uniaxial particles.[25]
- The main result of our investigation concerns the special effects of bent molecular shapes on the elastic constants. In general, molecular bending is accompanied by a lowering of the stiffness. For K_{11} and K_{22} this effect can be associated with the decrease of order, but such an explanation is not sufficient for K_{33}. This is much higher than the other elastic constants for elongated geometries and rapidly decreases with increasing the deviation from a linear shape, reaching even negative values for strongly bent structures. We have found that shape bending has the main responsibility for the decrease of the K_{33}/K_{11} ratio on going from PAA to 8CB, trough 5CB. These are generally considered as rod-like mesogens; but in the case of flexible mesogens, like *n*CBs, this is only the result of a conformational average. As can be seen in figs. 3 and 4, some of the conformers of 5CB and 8CB are roughly V-shaped; the effect is especially pronounced for 8CB, for which even the all-*trans* conformer exhibits some degree of bending. We think that, in general, the following picture can be drawn: most mesogens are far from rigid and the variety of accessible molecular shapes increases with the length of the flexible chains. In a mixture of conformers, the elongated structures will prevail, otherwise the nematic phase would not be found; however, the presence of V-shaped structures has the effect of reducing the restoring forces opposing bend distortions of the director.
- Some more comments should be deserved to the meaning of negative K_{33} values, since these would imply that the nematic phase with uniform director does not correspond a minimum of the free energy. Actually, the presence of a few conformers with negative contributions has only the effect of decreasing the average K_{33} value for mesogens like *n*CBs. However dramatic consequences can be expected for compounds characterized by a V-shape in their most stable conformations, as the so called ‘banana’ or ‘bent core’ mesogens. These systems

have been found to possess very peculiar properties, most of which remain poorly understood. They have scarce propensity to form nematic phases and almost no information on the elasticity of this is available: the values $K_{11} \sim K_{33} \sim 2$ pN were reported for 4-chloro-1,3-phenylene bis4-[4'-(9-decenyloxy)benzoyloxy]benzoate (T_{NI}=78°C), 7°C below the Isotropic-Nematic transition.[56] Both values are low, especially in view of the dimension of the mesogen; this is particularly remarkable for K_{33}, which is about one fifth of that of PAA at the same reduced temperature. However, such results do not appear surprising in the light of our findings on the effect of a bent shape on the elastic moduli of nematics. This kind of behavior was early predicted by Gruler [15] and then by Dozov,[57] in relation to bent-core mesogens. Interestingly, the propensity of bent-core LCs for spontaneous bending of the director been recently invoked to explain different phenomena, comprising the segregation into chiral domains of opposite handedness in the nematic phase [58] and the formation of stripe and labyrinthine patterns of the *c*-director in freely suspended polar smectic SmCPF films. [59] Certainly the elastic behavior of bent-core LCs deserves more attention, and we think that our methodology could be a useful tool in this context.

- We have also calculated the surfacelike elastic constants, k_{13} and k_{24}, of PAA, 5CB and 8CB. We have found that these are strongly affected by structural changes, even more than the bulk elastic constants. In fact, the results obtained for PAA, 5CB and 8CB differ in sign, magnitude and temperature dependence. Unfortunately, we cannot assess the quality of these predictions, for the scarcity and uncertainty of experimental data. The surfacelike elasticity remains poorly understood, though being involved in important phenomena occurring at interfaces, like surface anchoring and structure formation in films; further investigation in this field is required.

Acknowledgments

The beginning of this work was supported by Italian MIUR (PRIN 2005).

Abbreviations LC: liquid crystal; PAA: *para*-azoxyanisole; CB 4-*n*-alkyl-4'-cyanobiphenyl; 5CB: 4-*n*-pentyl-4'-cyanobiphenyl; 8CB: 4-*n*-octyl-4'-cyanobiphenyl; SI: Surface Interaction.

References

[1] D.-K. Yang, S.-T. Wu, *Fundamentals of Liquid Crystal Devices* (John Wiley & Sons, Chichester, 2006).

[2] C.W. Oseen, *Trans. Faraday Soc.*, 1933, **29**, 883-889.

[3] F.C. Frank, *Discuss. Faraday Soc.*, 1958, **25**, 19-28.

[4] C. Oldano, G. Barbero, *Phys. Lett.*, 1985, **110A**, 213-216.

[5] S. Faetti, M. Riccardi, *J. Phys. II (France)*, 1995, **5**, 1165-1191.

[6] O.D. Lavrentovich, V.M. Pergamenschik, *Int. J. Mod. Phys. B*, 1995, **9**, 2389-2437.

[7] M. Schadt, P.R. Gerber, *Z. Naturforsch.*, 1982, **37a**, 165-178.

[8] M. Schadt, *Ann. Rev. Mat. Res.*, 1997, **27**, 305-379.

[9] H. Shin, M.J. Bowick, X. Xing, *Phys. Rev. Lett.*, 2008, **101,** 037802:1-4.

[10] M. Ravnik, M. Škarabot,2 S. Žumer, U. Tkalec, I. Poberaj, D. Babič, N. Osterman, I. Muševič, *Phys. Rev. Lett.*, 2007, **99,** 247801:1-4.

[11] W.H. de Jeu, W.A.P. Claassen, *J. Chem. Phys.*, 1977, **67**, 3705-3712.

[12] D. Dunmur, in *Physical Properties of Liquid Crystals*, eds. D.A. Dunmur, A. Fukuda, G.R. Luckhurst (EMIS Datareviews Series, IEE, London, 2000).

[13] G. Vertogen, W.H. de Jeu, *Thermotropic Liquid Crystals*: *Fundamentals* (Springer, Berlin, 1988).

[14] S. Singh, *Phys. Rep.*, 1996, **277**, 283-384.

[15] H. Gruler, *J. Chem. Phys.*, 1974, **61**, 5408-5412.

[16] R.G. Priest, *Phys. Rev. A*, 1973,**7**,720-729.

[17] J.P. Straley, *Phys. Rev. A*, 1973,**8**,2181-2183.

[18] A. Poniewierski, J. Stecki, *Mol. Phys.*, 1979, **38**, 1931-1940.

[19] T.K. Lahiri, K. Rajesh, S. Singh, *Liq. Cryst.*, 1997, **22**, 575-578.

[20] W.M. Gelbart, A. Ben Shaul, *J. Chem. Phys.*, 1982, **77,** 916-933.

[21] A. Srivastava and S. Singh, *J. Phys.: Condens. Matter*, 2004, **16**, 7169-7182.

[22] J. Stecki, A. Poniewierski, *Mol. Phys.*, 1980, **41**, 1451-1461.[23] M.P. Allen, A.J. Masters, *J. Mater. Chem.*, 2001, **11**, 2678-2689.

[24] M.R. Wilson, *Int. Rev. Phys. Chem.*, 2005, **24**, 421-455.

[25] A.V. Zakharov and A. Maliniak, *Eur. Phys. J. E*, 2001, **4**, 85-91.

[26] M. Cestari, A. Bosco, A.Ferrarini, submitted.

[27] W. Maier, A. Saupe, *Z. Naturforsch. A*, 1959, **14A**, 882-900; *ibidem*, 1960, **15A**, 287-292.

[28] A. Ferrarini, G.J. Moro, P.L. Nordio, G.R. Luckhurst, *Mol. Phys.*, 1992, **77**, 1-15.

[29] A. Ferrarini, G.R. Luckhurst, P.L. Nordio, S.J. Roskilly, *J. Chem. Phys.*, 1994, **100**, 1460-1469.

[30] A . Ferrarini, F. Janssen, G.J. Moro, P.L. Nordio, *Liq. Cryst.*, 1999, **26**, 201-210.

[31] A. Ferrarini, G.J. Moro, P.L. Nordio, *Phys. Rev. E*, 1996, **53**, 681-688; A. Ferrarini, G.J. Moro, P.L. Nordio, *Mol. Phys.*, 1996, **87**, 485-499.

[32] A. Ferrarini, *Phys. Rev. E*, 2001, **64**, 021710:1-11.

[33] C. Greco, G.R. Luckhurst, A. Ferrarini, *J. Mater. Chem.*, 2007, **17**, 1039-1042.

[34] A. Ferrarini, G.J. Moro, *J. Chem. Phys.* **114**, 596-608 (2001).

[35] G.R. Luckhurst, G.W. Gray, *The Molecular Physics of Liquid Crystals* (Academic, London, 1979).

[36] Indeed, more complex expressions where obtained for the case for flexible molecules in ref. [26], but they reduce to the simpler form of eqs. (16) when the average torsional potential is similar in the isotropic and in the nematic phase, *i.e.* the average difference $<\Delta V>$ is small.

[37] C.J. Adam, S.J. Clark, M.R. Wilson, G.J. Ackland, J. Crain, *Molec. Phys.*, 1998, **93**, 947-954.

[38] M.J. Frisch et al , Gaussian 03, Revision C.02 (Gaussian Inc., Wallingford CT, 2004).

[38] V.A. Herrebout, B.J. van der Veken, A. Wang, J.R. Durig, *J. Phys. Chem.*, 1995, **99**, 578-585.

[40] M.F. Sanner, J.C. Spehner, A.J. Olson, *Biopolymers*, 1996, **38**, 305-320.

[41] D.R. Lide (Ed.), *Handbook of Chemistry and Physics* (CRC; Boca Raton, 1996).

[42] I.W. Hamley, S. Garnett, G.R. Luckhurst,S.J. Roskilly, J.S. Pedersen, R.M. Richardson, J.M. Seddon, *J. Chem. Phys.*, 1996,**104**, 10046-10054.

[43] L.G.P. Dalmolen, SJ. Picken, A.F. de Jong, W.H. de Jeu, *J. Phys. (France)*, 1985, **46**, 1443-1449.

[44] I. Pardowitz, S. Hess, *J. Chem. Phys.*, 1982, **76**, 1485-1489.

[45] W.H. de Jeu, W.A.P. Claassen, M.J. Spruijt, *Mol. Cryst. Liq. Cryst.*, 1976, **37**, 269-280.

[46] N.V. Madhusudana, R. Pratibha, *Mol. Cryst. Liq. Cryst.*, 1982, **89**, 249-257.

[47] M.J. Bradshaw, E.P. Raynes, J.D. Bunning, T.E. Faber, *J. Phys. (France)*, 1985, **46**, 1513-1520.

[48] G.-P. Chen, H. Takezoe, A. Fukuda, *Liq. Cryst.*,1989, **5**, 341-347.

[49] H.J. Coles, in *The Optics of Thermotropic Liquid Crystals*, eds. S. Elston, R. Sambles (Taylor & Francis, London, 1998).

[50] S. Faetti, V. Palleschi, *Liq. Cryst.*, 1987, **2**, 261-268.

[51] A. Ferrarini, G.R. Luckhurst, P.L. Nordio, S.J. Roskilly, *Liq. Crystals*, 1996, **21**, 373-382.

[52] V.M. Pergamenshchik, S. Zumer, *Phys. Rev. E*, 1999, **59**, R2531- R2534.

[53] H. Yokoyama, *Phys. Rev. E*, 1997, **55**, 2938-2957.

[54] P.I.C. Teixeira, V.M. Pergamenshchik, T.J. Sluckin, *Mol. Phys.*, 1993, **80**, 1339-1357.

[55] J. Stelzer, H.-R. Trebin, L. Longa, *J. Chem. Phys.*, 1995, **103**, 3098-3107; *ibidem*, 1997, **107**, 1295-1296.

[56] D. Wiant, J.T. Gleeson, N. Eber, K. Fodor-Csorba, A. Jakli, T. Toth-Katona, *Phys. Rev. E*, 2005, **72,** 041712:1-12.

[57] I. Dozov, *Europhys. Lett.*, 2001, **56**, 247-253.

[58] V. Görtz, C. Southern, N.W. Roberts, H.F. Gleeson, J.W. Goodby, *Soft Matter*, 2009, **5**, 463-471.

[59] A. Eremin, A. Nemes, R. Stannarius, G. Pelzl, W. Weissflog, *Soft Matter*, 2008, **4**, 2186-2191.

Captions to the Figures

Figure 1 Chemical structure of *para*-azoxyanisole (PAA), 4-*n*-alkyl-4'-cyanobiphenyl (nCB).

Figure 2 Geometry of the conformers of *para*-azoxyanisole (PAA) considered for the calculation of elastic constants, as obtained from DFT/B3LYP/6-31g** calculations.[38]

Figure 3 Geometry of four of the conformers of 4-*n*-pentyl-4'-cyanobiphenyl (5CB) considered for the calculation of elastic constants, as obtained from DFT/B3LYP/6-31g** calculations.[38] The labels **P** and **M** are used for positive (~ +30°) and negative (~ -30°) biphenyl twist angles, respectively. The symbols **t** (*trans*) and **g** (*gauche*) denote the conformational state of CH_2-CH_2 bonds. The other conformers, not shown in the figure, differ in the sign of the twist angle between the aromatic rings (**P** in place of **M**) and the sign of the chain torsional angles ($\mathbf{g}_-$ in place of $\mathbf{g}_+$).

Figure 4 Geometry of seven of the conformers of 4-*n*-octyl-4'-cyanobiphenyl (8CB) considered for the calculation of elastic constants, as obtained from DFT/B3LYP/6-31g** calculations.[38] The labels **P** and **M** are used for positive (~ +30°) and negative (~ -30°) biphenyl twist angles, respectively. The symbols **t** (*trans*) and **g** (*gauche*) denote the conformational state of CH_2-CH_2 bonds. The other conformers, not shown in the figure, differ in the sign of the twist angle between the aromatic rings and the sign of the chain torsional angles ($\mathbf{g}_+$ in place of $\mathbf{g}_-$).

Figure 5 Principal values of the Saupe matrix calculated for PAA, 5CB and 8CB, as a function of temperature. The dashed line shows the ratio $(S_{xx}-S_{yy})/S_{zz}$; this can range between 0 (uniaxial) and 1.

Figure 6 Bulk elastic constants of PAA, 5CB and 8CB, as a function of temperature. Left: calculated values; right: experimental data for PAA (open triangles[44] and circles[45]), for 5CB (dashed lines,[46] triangles,[47] open circles,[48] squares[49]) and for 8CB (dashed lines,[46] open circles,[47] squares[50]).

Figure 7 Ratio of the bulk elastic constants for PAA, 5CB and 8CB, as a function of temperature. Lines: calculated values; symbols: experimental data, from refs. [44,45] for PAA, [46-49] for 5CB and [46,47,50] for 8CB.

Figure 8 Bulk elastic constants calculated for PAA, 5CB and 8CB, as a function of the square of the largest principal value of the Saupe matrix, S_{zz}. The dotted lines should be intended as a guide for the eyes, to highlight deviations from linearity. In the plot for *n*CBs, solid lines are used for 5CB and dashed lines for 8CB.

Figure 9 Elastic constants calculated for single conformers of 8CB, as a function of the S_{zz}^2 , the square of the largest principal value of the Saupe matrix. The curves refer to the conformers shown in Fig. 4; the solid line is for the all-*trans* chain, the other lines for conformers with a single *gauche* in the alkyl chain; the numbers in the labels indicate the position of the *g* state (starting from the aromatic ring). For comparison, also the elastic constants of PAA, calculated for the single **C** conformer, are shown (triangles).

Figure 10 Surfacelike elastic constants of PAA, 5CB and 8CB, as a function of temperature.

Figure 1

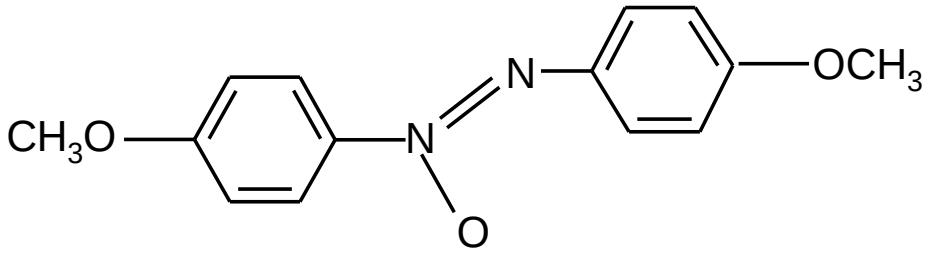

PAA

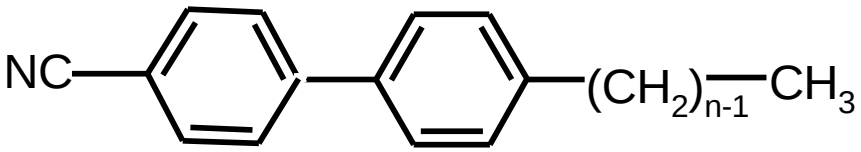

nCB

Figure 2

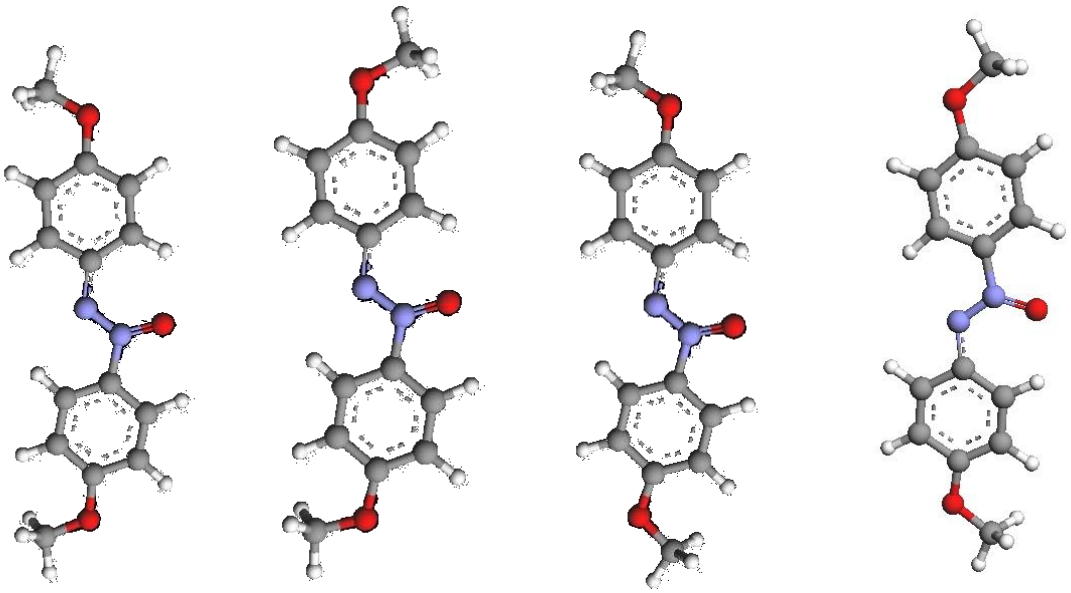

A **B** **C** **D**

Figure 3

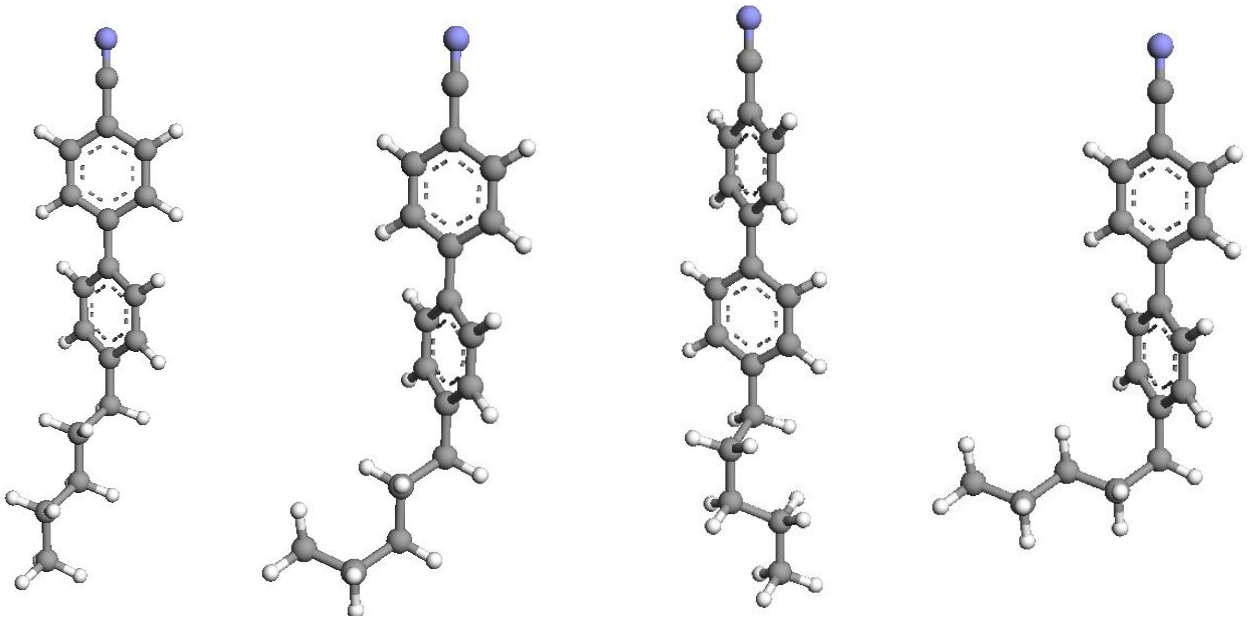

P*ttt*… ……..….P*ttg*$_+$… ……..…..P*tg*$_+$*t*…… …….P*g*$_+$*tt*

Figure 4

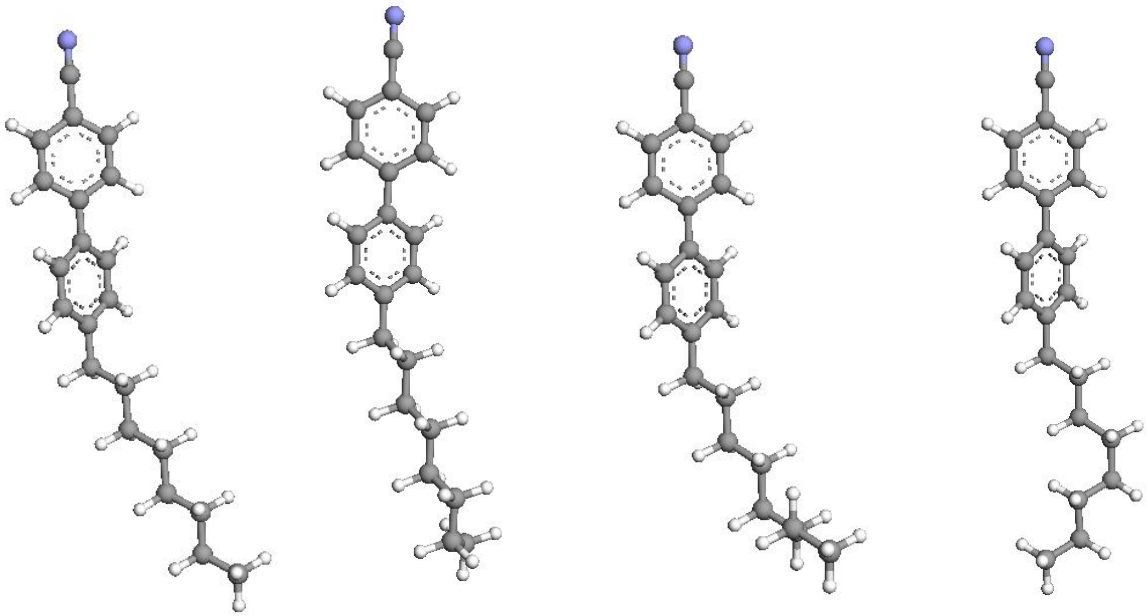

M*ttttt*… …M*ttttt*g…. …M*tttg*_*t*… …M*ttt*g_*tt*

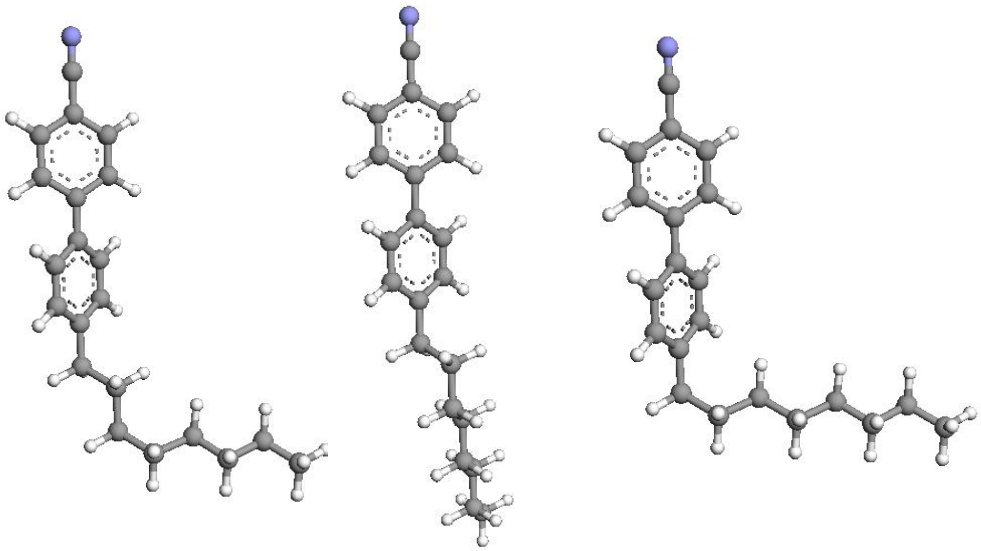

M*tt*g_*ttt* ……M*t*g_*tttt*… …M*g*_*ttttt*

Figure 5

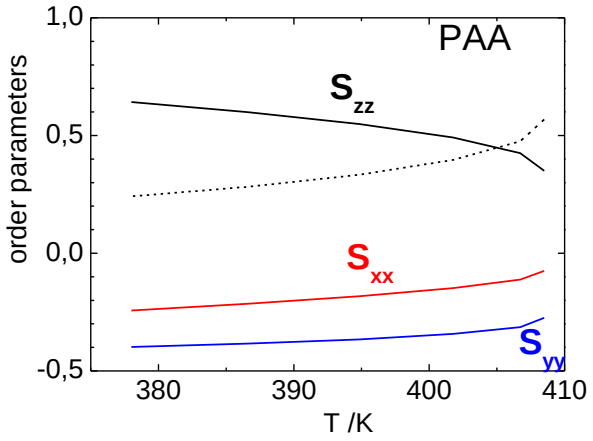
PAA
order parameters
1,0
0,5
0,0
-0,5
380
390
400
410
T /K
S zz
S xx
S yy

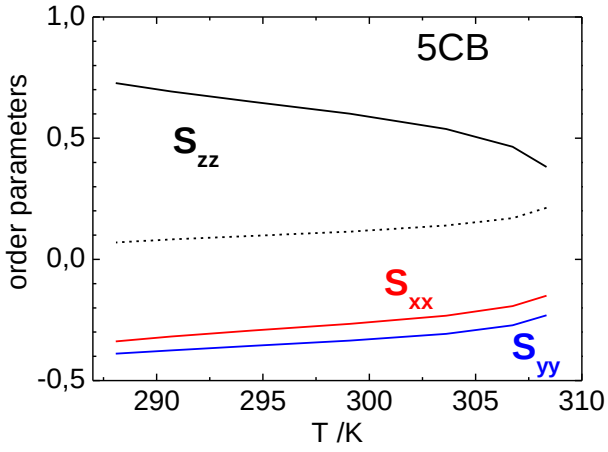
5CB
order parameters
1,0
0,5
0,0
-0,5
290
295
300
305
310
T /K
S zz
S xx
S yy

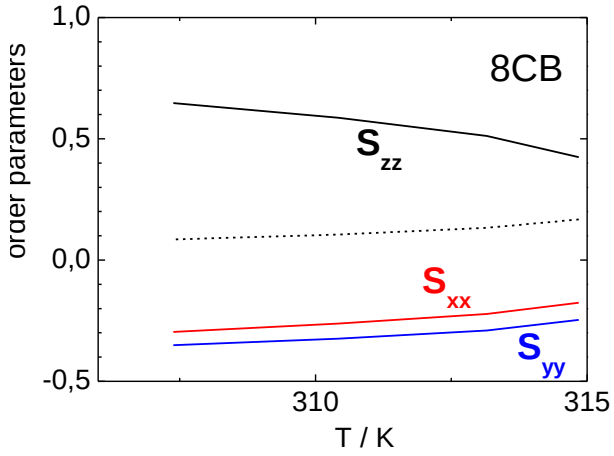
8CB
order parameters
1,0
0,5
0,0
-0,5
310
315
T / K
S zz
S xx
S yy

Figure 6

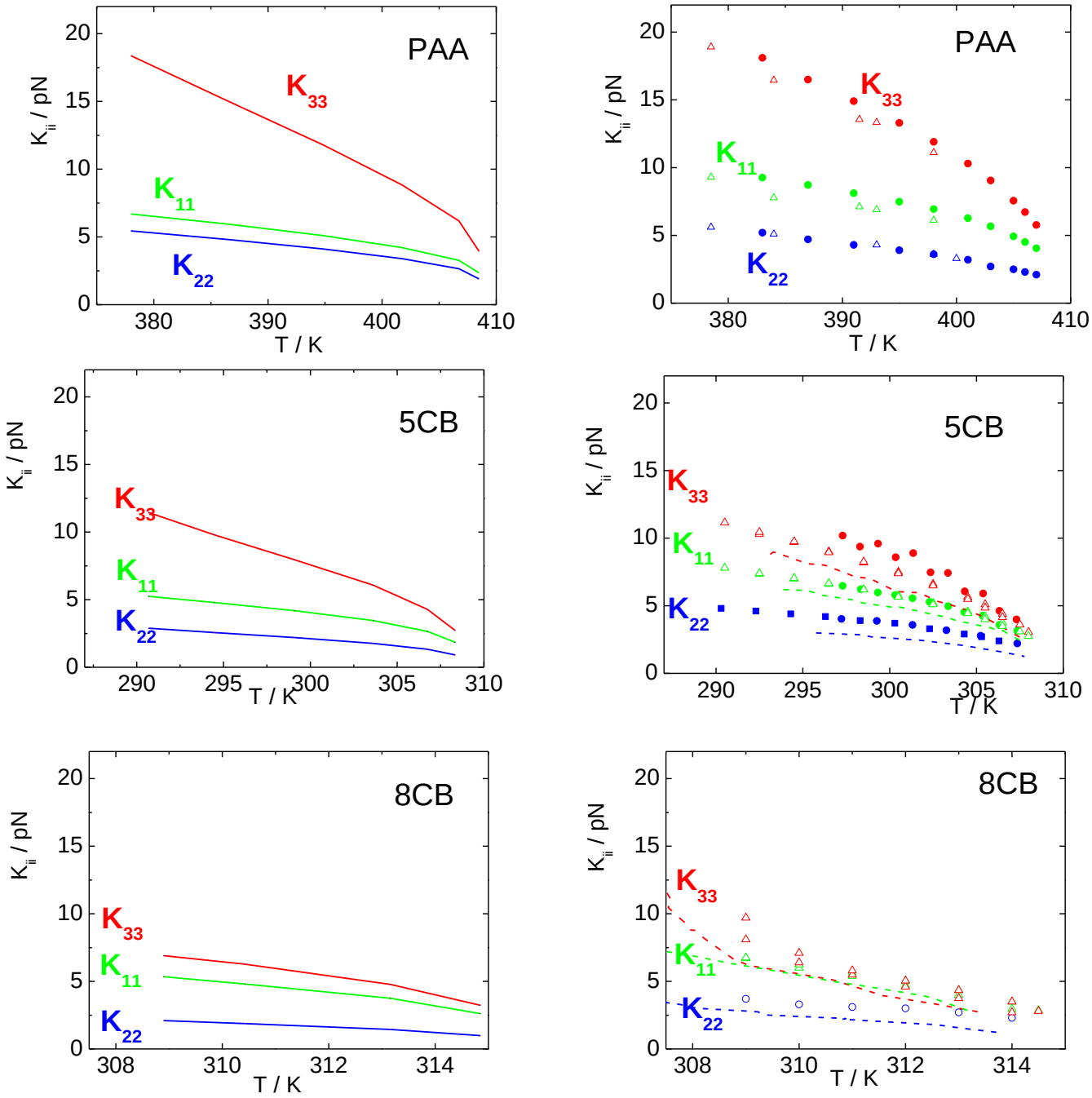

Figure 7

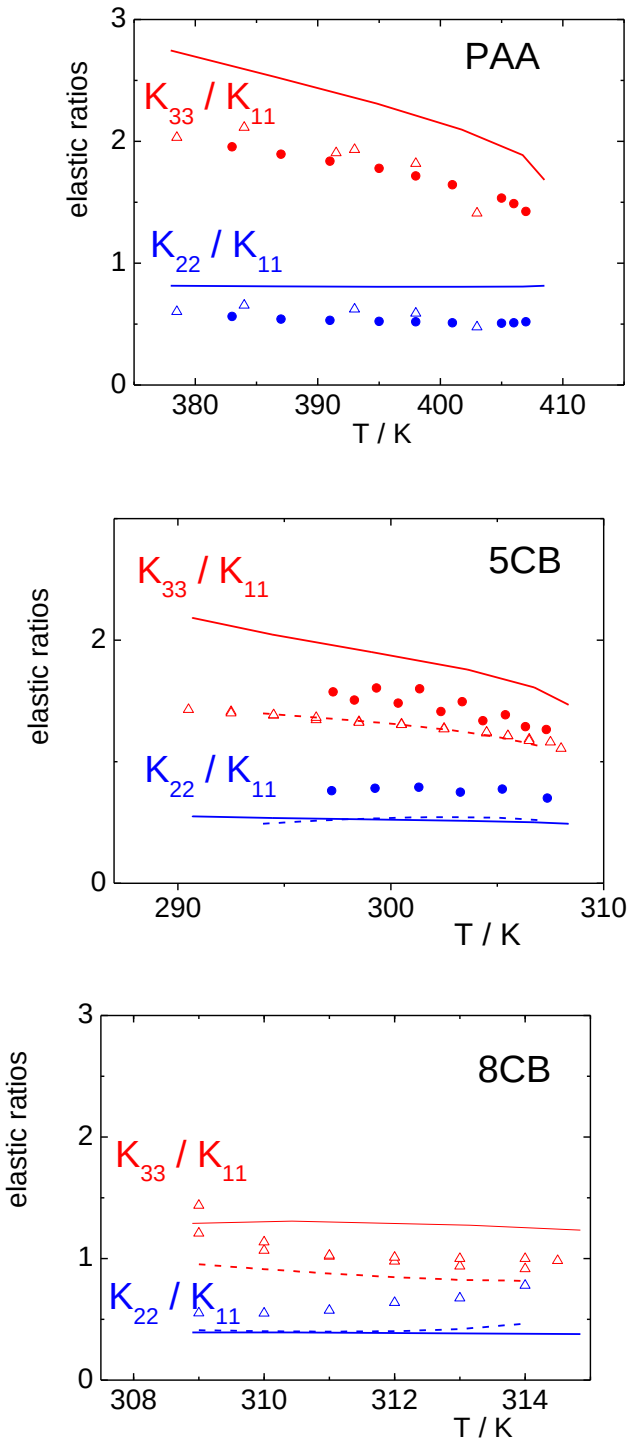
PAA
K_{33} / K_{11}
K_{22} / K_{11}
elastic ratios
T / K
5CB
K_{33} / K_{11}
K_{22} / K_{11}
elastic ratios
T / K
8CB
K_{33} / K_{11}
K_{22} / K_{11}
elastic ratios
T / K

Figure 8

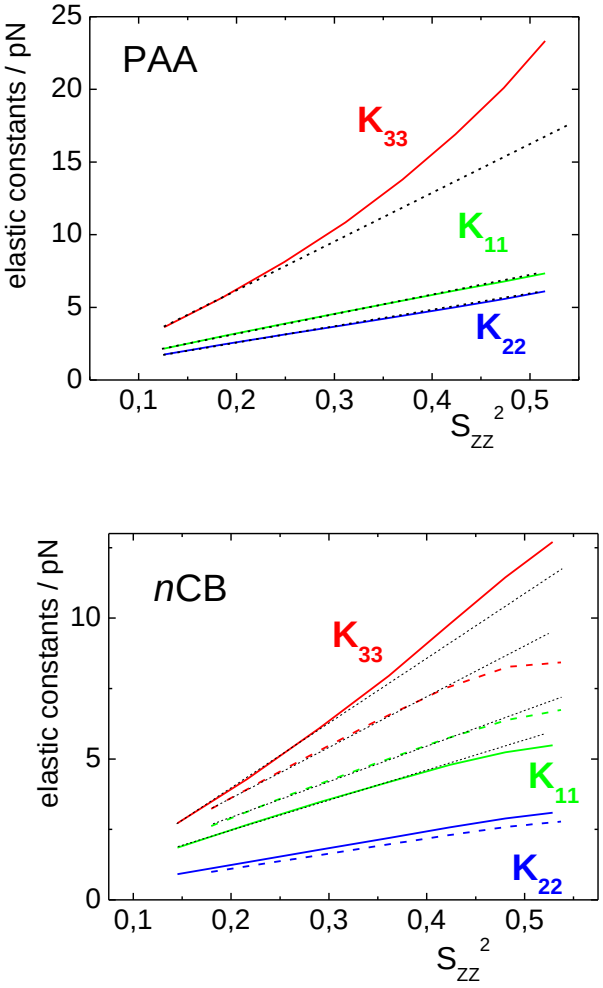
PAA
elastic constants / pN
25
20
15
10
5
0
0,1
0,2
0,3
0,4
0,5
S_{ZZ}^2
K_{33}
K_{11}
K_{22}
*n*CB
elastic constants / pN
10
5
0
0,1
0,2
0,3
0,4
0,5
S_{ZZ}^2
K_{33}
K_{11}
K_{22}

Figure 9

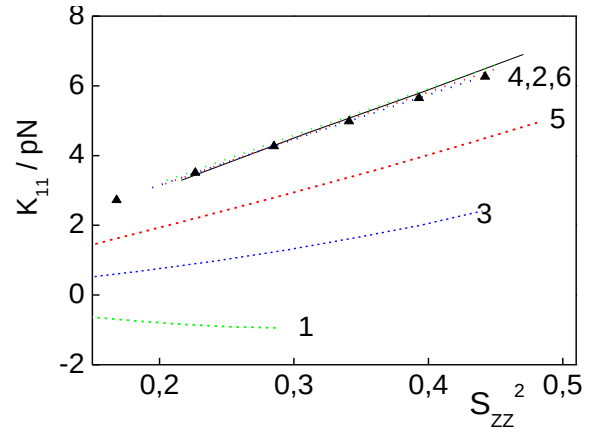
8
6
4
2
0
-2
K11 / pN
4,2,6
5
3
1
0,2
0,3
0,4
0,5
Szz 2

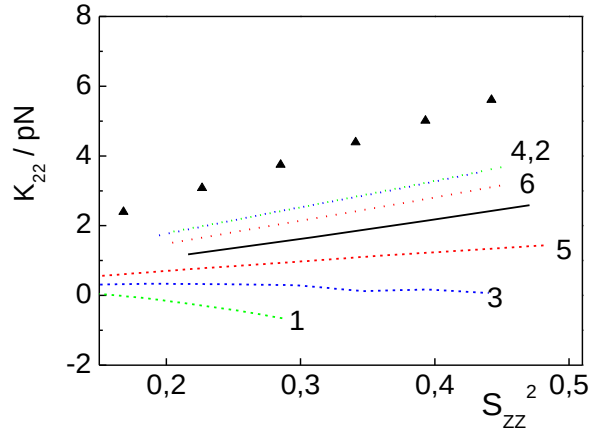
8
6
4
2
0
-2
K22 / pN
4,2
6
5
3
1
0,2
0,3
0,4
0,5
Szz 2

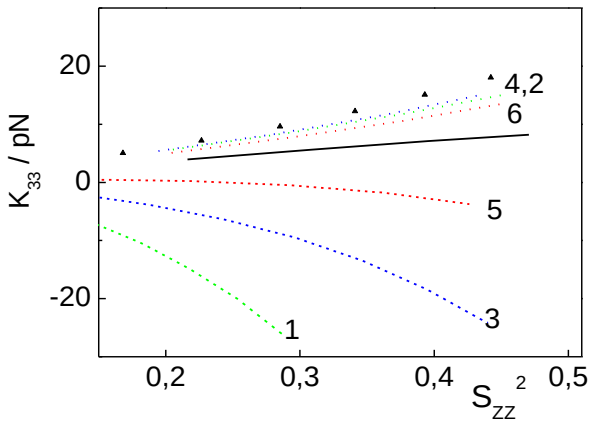
20
0
-20
K33 / pN
4,2
6
5
3
1
0,2
0,3
0,4
0,5
Szz 2

Figure 10

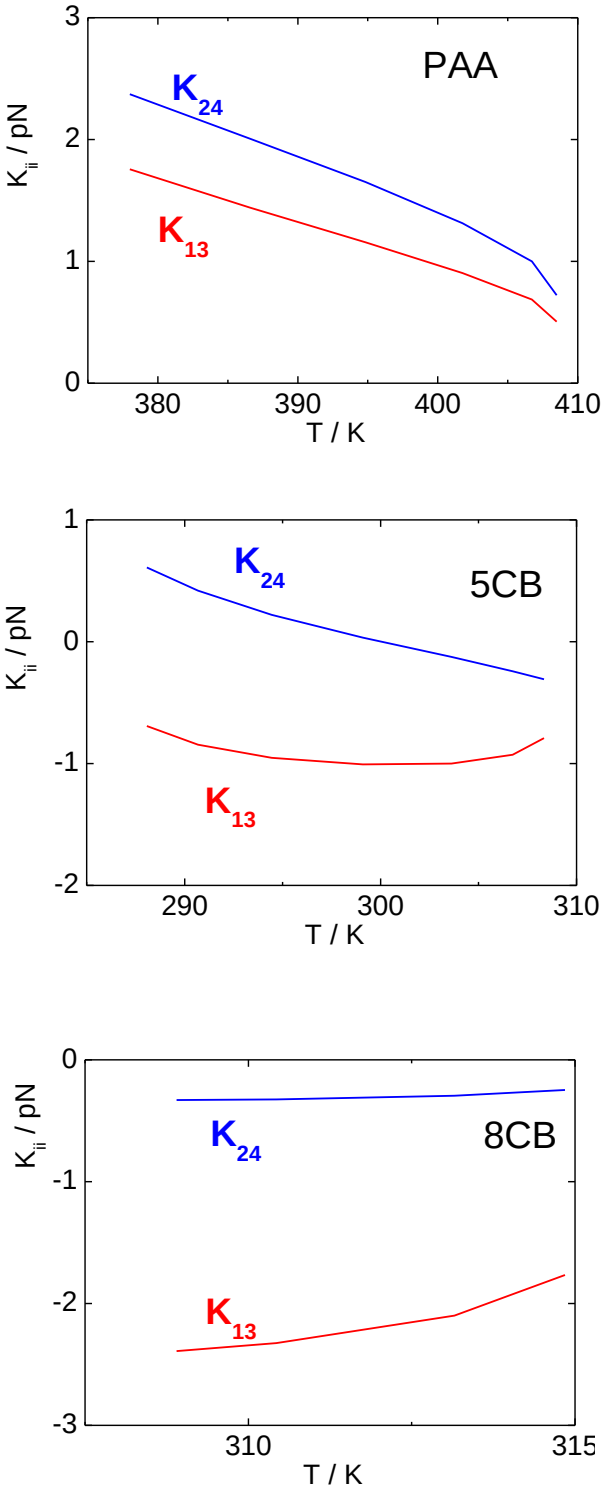

6

Results

Rotational Isomeric State approximation

6.1 Introduction

In this chapter we shall present the results obtained for the dielectric and elastic liquid crystal properties of CBOnOCB and CBOnOFF dimers, using the RIS approximation to take into account the molecular flexibility.

The number of conformers included in the calculations for each of the investigated systems is reported in Table 6.1. For symmetry reasons, this number for the CBOnOCB series is about a half of the number necessary for the CBOnOFF series.

Table 6.1: Number of conformers included in the calculations as a function of the number n of methylenes in the flexible spacer.

n	**CBOnOCB**	**CBOnOFF**
4	166	-
5	485	975
6	1368	2705
7	3250	6380
8	6700	13524

The chapter is organised as follows: firstly the ordering and thermodynamic properties at the NI transition will be presented; then, flexoelectric, dielectric and elastic properties will be reported. The theoretical predictions will be discussed in comparison to experimental data, when these are available.

6.2 Order parameters and NI transition properties

Figure 6.1 displays S_{zz}, the order parameter for the *para* axis of the biphenyl groups, as a function of the reduced temperature $T^* = T/T^{NI}$, where T^{NI} is the nematic isotropic transition temperature, for CBOnOCB and CBOnOFF dimers. For the sake of comparison, the results obtained for 5OCB are also reported in the same plot.

A clear difference appears between odd and even CBOnOCB dimers: at a given reduced temperature, the former have higher, the latter lower order parameters than 5OCB. Analogous behaviour is displayed by the CBOnOFF dimers, though these are generally lower.

Such odd-even effects were also observed experimentally; Table 6.2 reports the order parameters for the *para* axis of the biphenyl groups of the CBOnOCB dimers at the NI transition, obtained from NMR measurements [18, 72, 73], and those derived from measurements of the birefringence at a reduced temperature $T^* \sim 0.95$ [74].

Table 6.2: Experimental values of the order parameters S_{sz} at different temperatures, as a function of the number n of methylene groups in the flexible spacer.

nOCB				
			T^{NI} / K	S_{zz} [16]
5OCB			341	0.28
	CBOnOCB			
n	T^{NI} / K	S_{zz}^{NI} [18, 72, 73]	T / K	S_{zz} [74]
4	523	-	499	0.59
5	459	0.31	433	0.47
6	494	0.45	491	0.59
7	454	0.32	429	0.50
8	474	0.48	451	0.59

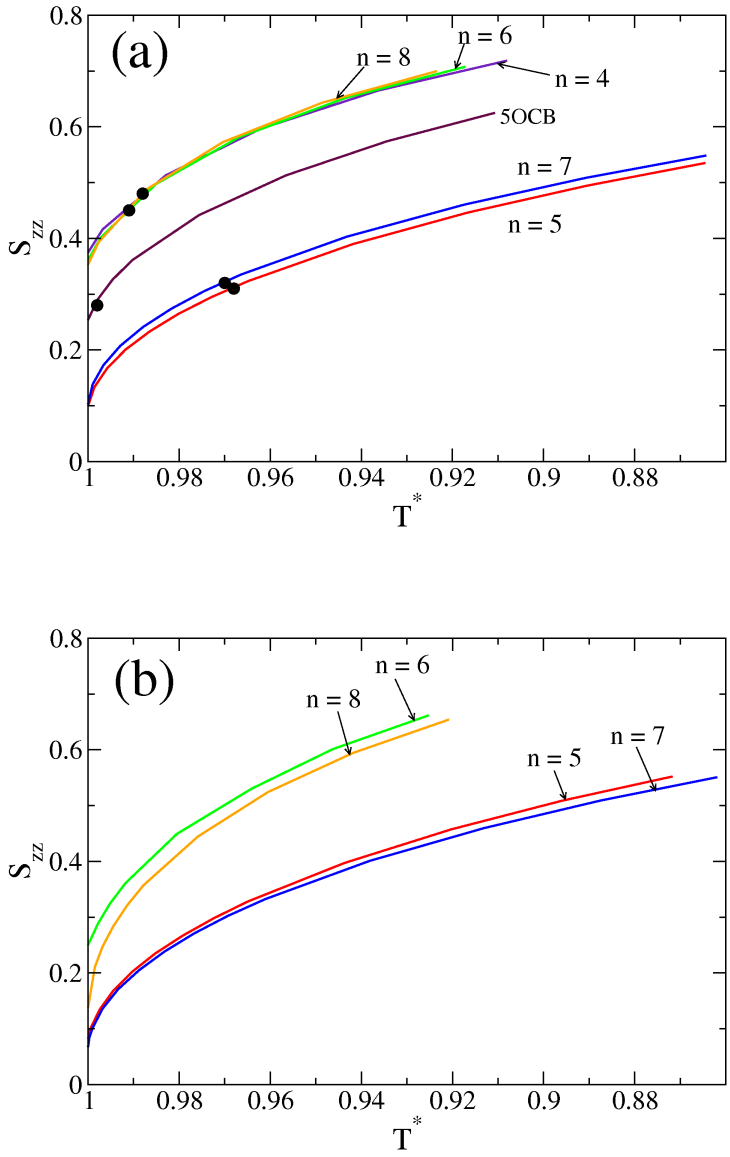

Figure 6.1: Calculated order parameter S_{zz} as a function of the reduced temperature $T^* = T/T_{NI}$ for the CBOnOCB (a) and CBOnOFF (b) dimers, and for 5OCB, whose chemical structures are reported in Figure 1.5. The order parameter S_{zz} is the largest principal value of the Saupe matrix and n is the number of methylene groups in the flexible spacer. The black circles denote the experimental values of S_{zz} at the NI transition found for CBOnOCB (a) and reported in Table 6.2.

If we compare the calculated results, displayed in Figure 6.1a, with the experimental data reported in Table 6.2, we can see that the order parameter for 5OCB at the NI transition is correctly predicted and those for even CBOnOCB dimers are slightly underestimated; the discrepancy increases in the case of odd dimers, for which too low order parameters are predicted at the NI transition. The experimental order parameters at the NI transition are shown by black circles in Figure 6.1.

Table 6.3 collects the entropy changes at the NI transition, $\Delta S^{NI}/R$, calculated as explained in Sec. 2.4.2. The measured entropy changes for CBOnOCB dimers are also reported in the table. Only qualitative agreement is found: the calculated values display strong odd-even effects, as the experimental data, but the predicted entropy changes are too small. The agreement between experimental and calculated data considerably improves, if the nematic-isotropic entropy differences are calculated at order parameters equal to the experimental values, shown in Table 6.2.

Table 6.3: Experimental (Ref. [18]) and calculated entropy difference at the NI transition, ΔS^{NI}, as a function of the number n of methylene groups in the alkyloxy chain. The numbers in brackets give the values calculated at the experimental S_{zz}^{NI} value (see Table 6.2).

	CBOnOCB			**CBOnOFF**
	$\Delta S^{NI}/R$			$\Delta S^{NI}/R$
n	exp.	calc.		calc.
4	-	-0.70		-
5	-0.66	-0.06	(-0.55)	-0.04
6	-1.98	-0.70	(-1.07)	-0.32
7	-0.78	-0.06	(-0.60)	-0.03
8	-2.01	-0.72	(-1.33)	-0.11

Indeed, the location of the NI transition can be critical. It is identified as the point at which the Helmholtz free energy difference between nematic and isotropic phases vanishes, $\Delta A^{NI} = 0$. As explained in chapter 2, in our mean field calculations the free parameter is ε, the orienting strength in the nematic phase. The entropy difference and the internal energy difference between the nematic and isotropic phases are decreasing functions of ε, i.e. they decrease with increasing order. The NI transition results from the trade-

off between these two contributions, and can be significantly affected by relatively small changes in the orienting potential $U(\Omega)$.

This point is illustrated by the simple model of nematics composed by rigid molecules; the orienting potential can be expressed by the generalised Maier-Saupe form [75]:

$$U(\Omega) = -c \langle X_{20} \rangle X_{20}(\Omega) \tag{6.1}$$

where Ω are the Euler angles specifying the molecular orientation in the laboratory frame and c is a constant for a given system, related to the strength of intermolecular interactions, which depends on the nature of molecules. The function $X_{20}(\Omega)$ is defined as

$$X_{20}(\Omega) = D^2_{00}(\Omega) + \lambda[D^2_{02}(\Omega) + D^2_{0-2}(\Omega)], \tag{6.2}$$

where $D^2_{0m}(\Omega)$ are elements of Wigner rotation matrices [76] and λ is a parameter specifying the biaxiality of the orienting potential, which can be traced back to the biaxiality of intermolecular interactions. The angular brackets denote the orientational average;

$$\langle X_{20} \rangle = \frac{\int d\Omega X_{20}(\Omega) e^{\langle X_{20} \rangle X_{20}(\Omega)/T^{SC}}}{\int d\Omega e^{\langle X_{20} \rangle X_{20}(\Omega)/T^{SC}}} \tag{6.3}$$

with the scaled temperature $T^{sc} = k_B T/c$. The nematic-isotropic free energy difference, ΔA^{NI}, can then be expressed as function of the order parameter $\langle X_{20} \rangle$ [75] as shown in Sec. 2.4.2. Figure 6.2 shows the order parameter $\langle X_{20} \rangle$, as a function of the scaled temperature T^{sc}, for two different values of the biaxiality parameter, $\lambda = 0.1$ and $\lambda = 0.4$. The curves are obtained by minimising ΔA^{NI} with respect to $\langle X_{20} \rangle$ at each value of the scaled temperature T^{sc}. In the isotropic phase $\langle X_{20} \rangle = 0$, whereas in the nematic phase $\langle X_{20} \rangle > 0$. We can see in the figure that for higher biaxiality the NI transition occurs at a lower value of the scaled temperature.

In the SI model, the orienting potential is parametrised according to the anisometry of the molecular surface; in particular, the biaxiality appearing in the orienting potential is determined by the shape biaxiality of molecules. The location of the NI transition at too low order, and then the underestimation of transition properties, is probably an indication of some overestimation of the biaxiality of the orienting mean field by the SI model. To check this point, we can look at the biaxiality of order, expressed by the difference of the two lowest eigenvalues of the Saupe ordering matrix, $S_{xx} - S_{yy}$. In Table 6.4, the differences measured for CBOnOCB dimers at the NI transition are compared with those

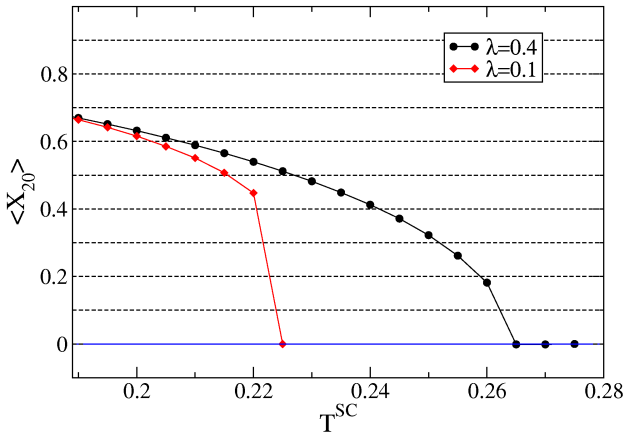

Figure 6.2: $\langle X_{20} \rangle$ order parameter as a function of the scaled temperature T^{sc}, for a model system of rigid biaxial molecules. The two curves refer to different values of the molecular biaxiality (λ).

calculated, in correspondence of the experimental S_{zz} values at the transition. We can see that indeed the predicted biaxiality of order is slightly larger than that determined by experiment and the discrepancy is generally higher for odd dimers. Though differences are small, they can have non negligible effects on the location of the NI transition, just because this is determined by a delicate balance of contributions; the elastic and dielectric LC properties which will be presented in the following are less sensitive to small changes of the biaxiality of the orienting potential.

6.3 Flexoelectric coefficients

In this section we shall present the results obtained for the flexoelectric coefficients of the CBOnOCB and CBOnOFF dimers and the 5OCB monomer, shown in Figure 1.5. Splay and bend flexoelectric coefficients were calculated according to Eqs. 2.17 and 2.18, giving v the volume per molecule, the values obtained from the molecular surface calculation [68]; the set of atomic charges defined in chapter 4 were used.

Experimentally it was found that dimers show a particularly strong flexoelectric coupling, much stronger than that measured for typical mesogens [77], comprising nOCB monomers [12, 13]. Usually, in the literature the flexoelectric behaviour is interpreted in

Table 6.4: Experimental (Ref. [18]) and calculated biaxiality of order, $S_{xx} - S_{yy}$, as a function of the number n of methylene groups in the alkyloxy chain. Experimental and calculated data refer to the value of the S_{zz} order parameters measured at the NI transition (see Table 6.2).

nOCB		
	$S_{xx} - S_{yy}$	
5OCB	calc.	0.07
	CBOnOCB	
	$S_{xx} - S_{yy}$	
n	exp.	calc.
4	-	
5	0.03	0.09
6	0.03	0.06
7	0.04	0.09
8	0.02	0.07

terms of electric and steric dipoles, according to the Meyer model [10]. This is a clever model, which gives a direct insight into the molecular origin of the flexoelectricity. However, when dealing with real molecules the whole charge distribution and the real shape have to be taken into account. For example, vanishing flexoelectric coefficients would be predicted for the even CBOnOCB dimers on the basis of simple considerations on the all-*trans* conformer, in clear contrast to the experimental evidence.

Figure 6.3 reports the flexoelectric coefficients e_1 and e_3 calculated for the CBOnOCB and CBOnOFF dimers, as a function of the order parameter S_{zz}, the highest principal value of the Saupe matrix. For the sake of comparison, the flexoelectric coefficients calculated for 5OCB are also reported.

We can see in Figure 6.3a that the splay coefficients of the CBOnOCB dimers have approximately the same dependence on order, independently of the number n of methylene units in the spacer. For all compounds e_1 is positive and steadily grows with the order parameter S_{zz} in the examined range. A similar behaviour is found for the CBOnOFF dimers in Figure 6.3b, but the slope of e_1 as a function of S_{zz} is lower in this case, by almost a factor of two. We can see in Figure 6.3a that also the splay flexoelectric coefficient

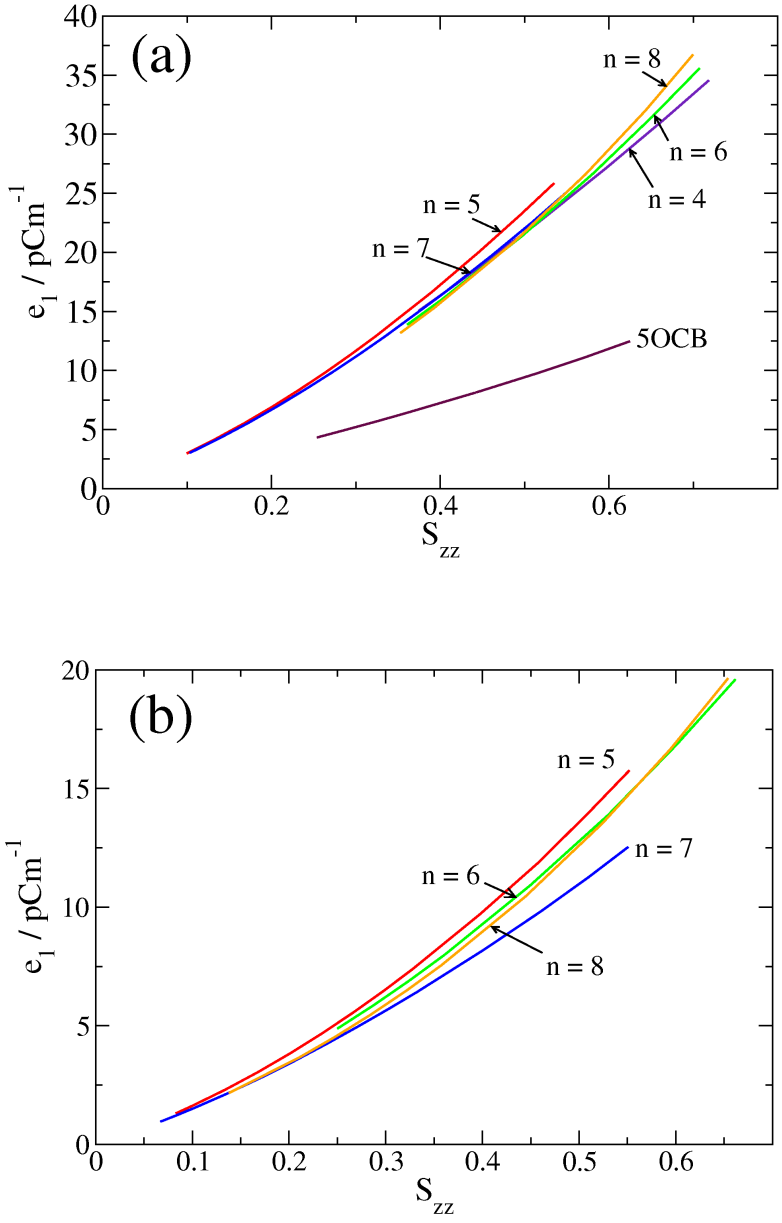

Figure 6.3: Splay flexoelectric coefficient e_1 calculated for the CBOnOCB (a) and CBOnOFF (b) dimers and for 5OCB as a function of the order parameter S_{zz}, the largest principal value of the Saupe matrix. n is the number of methylene groups in the spacer.

calculated for 5OCB is positive and increases with the degree of order; however it is much lower than that of dimers, despite the presence of a strong longitudinal electric dipole.

From our results we infer that the splay flexoelasticity of the systems under investigation does not strongly depend on specific molecular features or on the presence of net dipoles, but is determined in a more general way by the overall distribution of charges in an extended space region, as described by higher order electric multipoles.

Figure 6.4 shows the bend flexoelectric coefficients of the CBOnOCB and CBOnOFF dimers, in addition to that of 5OCB. We can see that e_3 exhibits strong odd-even differences; it is large, and increases with the order parameter for even dimers, whereas for the odd dimers it is much smaller and reaches a maximum at $S_{zz} \sim 0.3$. Again, similar behaviour is predicted for CBOnOCB and CBOnOFF dimers, though smaller values are obtained in the latter case. The e_3 coefficient calculated for 5OCB exhibits a dependence on order analogous to that of the even CBOnOCB dimers, but it is significantly smaller.

We can try to understand the results obtained for the bend flexoelectric coefficient in terms of the bend angle β between the cyanobiphenyl units and the transverse electric dipole moment $\mu_\perp$. The all-*trans* conformer of odd CBOnOCB dimers has a significant transverse electric dipole, whereas no net dipole is present in the all-*trans* conformers of even dimers. However the situation can strongly change from one conformer to another, by virtue of the change of the angle between the cyanobiphenyl units, which are responsible for the major contribution to the molecular dipole. Figure 6.5 shows the probability distribution of the β angle for CBO5OCB and CBO6OCB, calculated at two different values of the S_{zz} order parameter. We can see that the distribution looks quite different for the odd and the even dimer. In the case of CBO5OCB, the probability is concentrated in the region $90° < \beta < 150°$; this means that most of the conformers will bear a transverse dipole. On the other hand, for CBO6OCB high probability around 180° is predicted, i.e. antiparallel cyanobiphenyls, in addition to a rather broad distribution comprising the region $30° < \beta < 120°$. Thus, in the average, a significantly higher transverse dipole is expected for CBO5OCB than for CBO6OCB. According to the Meyer model [10], bent molecules with an outward pointing transverse dipole should yield a negative e_3 coefficient (see Figure 1.4). So, the differences between the bend flexoelectric coefficients of odd and even CBOnOCB dimers, in Figure 6.4, are compatible with the following picture: the quadrupolar contribution is similarly large and positive in both systems, whereas the

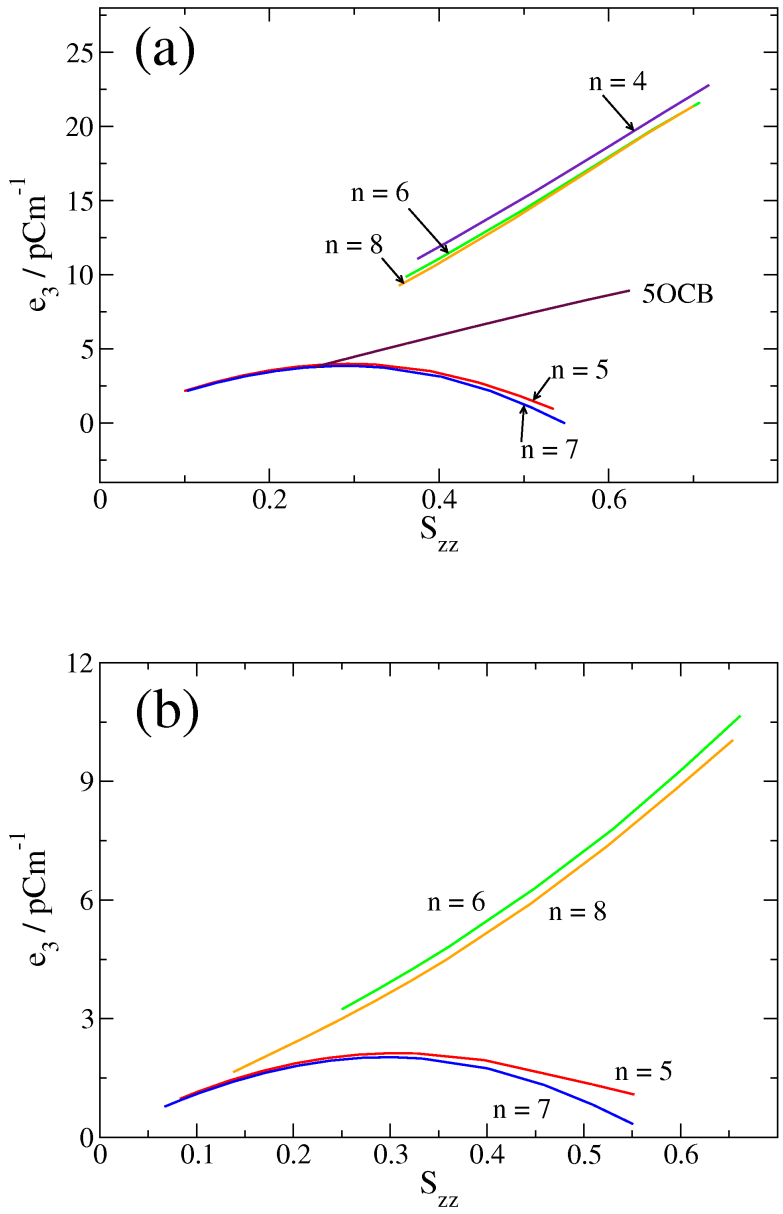

Figure 6.4: Bend flexoelectric coefficient e_3 calculated for the CBOnOCB (a) and CBOnOFF (b) dimers and for 5OCB as a function of the order parameter S_{zz}, the largest principal value of the Saupe matrix. n is the number of methylene groups in the spacer.

dipolar contribution is much higher for odd dimers. Being negative, it has the effect of significantly reducing the overall e_3 value.

For the comparison with experiments, the relevant quantity is the *flexoelastic ratio*, defined as [12, 13]:

$$e = \frac{\bar{e}}{K} \tag{6.4}$$

where $\bar{e}$ is one half of the flexoelastic anisotropy:[1]

$$\bar{e} = \frac{e_1 - e_3}{2} \tag{6.5}$$

and K is the effective elastic constant:

$$K = \frac{K_{11} - K_{33}}{2} \tag{6.6}$$

with K_{11} and K_{33} being the splay and bend elastic constants.

Figure 6.6 shows the difference $\bar{e}$ calculated for the CBOnOCB and the CBOnOFF dimers as a function of the order parameter S_{zz}. It follows from the expressions of the flexoelectric coefficients, Eqs. 2.17 and 2.18, that the difference $\bar{e}$ is only determined by the dipolar contribution. Thus, in view of the considerations presented above, it is not surprising that the values for odd CBOnOCB dimers are significantly higher than those for the even members, at the same order parameter S_{zz}, and both are higher than the value obtained for 5OCB.

6.4 Dielectric permittivity

Experimentally it was found that CBOnOCB dimers exhibit positive, yet modest dielectric anisotropy $\Delta\epsilon = \epsilon_{\parallel} - \epsilon_{\perp}$, in comparison to the corresponding monomers nCBO [12–14]. This result is not obvious, especially for odd dimers. In fact, from simple considerations on the all-*trans* conformer, a vanishing dipole contribution to the permittivity would be expected for even dimers (with no electric dipole), along with negative dielectric anisotropy for the odd members (with transverse dipole), as shown in Figure 6.7.

The molecular flexibility has to be considered to explain the experimental findings; the alkyl spacer guarantees a certain degree of decoupling of the terminal dipoles and

[1] Note that due to a different definition of the e_3 sign, Coles and coworkers define the flexoelectric anisotropy as $e^* = e_1 + e_3$ [12, 13].

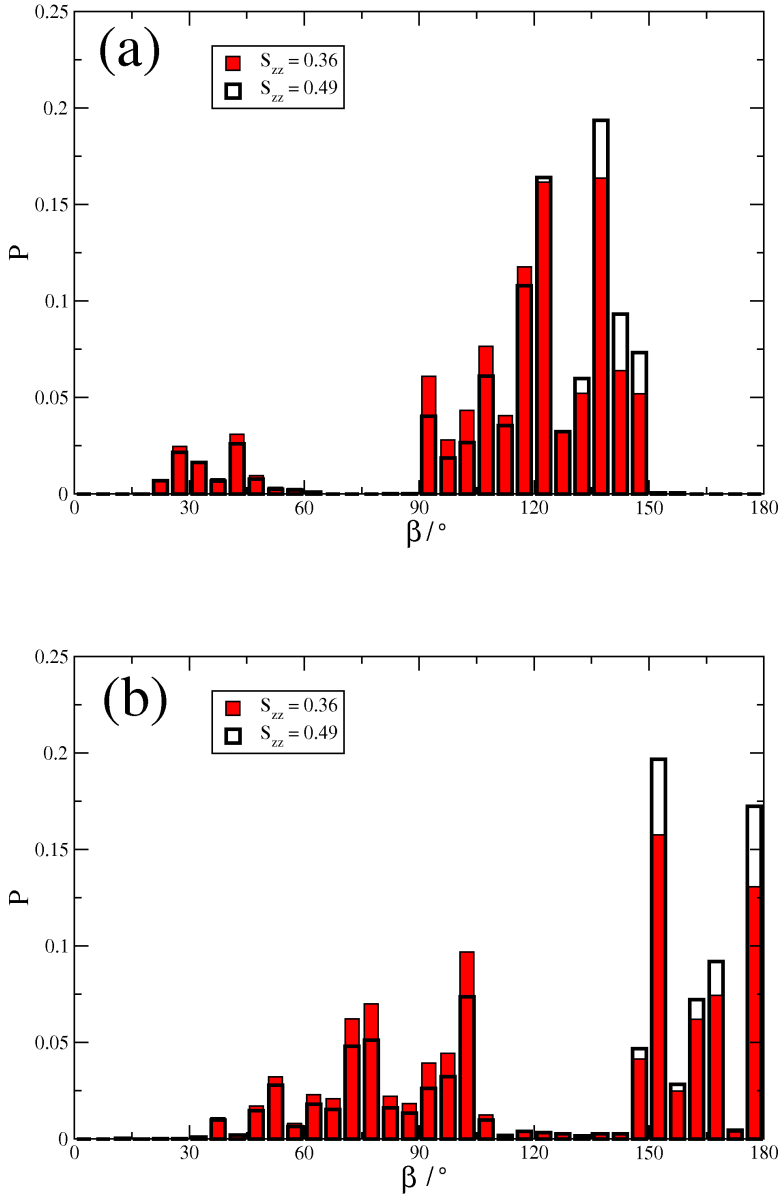

Figure 6.5: Probability distribution of the angle β between the *para* axes of the two cyanobiphenyl units, calculated for CBO5OCB (a) and CBO6OCB (b). Red and white are used to distinguish the distributions obtained with order parameter $S_{zz} = 0.36$ and $S_{zz} = 0.49$, respectively

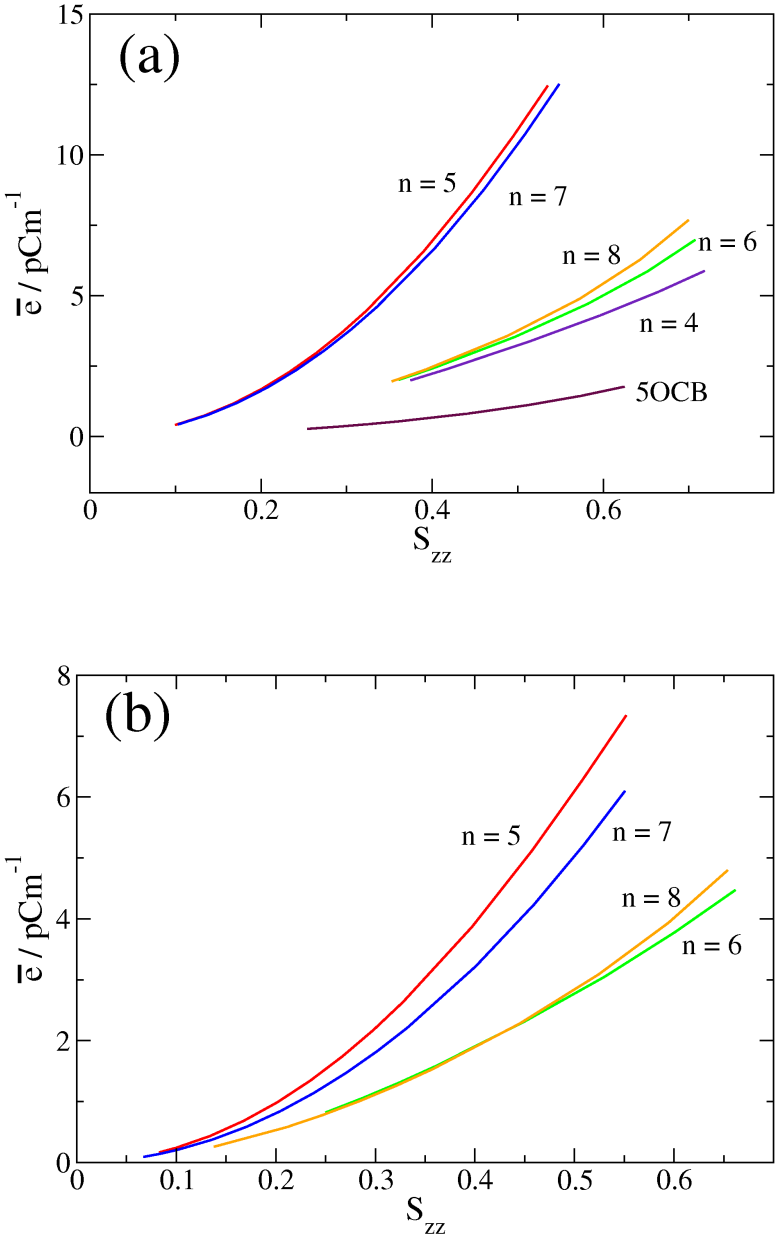

Figure 6.6: Flexoelectric difference $\bar{e} = (e_1 - e_3)/2$ calculated for the CBOnOCB (a) and CBOnOFF (b) dimers as a function of the order parameter S_{zz}, the largest principal value of the Saupe matrix. n is the number of the methylene units in the spacer

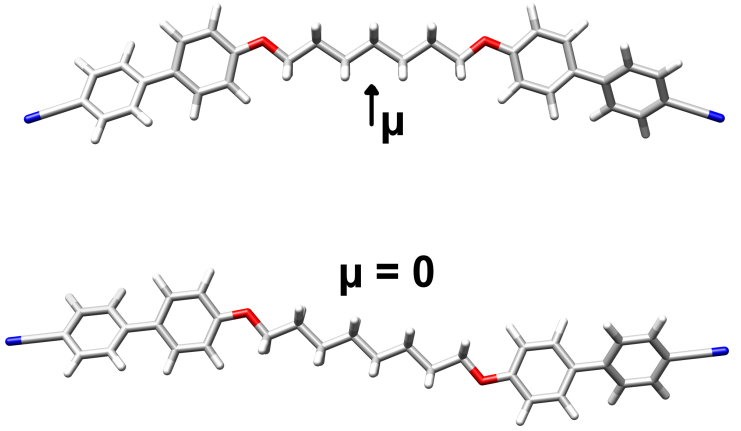

Figure 6.7: All-*trans* conformer of CBO7OCB and CBO8OCB.

allows molecular conformations with a dipole component parallel to the long molecular axis to give a significant contribution. Figure 6.8 shows $\epsilon_{\parallel}$ and $\epsilon_{\perp}$, the components of the permittivity tensor parallel and perpendicular to the nematic director, measured for the symmetric CBO10OCB [78] and CBO11OCB [79] dimers. Another interesting feature appears in the figure: the dielectric anisotropy $\Delta\epsilon$ decreases with lowering temperature, i.e. as ordering increases. This is the opposite of the usual behaviour of nematics formed by mesogens with longitudinal dipole [30], whose dielectric anisotropy increases with the alignment to the director.

With the purpose of understanding the temperature dependence of the dielectric anisotropy of the nematic phase of CBOnOCB and CBOnOFF dimers, we have calculated the mean square dipole components parallel and perpendicular to the director, $\left\langle \mu^2_{\parallel(\perp)} \right\rangle$. These are related to the static permittivity by Eq. 2.12. Being interested in the anisotropy of the permittivity, rather than in its average value, we have reported in the figures the ratio $\left(\left\langle \mu^2_{\parallel(\perp)} \right\rangle - \langle \mu^2 \rangle_{\text{iso}} \right) / \langle \mu^2 \rangle_{\text{iso}}$, where $\langle \mu^2 \rangle_{\text{iso}}$ is the mean square value of the dipole in the isotropic phase. The temperature dependence of the mean square dipole components was determined using Eq. 2.11.

For the sake of comparison, the results obtained for 5OCB are shown in Figure 6.9. Here we can see the normal behaviour of mesogens with longitudinal dipole, with $\left\langle \mu^2_{\parallel} \right\rangle - \left\langle \mu^2_{\perp} \right\rangle > 0$, which increases with lowering temperature.

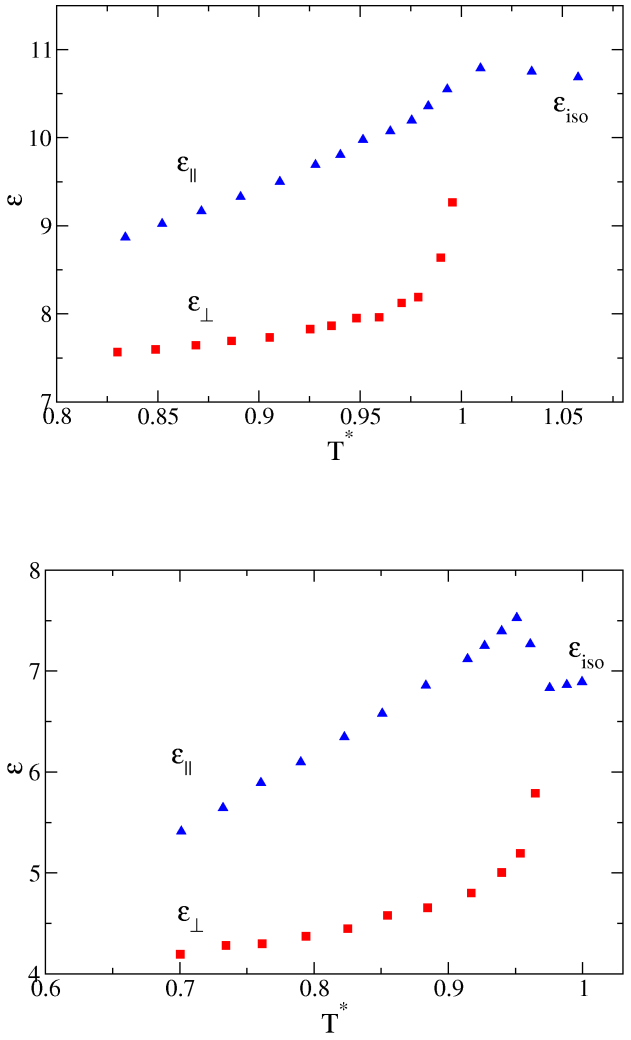

Figure 6.8: Experimental dielectric permittivity as a function of the temperature for the CBO10OCB (top) and CBO11OCB (bottom), from Refs [78] and [79], respectively.

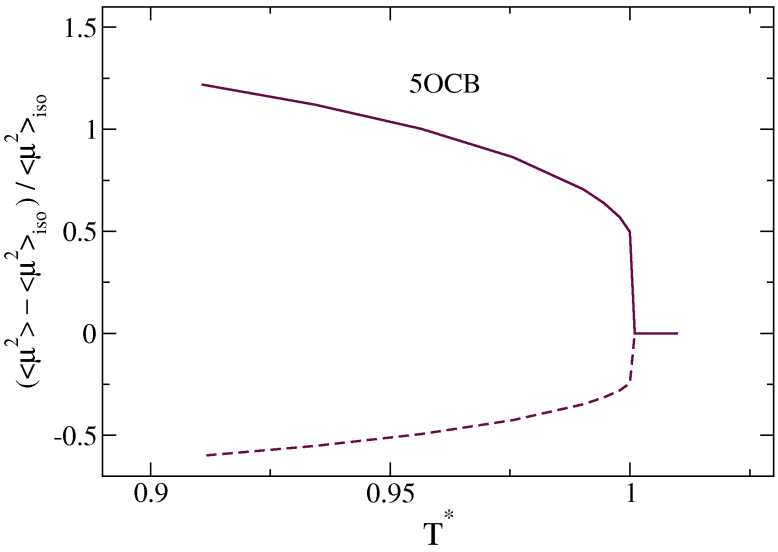

Figure 6.9: Scaled dipole moment $\left(\langle\mu^2_{\parallel(\perp)}\rangle - \langle\mu^2\rangle_{\rm iso}\right) / \langle\mu^2\rangle_{\rm iso}$ as a function of the reduced temperature T^*, calculated for the monomer 5OCB. Continuous and dashed lines indicate the parallel and perpendicular component, respectively.

Figures 6.10 and 6.11 display the square dipole components of CBOnOCB and CBOnOFF dimers, obtained from our calculations, as a function of the reduced temperature T^*. For all the systems under investigation we have obtained $\left\langle\mu^2_{\parallel}\right\rangle > \langle\mu^2_{\perp}\rangle$, in keeping with the experimental data [12–14]. For CBOnOCB dimers, the ratio $\left(\left\langle\mu^2_{\parallel(\perp)}\right\rangle - \langle\mu^2\rangle_{\rm iso}\right) / \langle\mu^2\rangle_{\rm iso}$ increases with the length of the alkyl spacer, which can be ascribed to the weakening of the correlation between the molecular arms and the stabilisation of the more elongated conformers. In the case of even CBOnOCB dimers, the temperature dependence of $\left\langle\mu^2_{\parallel}\right\rangle$ and $\langle\mu^2_{\perp}\rangle$ is in qualitative agreement with that found experimentally for the member with n=12. Somewhat larger differences between theoretical and experimental data appear for the odd members.

For CBOnOFF dimers the ratio $\left(\left\langle\mu^2_{\parallel(\perp)}\right\rangle - \langle\mu^2\rangle_{\rm iso}\right) / \langle\mu^2\rangle_{\rm iso}$ is generally larger than for the corresponding CBOnOCB dimers. A relatively small influence of the spacer length is found among the odd members, as well as among the even members, in agreement with the experimental finding that $\Delta\epsilon$ is practically the same for different odd dimers ($n = 5, 7, 9, 11$) and for different even dimers ($n = 6, 8, 10, 12$) [12].

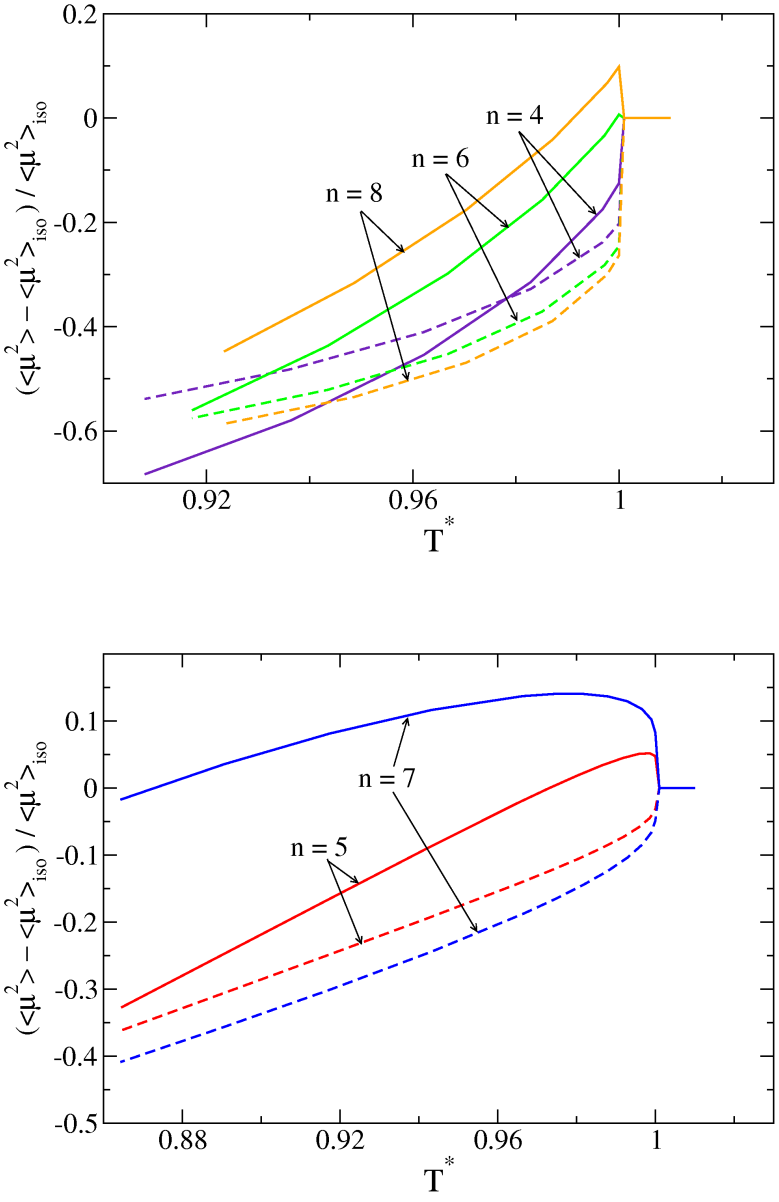

Figure 6.10: Scaled dipole moment $\left(\langle\mu^2_{\parallel(\perp)}\rangle - \langle\mu^2\rangle_{\mathrm{iso}}\right) / \langle\mu^2\rangle_{\mathrm{iso}}$ as a function of the reduced temperature T^*, calculated for the CBOnOCB dimers. Top: even dimers; bottom: odd dimers. n is the number of the methylene units in the spacer. Continuous and dashed lines indicate the parallel and perpendicular components, respectively.

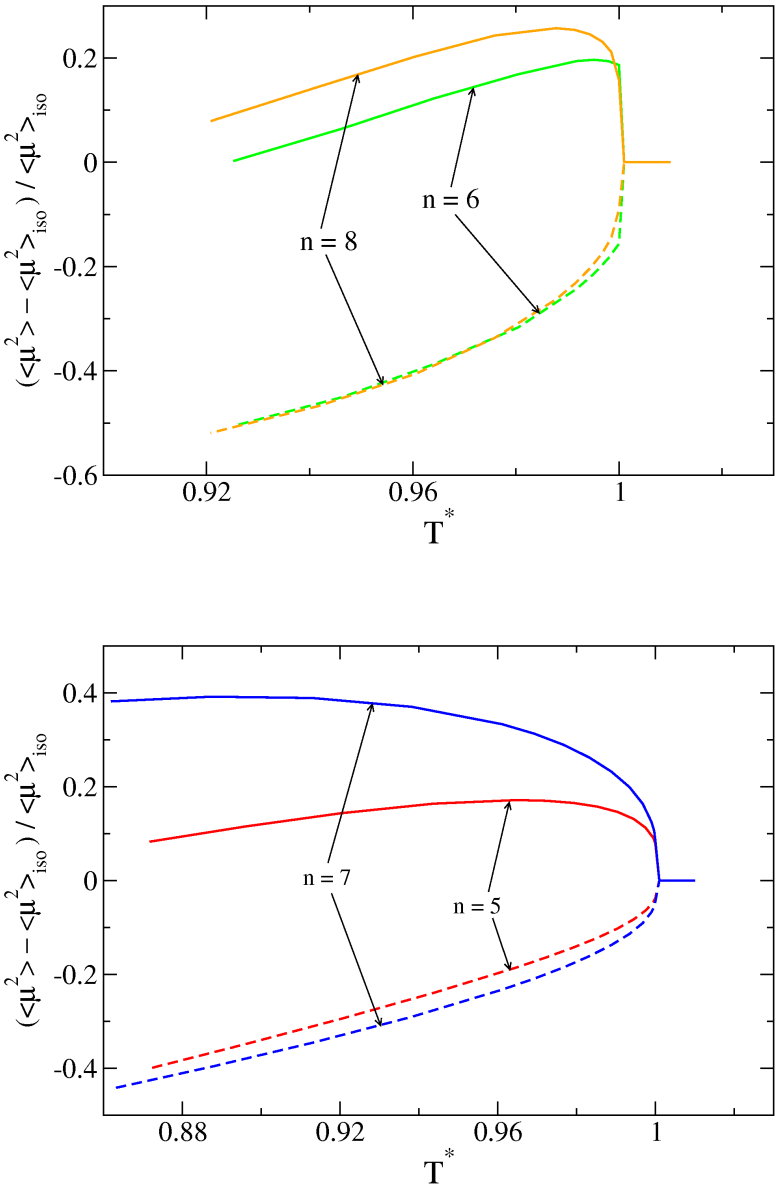

Figure 6.11: Scaled dipole moment $\left(\langle\mu^2_{\parallel(\perp)}\rangle - \langle\mu^2\rangle_{\mathrm{iso}}\right) / \langle\mu^2\rangle_{\mathrm{iso}}$ as a function of the reduced temperature T^*, calculated for the CBOnOFF dimers. Top: even dimers; bottom: odd dimers. n is the number of the methylene units in the spacer. Continuous and dashed lines indicate the parallel and perpendicular components, respectively.

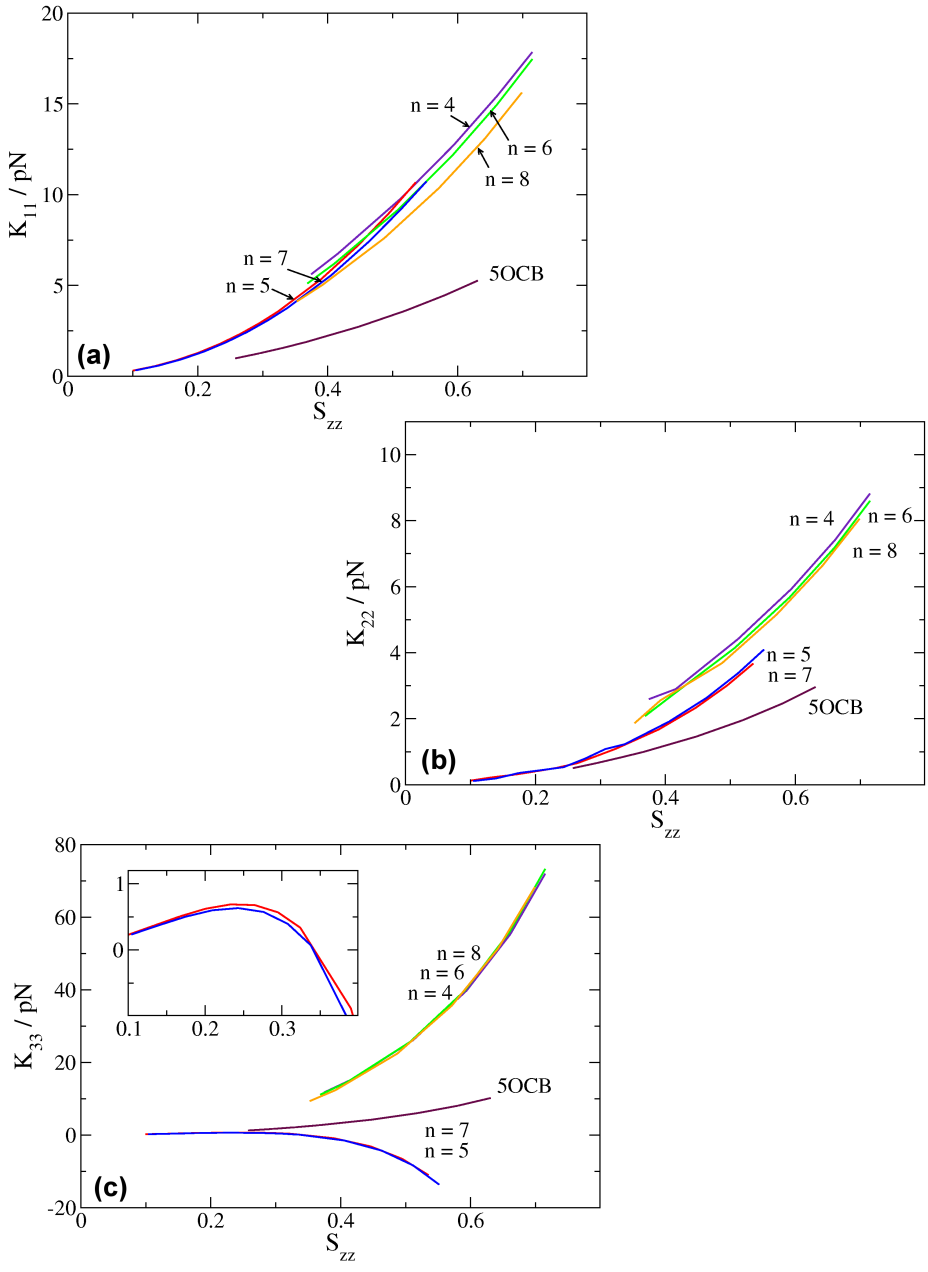

Figure 6.12: Elastic constants calculated for CBOnOCB dimers as a function of the order parameter S_{zz}, the largest principal value of the Saupe matrix. n is the number of methylenes in the flexible spacer. The onset shows that K_{33} is slightly positive at lower order.

6.5 Elastic constants

Figure 6.12 shows the splay, twist and bend elastic constants of the CBOnOCB dimers as a function of S_{zz}, the largest eigenvalue of the Saupe matrix. For the sake of comparison, also the results obtained for the 5OCB monomer are shown. We can see that the splay stiffness for dimers is significantly higher than that of 5OCB and similar dependence on the order parameter is exhibited by odd and even dimers: at the same S_{zz} value, very close splay moduli are predicted for them. Analogous considerations can be made for the twist elastic constants, although some more differences appear between odd and even dimers; for all compounds $K_{22} < K_{11}$, as usual for thermotropic low molar mass mesogens. A more peculiar behaviour is exhibited by the bend stiffness which, as already shown for some typical mesogens in chapter 5, is more sensitive to changes in the molecular structure. Here, huge odd-even differences appear, with K_{33} (Figure 6.12c) much higher than that of the monomer for even dimers, and much lower for odd dimers. On one side, the big values obtained for even dimers can be explained by their large molecular dimension; in fact, stiff polymers are characterised by high bending stiffness [80]. On the other side, the drop of the K_{33} values calculated for odd dimers can be traced back to their V-shape; the importance of deviations from a linear shape emerged from the study of the elastic constants of typical mesogens, in chapter 5. Figure 6.13 shows that the elastic constants calculated for members of the CBOnOFF and the CBOnOCB series have similar temperature dependence, though the former have smaller magnitude.

It is interesting to analyse whether our results are affected by the molecular flexibility. In Figure 6.14 the elastic constants obtained for CBO7OCB and CBO8OCB after averaging over all conformers are compared with the values calculated for the single all-*trans* conformers. Somehow surprisingly, we can see that the K_{ii} values for the all-*trans* conformer of CBO7OCB, though smaller than those for the all-*trans* conformer of CBO8OCB, exhibit analogous temperature dependence. The influence of conformational averaging can be easily understood in the case of CBO8OCB. The very elongated all-*trans* conformer is expected to be highly ordered and to give a strong contribution to the stiffness in the nematic phase; this effect is washed out by the other, less extended conformers. The same considerations can apply to CBO7OCB, but with a more dramatic result, by virtue of the more bent shape, in the average, of this compound. Figure 6.15 shows the

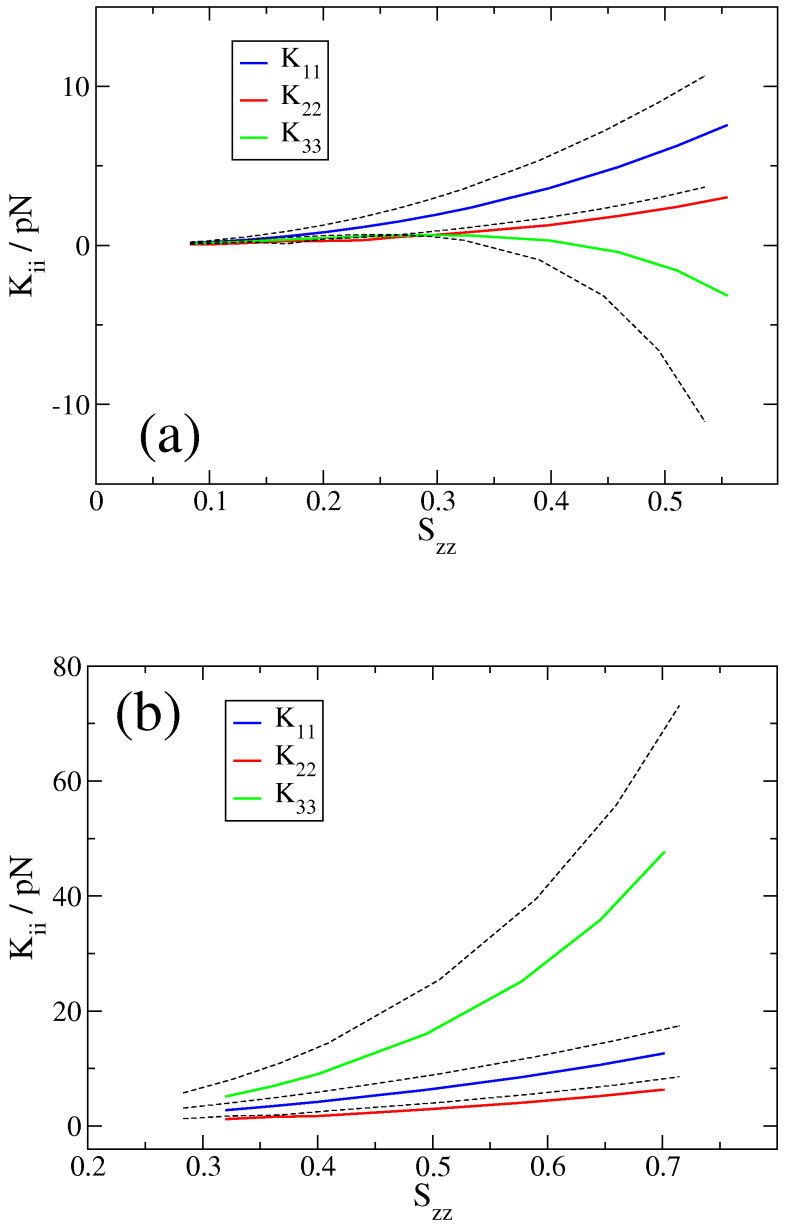

Figure 6.13: Elastic constants calculated for the CBO5OFF (a) and CBO6OFF (b) dimers. For the sake of comparison, the elastic constants for CBO5OCB (a) and CBO6OCB (b) are also reported (dashed lines).

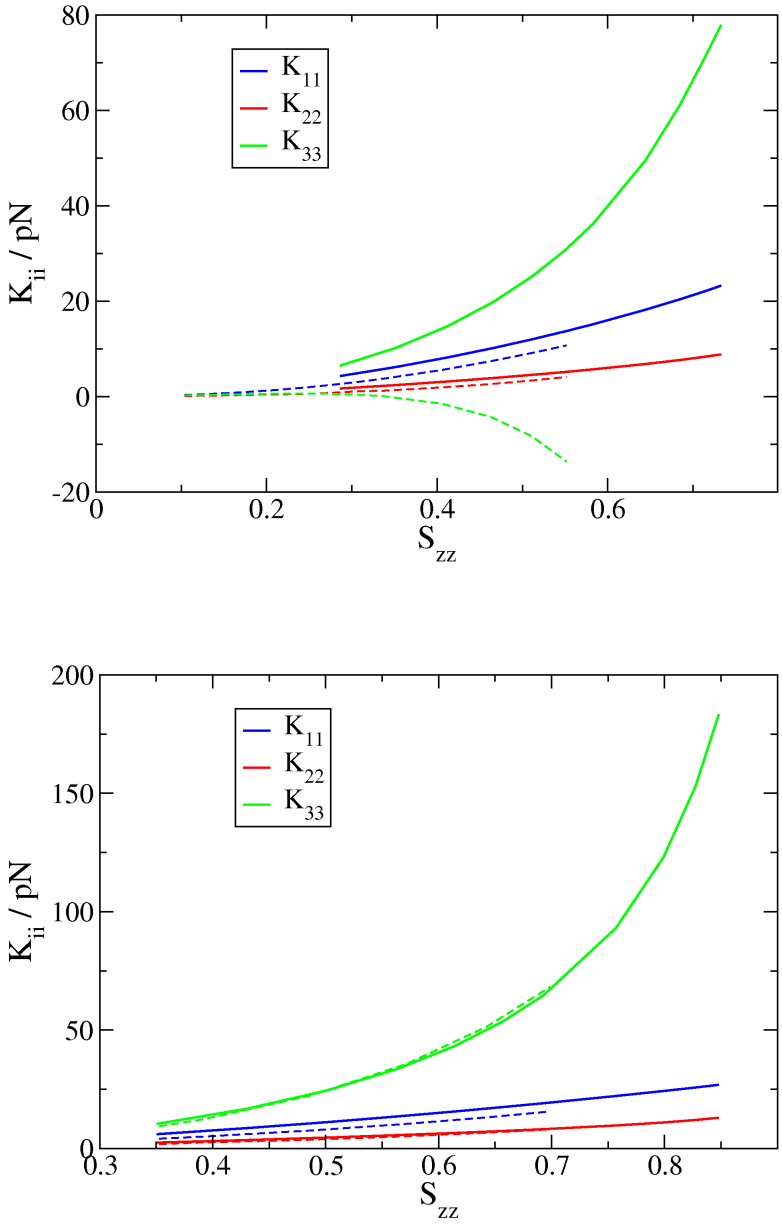

Figure 6.14: Elastic constants calculated for the all-*trans* conformer of CBO7OCB (top) and CBO8OCB (bottom), as a function of the order parameter S_{zz}, the largest principal value of the Saupe matrix. For the sake of comparison, the elastic constants obtained after averaging over all conformers are also reported (dashed lines).

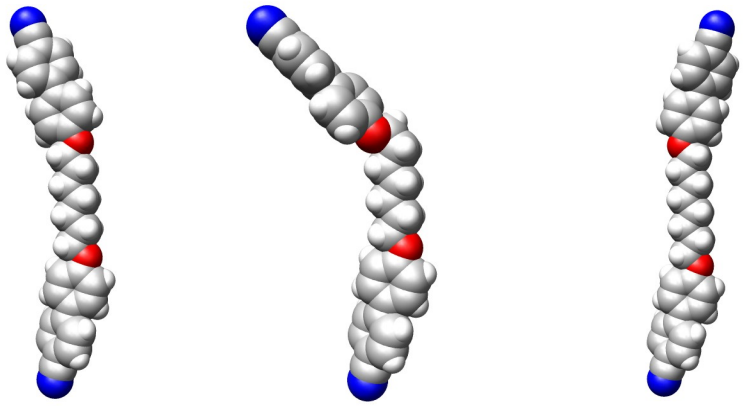

Figure 6.15: CPK representation of the all-*trans* (left) and the tg^+ttttt (centre) conformers of CBO7OCB, and of the all-*trans* conformer of CBO8OCB (right).

all-*trans* conformer of CBO7OCB together with another conformer, with a *gauche* in the second chain bond, for which low K_{11} and K_{22} and very negative K_{33} are predicted. We can see that the shape of the all-*trans* conformer of CBO7OCB is only slightly more bent than that of the all-*trans* conformer of CBO8OCB, but the other conformer has a clear V-shape.

In Figure 6.16 we can see that the splay and twist elastic constants of odd and even CBOnOCB dimers are approximately proportional to S_{zz}^2, with a similar proportionality factor, larger than for the monomer. On the contrary, the dependence of K_{33} on S_{zz}^2 exhibits significant deviations from linearity.

We can try to compare our predictions with the experimental behaviour. The elastic constants predicted for 5OCB fall in the range typical of most low molar mass rod-like mesogens (see for instance the results reported in chapter 5), and are in keeping with the experimental data reported for this system [81]. More unusual, and in this sense more interesting, is the behaviour predicted for dimers. Scarce experimental information is available in this case; however, the good agreement found for systems allowing a comparison with experiments (for example those presented in chapter 5), gives us confidence in our predictions. The splay elastic constants of CBOnOCB dimers were measured by Tsvetkov and coworkers [14]; their results at the temperatures reported in the fourth column of Table 1.1 are shown in Figure 6.17. We can see clear odd-even effects: val-

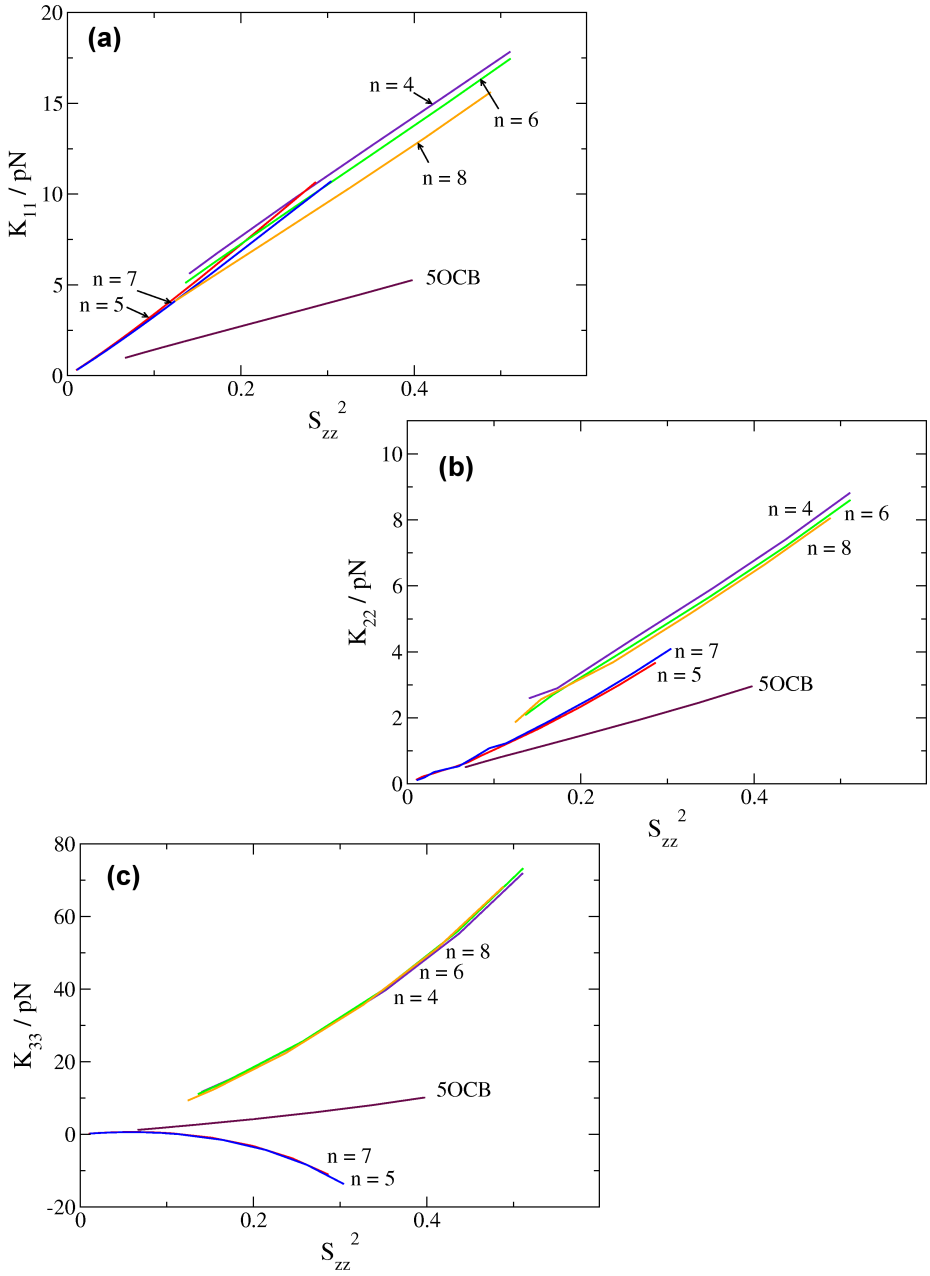

Figure 6.16: Elastic constants calculated for CBOnOCB dimers as a function of the square of the order parameter S_{zz}, the largest principal value of the Saupe matrix. n is the number of methylenes in the flexible spacer.

ues comparable to those typical of low molar mass mesogens are found for odd dimers, whereas the even homologous exhibit a higher stiffness. In the light of our results, we can explain this behaviour in terms of the different degree of order of odd and even dimers: at the same reduced temperature, the former have lower splay elastic constants because they are less ordered. This is different from the simple interpretation which would ascribe the decrease of resistance to splay deformation to the wedge shape of odd dimers. In Figure 6.17, also the values obtained from our calculations are displayed, and the agreement between theory and experiment clearly appears. Coles and colleagues have measured the splay elastic constants of CBOnOFF dimers with n= $5-12$ at a reduced temperature $T^* \simeq 0.95$ [82]; these are slightly lower than those reported by Tsvetkov for CBOnOCB at a similar reduced temperature [74]. The uncertainty of the experimental data and that affecting the temperature dependence of the calculated elastic constants preclude quantitative comparisons; however the decrease of K_{11} from CBOnOCB at the same reduced temperature is in agreement with our predictions. No experimental values are reported for the twist elastic constants of CBOnOCB or CBOnOFF dimers. Odd-even effects, with lower K_{22} values for odd n values, were inferred for CBOnOCB dimers from ESR experiments [83] and for CBOnOFF dimers from helical twisting power measurements [82]. This can explained by the theoretical results shown in Figures 6.12 and 6.13, in view of the lower degree of order in the nematic phase of odd dimers, at a given reduced temperature. No experimental values are reported for the twist elastic constants of CBOnOCB or CBOnOFF dimers.

The behaviour of the bend elastic constants is particularly intriguing. We can see in Figure 6.12c that K_{33} is very small and positive at low order, but becomes even negative at high ordering. This is a really unexpected result, rich of implications, since negative bending stiffness would promote spontaneous bending of the nematic director. This 'pathological' elasticity was predicted some years ago for V-shaped molecules [84], and was recently invoked to explain the segregation into domains of opposite handedness, exhibited by bent-core mesogens [85]. A negative bend elastic constant was recently assumed to explain the formation of stripe and labyrinthine patterns in freely suspended polar smectic SmCPF films of a bent-core mesogen [86]. No indication of this kind has been reported for the LC dimers under investigation, but certainly these were not studied as thoroughly as bent-core mesogens; we hope that our results can stimulate further

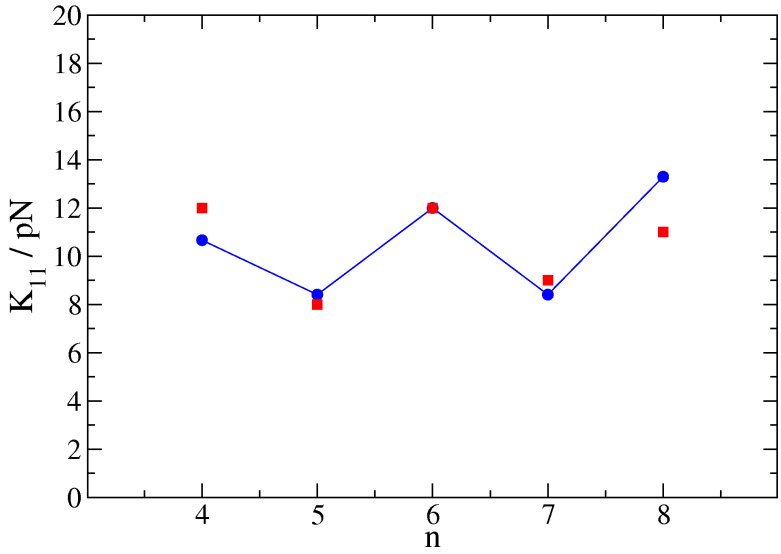

Figure 6.17: Experimental [14] and calculated splay elastic constants of CBOnOCB dimers, at the temperatures reported in the fourth column of Table 1.1. n is the number of methylenes in the flexible spacer.

experimental study of these systems. At the moment, we are not able to assess the degree of reliability of our results and we cannot exclude that the negative K_{33} values derive from the magnification of some effect by our model. We believe anyway that the strong decrease of bend stiffness predicted for odd dimers is physically meaningful. It is a clear manifestation of the relationship between bend elasticity and bent molecular shape, already evidenced in chapter 5 for typical thermotropic mesogens. This seems to be a peculiarity of the bend elasticity. The splay and twist elastic constants do not seem to be especially sensitive to specific molecular features; they rather seem to feel the change of molecular structure in a rather generic way, through a change of orientational order. Probably these aspects have not been sufficiently explored, only a few references can be found in the literature. Gleeson et al. report values of about 2 pN for K_{11} and K_{33} of a bent-core nematic system [87]; the low value of the elastic constants and of the K_{33}/K_{11} ratio can be hardly explained, in comparison to the elasticity of smaller mesogens. Dodge et al. found that a tiny amount of bent-shaped mesogens can dramatically lower the bend elastic constant of rod-like nematics (8OCB) [88], an effect which could not be

explained by simple models. Madhusudana and coworkers [89] measured the splay and bend elastic constants of mixtures of 8OCB and bent-core mesogens. They found that both decrease with increasing concentration of bent-core molecules, but K_{33} exhibits a much stronger change, together with an unexplained temperature dependence. Our results for odd dimers can provide a general explanation for these findings. Of course, the investigation of specific systems is needed to give a definite answer, but we think that our atomistic model can provide new insight into this matter.

To conclude the discussion on the elastic constants of LC dimers, it might be worth mentioning the recent discovery that chirally doped mixtures of odd FFOnOFF dimers can form Blue Phases with a temperature range of about 50°, enormously broader than the typical range of about 1° [15]. This unusual behaviour, very promising for the development of fast response applications, raised a number of questions, first of all on what special properties the employed material should have [90]. Our results suggest that one of the special features could just be the unusual elasticity of LC dimers. The Blue Phases are not fully understood; however, recent calculations have shown that their stability is affected by the relative values of the elastic constants [91].

7

Results

Monte Carlo sampling of conformations

7.1 Introduction

According to the expressions reported in chapter 2, the dielectric and elastic LC properties are calculated as orientational-conformational averages of molecular properties. In the previous chapter we presented the results obtained using the RIS approximation [31] to treat the conformational degrees of freedom.

According to this approximations the fluctuations within the minima of the torsional potential are neglected. This is not justified if the barriers between the minima of the torsional potential are not higher than a few k_BT units. This occurs, for instance, for the torsional potential around the phenyl-methylene bond of the CBnCB dimers, shown in Figure 4.4a. In general, the RIS approximation can be safely adopted for alkyl chains; however, there may be cases in which the small amplitude oscillations in the potential wells can have non-negligible effects. The dimers studied in this thesis could be an example: the superposition of small rotations around a large number of bonds could produce significant changes of the molecular shape. Thus, a dimer which cannot be well accommodated in the nematic phase, with a low energetic cost could change its shape, to make it more suitable to the ordered environment [62, 63]. To check whether small amplitude rotations around the minima can influence the elastic and dielectric properties of the systems under

investigation, for some of them we have performed calculations using Monte Carlo (MC) sampling of the torsional angles. The results are presented in this chapter. The MC procedure as implemented in our methodology is described in Sec. 4.5.

Calculations with MC sampling of conformations can be significantly more expensive than those based on the RIS approximation. Table 7.1 reports the number of MC steps and of accepted conformations in the calculations of the elastic constants of CBOnOCB dimers. These can be compared with the number of conformers for analogous calculations with the RIS approximation (see Table 6.1).

Table 7.1: Number of MC steps and number of accepted conformations in calculations of the elastic constants of CBOnOCB dimers. n is the number of methylenes in the flexible spacer.

	CBOnOCB	
n	MC steps	accepted
4	25000	12371
5	50000	26655
6	40000	21511
7	140000	71051
8	75000	34715

The number of MC steps was determined on the basis of the convergence of local and global properties. Figure 7.1 shows the distribution of the φ_3 dihedral (see Figure 4.5) obtained for the CB7CB dimer with a number of 22000 MC steps; we can see that the whole range of torsional angles is sampled.

Figure 7.2 reports the calculated flexoelectric coefficients and elastic constants of the CBO5OCB dimer, as a function of the number of accepted conformations. The figure shows that the number of steps needed for convergence may depend on the property. We have found that in general the flexoelectric coefficients converge faster than the elastic constants; among these, the bend modulus K_{33} has been found to be particularly critical, especially for odd dimers.

Figure 7.3 shows S_{zz}, the largest principal value of the Saupe matrix, as a function of the reduced temperature $T^* = T/T^{NI}$ obtained for CBO5OCB and CB7CB with MC sampling of conformations. For the sake of comparison, the RIS results for the same

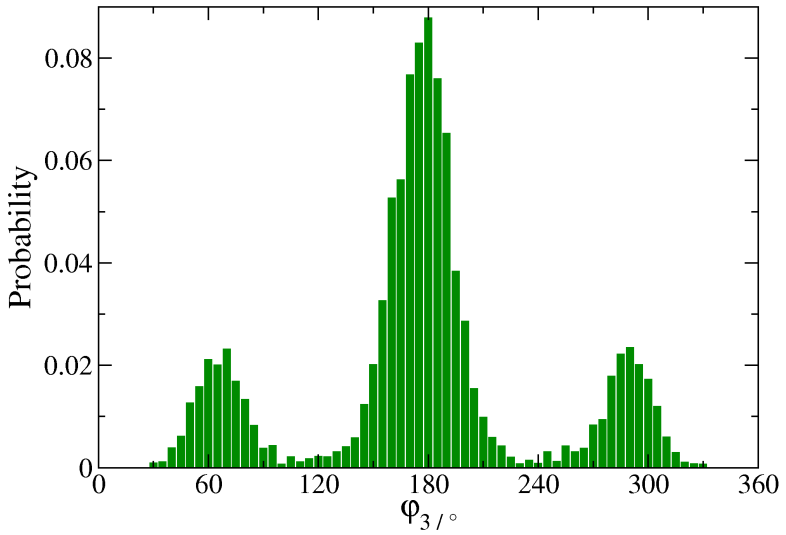

Figure 7.1: Probability distribution of the φ_3 torsional angle (see Figure 4.5) for the CB7CB dimer (22000 MC steps).

systems are also shown in the figure. We can see that for both systems the NI transition is shifted at slightly higher order parameter and the predicted S_{zz} value increases over the whole temperature range, when the geometric constraints of the RIS approximation are relaxed. This can be understood, on the basis of the considerations presented at the beginning of this section.

In the following, we shall report the flexoelectric coefficients, dielectric constants and elastic constants calculated for dimers using MC sampling of conformations. We shall focus on the cases which exhibit significant differences from the RIS results.

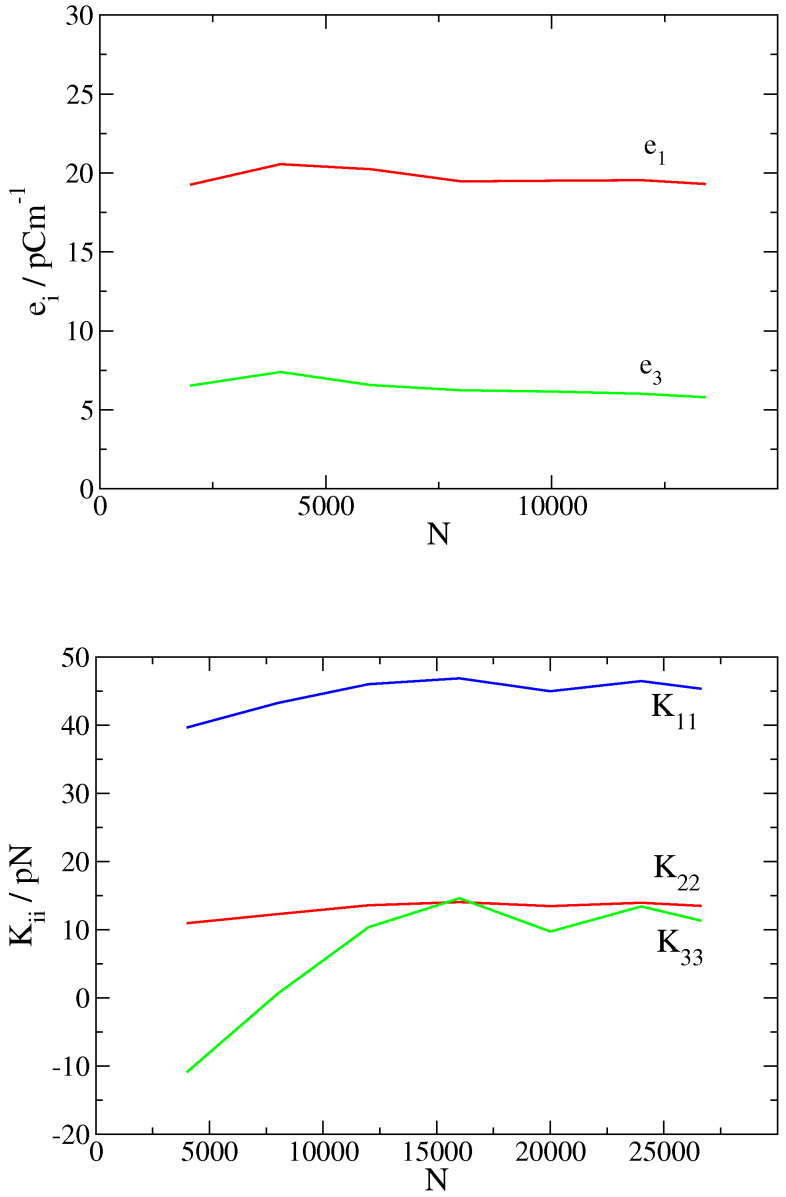

Figure 7.2: Calculated flexoelectric coefficients (top) and elastic constants (bottom) of the CBO5OCB dimer, as a function of the number of accepted conformations.

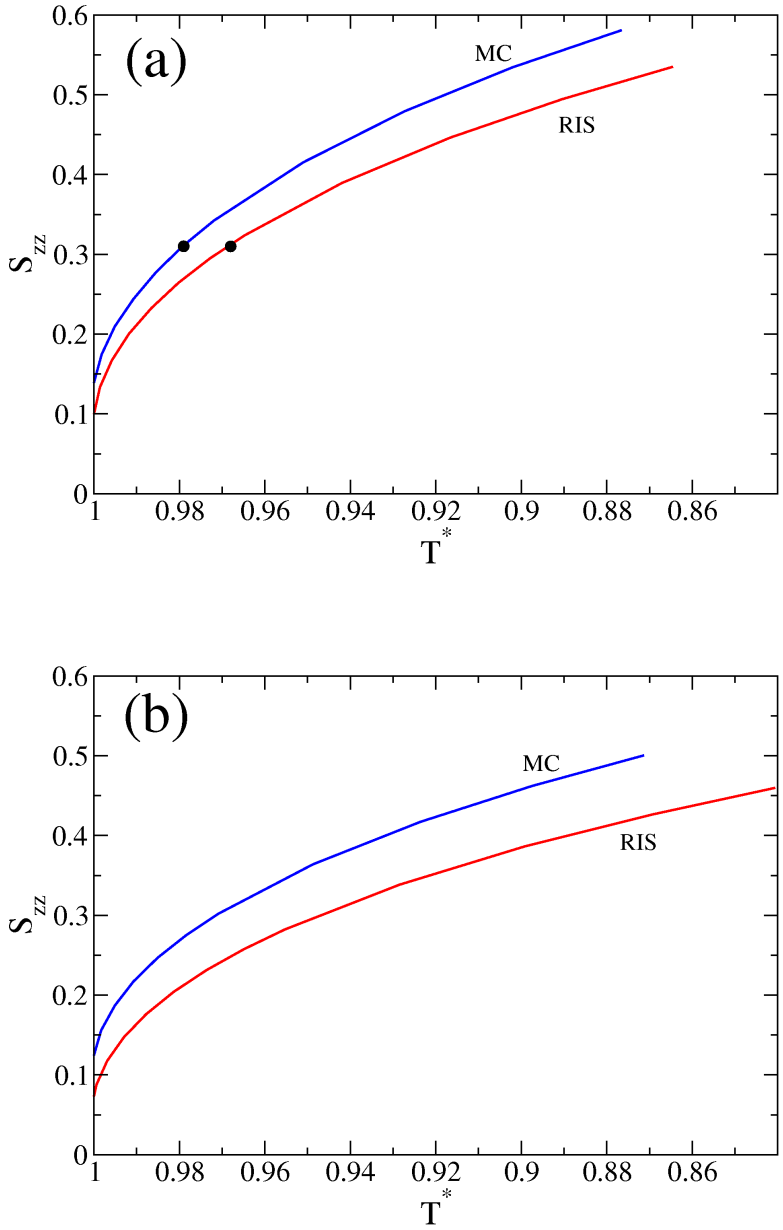

Figure 7.3: S_{zz} order parameter as a function of the reduced temperature T^* for the CBO5OCB (a) and CB7CB (b) dimers: results obtained by MC sampling of conformations (blue) and RIS approximation (red). S_{zz} is the largest eigenvalue of the Saupe matrix. The black circles show the experimental order parameters at the NI transition [18].

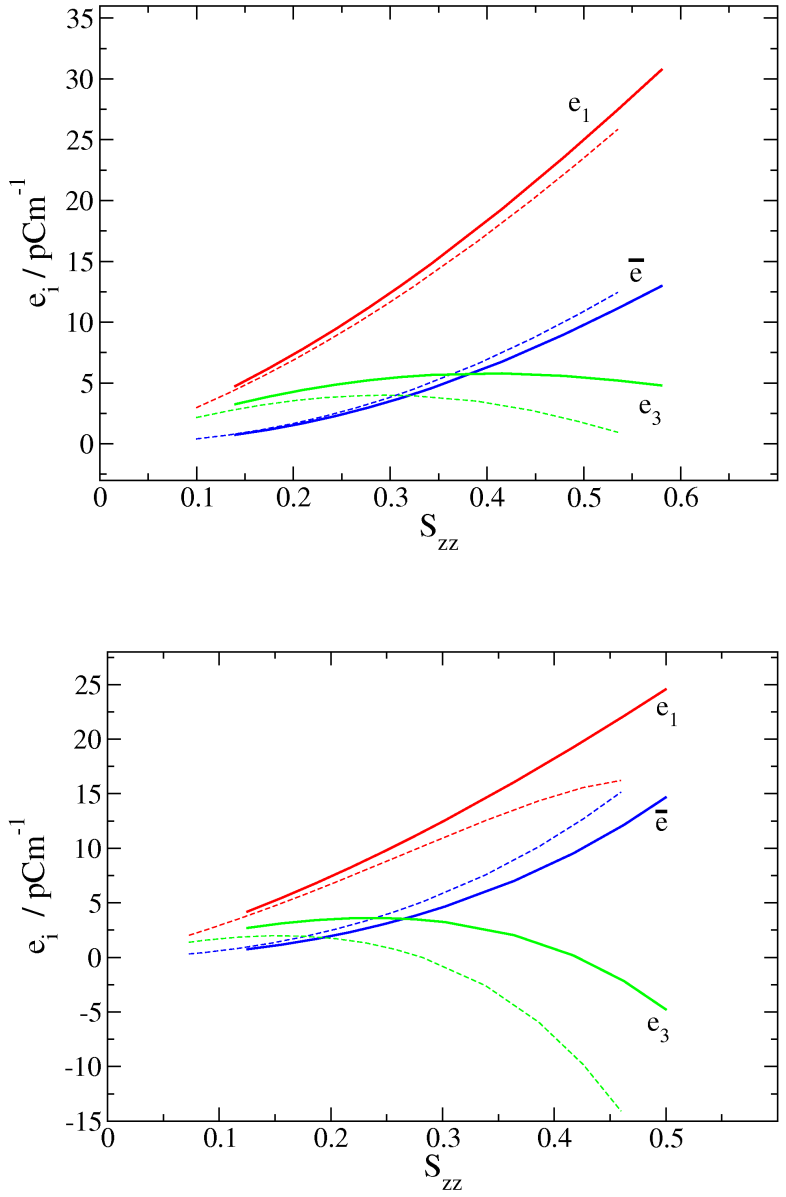

Figure 7.4: Flexoelectric coefficients calculated for CBO5OCB (top) and CB7CB (bottom), by MC sampling (continuous lines) and RIS approximation (dashed lines).

7.2 Flexoelectric coefficients

Figure 7.4 shows the splay e_1, bend e_3 and effective $\bar{e} = (e_1 - e_3)/2$ flexoelectric coefficients calculated for CBO5OCB and CB7CB. For the sake of comparison the results obtained by the RIS approximation are also reported. We can see that for both systems the dependence on order of e_1 is not strongly influenced by the MC sampling, whereas significant effects, from the quantitative point of view, are found for e_3.

7.3 Dielectric permittivity

Figure 7.5 displays the scaled mean square components of the electric dipole, parallel and perpendicular to the nematic director, calculated for CBO5OCB with MC sampling of conformations. The temperature dependence of the parallel component is quite different from that predicted using the RIS approximation, and shows better qualitative agreement with the experimental behaviour reported for CBO11OCB (Figure 6.8). The main reason behind the difference is the change of the temperature dependence of the Saupe matrix, shown in Figure 7.3.

Figure 7.6 shows the measured temperature dependence of the dielectric permittivity for CB7CB [92]. The analogy with the results shown in Figure 6.8 for CBO10OCB and CBO11OCB appears, with positive dielectric anisotropy, which decreases with lowering temperature. The results obtained using the RIS approximation and MC sampling of conformations for CB7CB are reported in Figure 7.7. We can see that a completely wrong temperature dependence is predicted in the former case.

To understand the reason for the large differences between RIS and MC results found for CB7CB, it is useful to look at the probability distribution of the β angle between the *para* axes of the cyanobiphenyl units, shown in Figure 7.8. Very different distributions are obtained with the two methods. The RIS distribution is sharp and changes only slightly with the degree of order: in most of the conformers the angle between the two arms is close to 120°. The β distribution obtained by MC sampling is much broader and is sensitive to the degree of order: we can see that the increase of order favours the more elongated conformations, which can be better accommodated in the nematic environment. As shown in Figure 7.9, these conformations are characterised by a low dipole moment;

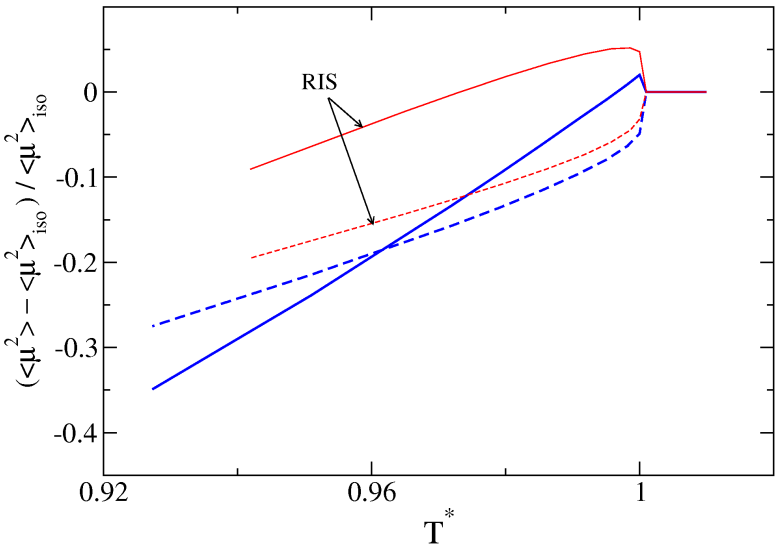

Figure 7.5: Scaled dipole moment $\left(\langle\mu^2_{\parallel(\perp)}\rangle - \langle\mu^2\rangle_{\rm iso}\right) / \langle\mu^2\rangle_{\rm iso}$ as a function of the reduced temperature T^*, calculated for CBO5OCB by MC sampling (blue) and RIS approximation (red). Continuous and dashed lines indicate the parallel and perpendicular component, respectively.

this is the reason for the decrease of the mean square dipole components with lowering temperature.

It is worth considering in some more detail the difference between CBO5OCB and CB7CB: the replacement of the oxygen atoms with methylenes has a twofold effect. (i) The rotation around the bond connecting aromatic ring and flexible chain is significantly less restricted in CB7CB than in CBO5OCB, as appears from comparison of the torsional potentials shown in Figures 4.4a and 4.1b. Indeed, given the height of the torsional barriers, the RIS approximation is clearly inadequate in the case of CB7CB.

(ii) The C_{ar}-O-C angle (119°) is slightly larger than the C_{ar}-C-C (113°) angle; as a consequence the conformations of CBO5OCB are in average more elongated than those of CB7CB. As shown by comparison of Figures 7.8 and 7.10, such a seemingly small difference in bond angles allows the CBO5OCB conformers to have a distribution of the β angle wider than that found in the case of CB7CB, for which the only available angles are essentially those tetrahedral. This is another reason why no dramatic differences appear between RIS and MC results in the case of CBO5OCB.

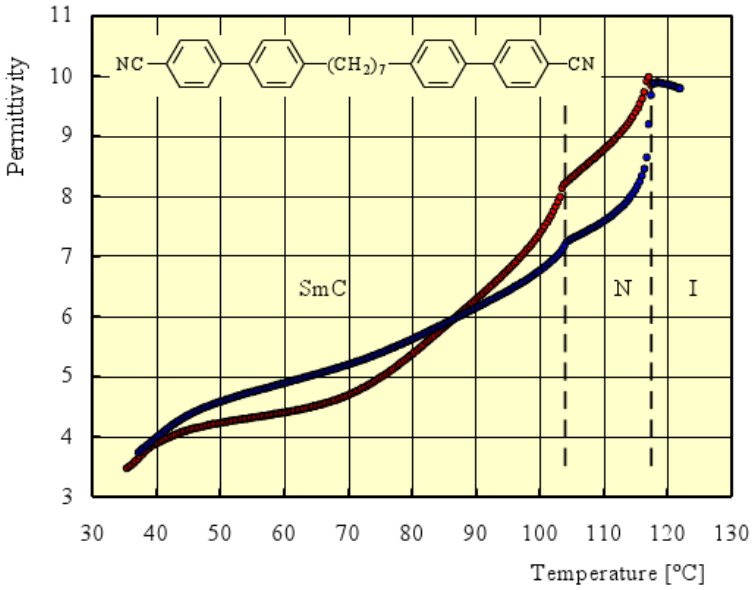

Figure 7.6: Experimental dielectric constants for the CB7CB [92]. I and N denote the isotropic and nematic phase, respectively.

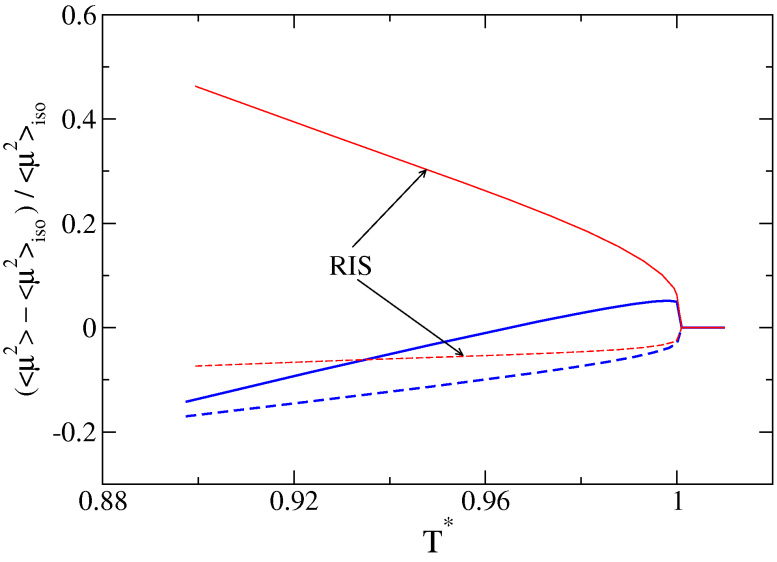

Figure 7.7: Mean square components of the molecular dipole as a function of the reduced temperature T^*, calculated for CB7CB, employing MC sampling of torsional angles (blue) and the RIS approximation (red). Continuous and dashed lines indicate the parallel and perpendicular components, respectively.

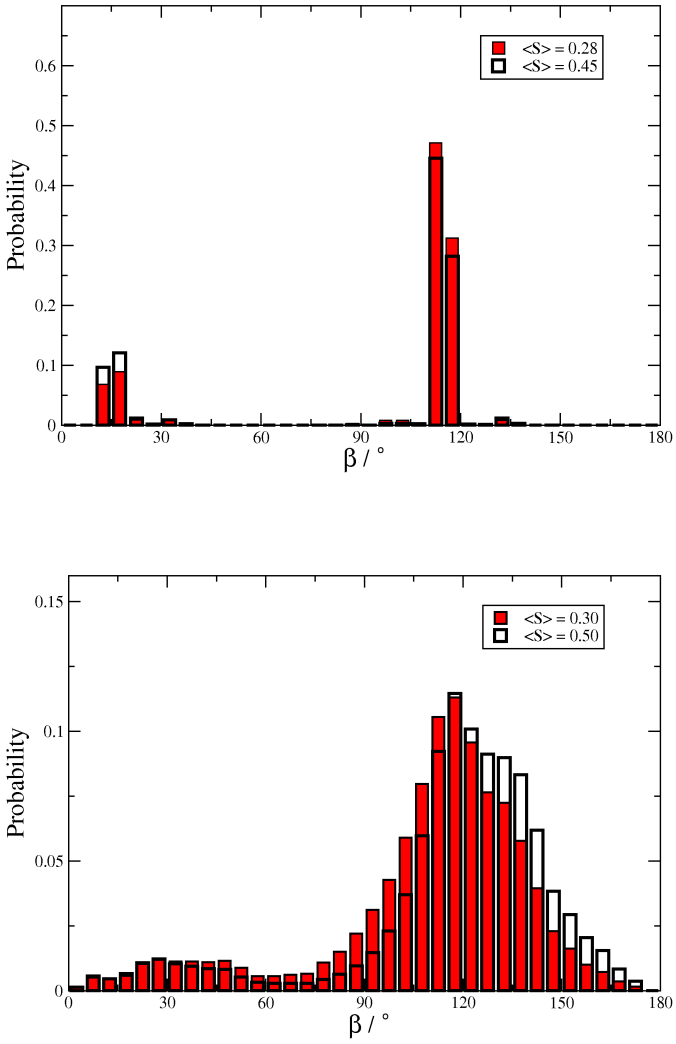

Figure 7.8: Probability distribution of the β angle between the *para* axes of the cyanobiphenyl units of CB7CB, calculated at two values of the order parameters S_{zz}. Top: RIS approximation; bottom: MC sampling of torsional angles. S_{zz} is the largest principal value of the Saupe matrix.

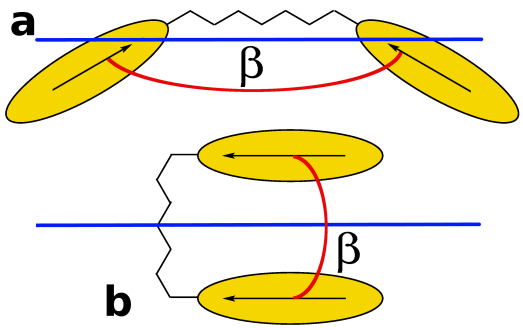

Figure 7.9: Cartoon of two dimer conformations with very different elongation and dipole moment.

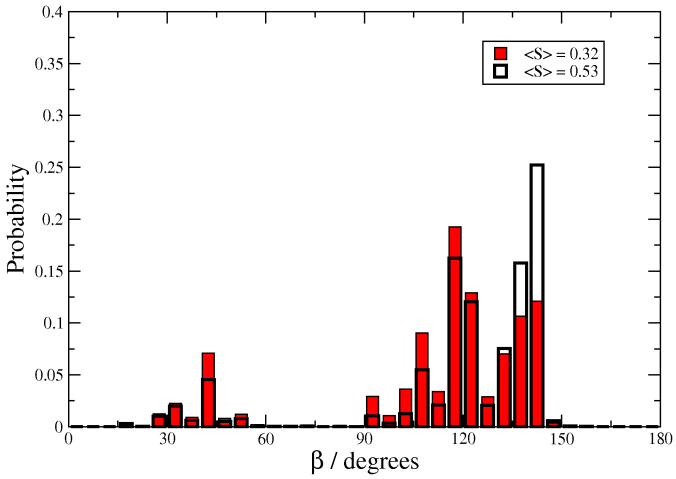

Figure 7.10: Probability distribution of the β angles between the *para* axes of the cyanobiphenyl groups of CBO5OCB, calculated with the RIS approximation at two distinct values of the order parameter. S_{zz} is the largest principal value of the Saupe matrix.

7.4 Elastic constants

Figure 7.11 shows the elastic constants calculated for CBO5OCB and CBO6OCB, employing the MC sampling of torsional angles. It is interesting to compare these results with those obtained with the RIS approximation, also reported in figure with dashed lines. A clear difference emerges for the bend elastic constant, the most sensitive to the sampling procedure, whereas similar results are found for the splay and twist elastic constants.

Figure 7.12 reports the elastic constants calculated for all the CBOnOCB dimers.

7.5 Interpretation of experiments

Collecting the results reported in the two last chapters, we can now try to interpret the experimental results of Coles and coworkers [12, 13]. They have reported the flexoelastic ratio $\bar{e}/\bar{K}$, with $\bar{e} = (e_1 - e_3)/2$ and $\bar{K} = (K_{11} + K_{33})/2$, for CBOnOFF dimers at a reduced temperature $T^* \simeq 0.95$ [12], for CBO8OCB at the same reduced temperature [13], and for 7OCB at $T^* \simeq 0.98$ [13]. These data are shown in Table 7.2. For the CBOnOFF series we can see clear odd-even effects: the flexoelectric ratios measured for the odd members are about twice as large as those determined for the even members; the latter are close to the value reported for 7OCB. Moreover, the flexoelastic ratio for CBO8OCB and CBO8OFF are similar.

Table 7.2 also shows the flexoelectric coefficients, along with the elastic constants and their ratios, calculated for the CBOnOCB dimers and for 5OCB. In the table the values for dimers refer to the order parameters listed in Table 6.2, which were determined by Tsvetkov and colleagues for the CBOnOCB series at a reduced temperature $T^* \simeq 0.95$ [74]. Flexoelectric coefficients and elastic constants exhibit oscillations with the number of methylenes in the spacer, with regularly lower values for the odd members. In particular, K_{11} and e_1 are higher for even members, simply as a consequence of the higher order parameter at the given reduced temperature. In the case of K_{33} and e_3, the reason behind the odd-even differences is less trivial, i.e. the special effect of shape bending on bend deformations of the nematic director, and very strong oscillations are found. Then, the effective flexoelectric coefficients and the effective elastic constants are bigger and smaller for even dimers. The final result is that the flexoelastic ratio, which is the

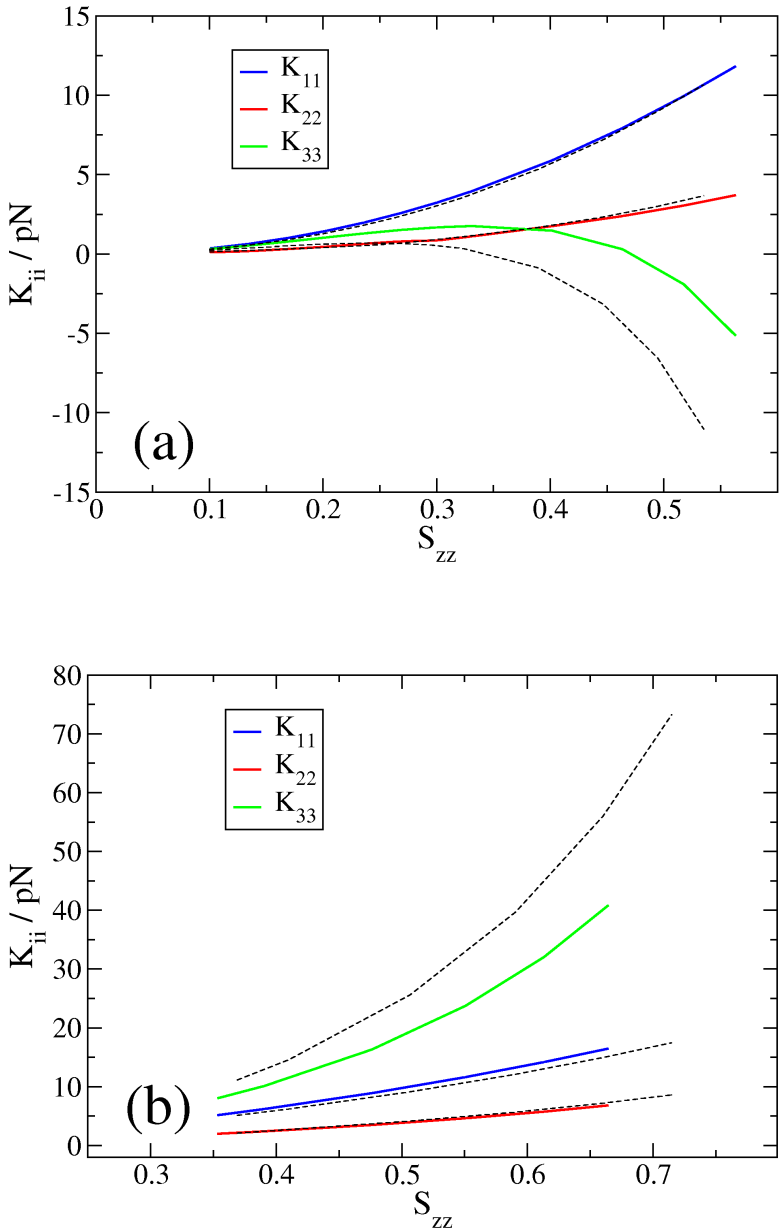

Figure 7.11: Elastic constants calculated for CBO5OCB (a) and CBO6OCB (b), by MC sampling of torsional angles (solid lines). For the sake of comparison, the results obtained for the same systems using the RIS approximation are also shown (dashed lines). S_{zz} is the largest principal value of the Saupe matrix.

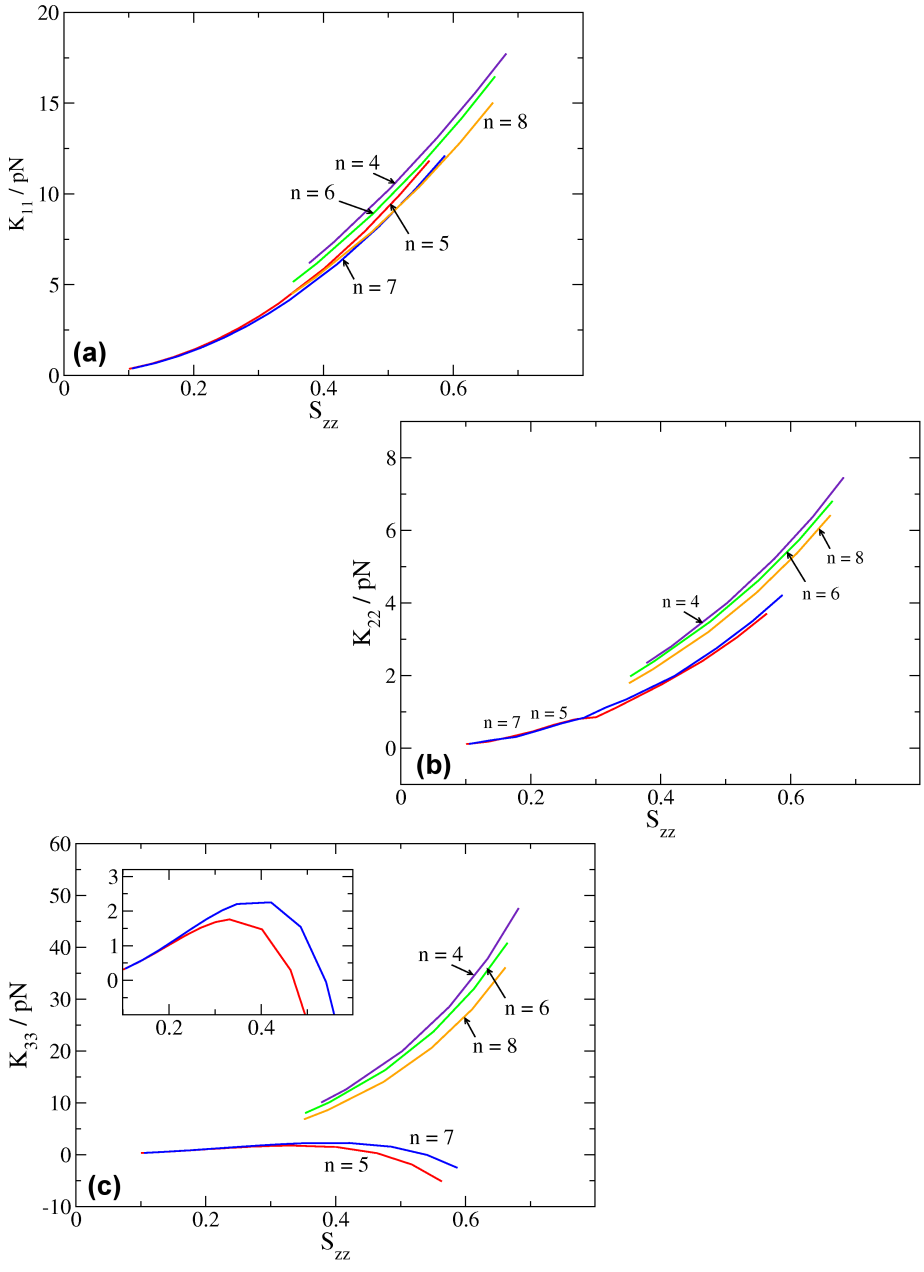

Figure 7.12: Splay elastic constants obtained for CBOnOCB dimers as a function of the order parameter S_{zz}. MC sampling of the torsional angles is used. n is the number of methylenes in the flexible spacer.

measured quantity, also displays odd-even oscillations, with lower values for the even dimers.

Reminding that, as shown in chapter 6, at a given reduced temperature both elastic constants and flexoelectric coefficients predicted for CBOnOFF dimers are slightly lower than those obtained for CBOnOCB dimers, we can compare the flexoelastic ratios calculated for the latter with corresponding values measured for the former. The results reported in Table 7.2 show the good agreement between theoretical predictions and experimental data. The quality of these results can be better appreciated, considering that presently no other method exists, which could provide any reliable estimates of elastic constants or flexoelectric coefficients of these systems.

A last comment deals with the comparison between mesogenic dimers and the corresponding monomers. In agreement with experiment, the flexoelastic ratio predicted for 5OCB is similar to that obtained for even dimers. However, this value for 5OCB results from the ratio of an effective flexoelectric coefficient and an effective elastic constant which are about an order of magnitude smaller than those of dimers.

Table 7.2: Flexoelectric coefficients and elastic constants calculated for CBOnOCB dimers and for 5OCB at the order parameters reported in Table 6.2. Experimental values of the flexoelastic ratio $\bar{e}/\bar{K}$ are also reported [12, 13].

	CBOnOCB							
n	e_1 / pC m^{-1}	e_3 / pC m^{-1}	$\bar{e}$ / pC m^{-1}	K_{11} / pN	K_{33} / pN	$\bar{K}$ / pN	$\bar{e}/\bar{K}$ calc. / C N^{-1} m^{-1}	$\bar{e}/\bar{K}$ exp. / C N^{-1} m^{-1}
4	27	18	4.5	13	30	21.5	0.2	-
5	22	2	10	8	0	4	2.0	(1.45)[a]
6	27	17	5	13	28	20.5	0.25	(0.45)[a]
7	22	1	10.5	9	1	5	2.0	(1.29)[a]
8	28	17	5.5	12	25	18.5	0.3	0.6 (0.52)[a]
	nOCB							
n	e_1 / pC m^{-1}	e_3 / pC m^{-1}	$\bar{e}$ / pC m^{-1}	K_{11} / pN	K_{33} / pN	$\bar{K}$ / pN	$\bar{e}/\bar{K}$ calc. / C N^{-1} m^{-1}	$\bar{e}/\bar{K}$ exp. / C N^{-1} m^{-1}
5	7	6	0.5	2	3	2.5	0.2	0.4[b]

[a] the experimental values in brackets refer to CBOnOFF [12].

[b] the experimental value refers to 7OCB [13].

Summary

This thesis focuses on the development and the application of a computational methodology, based on a molecular field theory and atomistic modelling, to connect dielectric and elastic properties of nematic liquid crystals to the structure of the constituent molecules.

Chapter 1 is a general introduction on the subject of the thesis. Firstly, the problem of the connection between materials properties and structure of the molecular constituents is introduced, with special reference to the case of liquid crystals, and the object of this work is presented. The main features of liquid crystals are then recalled, considering in particular the elastic and dielectric properties, investigated in this thesis, which are directly involved in the electro-optical behaviour. We also show the molecular systems to which the theoretical- computational methodology developed here has been applied. These have the common structure of two mesogenic, rather rigid units, connected by a flexible spacer. For these reasons they are called 'dimers'. These mesogens have several reasons of interest: their liquid crystal properties are very sensitive to changes in the molecular structure and exhibit some unusual and unexplained features. Therefore they can been devised as a benchmark for molecular modelling of liquid crystals.

In chapter 2 the theoretical framework is presented. After a review of the state of the art of the computational methods for the study of liquid crystals, we present the molecular field approach used in this thesis, which is based on the 'Surface Interaction' (SI) model. Herein, the relation between molecular and mesoscale level is introduced through the assumption that each element of the molecular surface tends to align to the nematic director. A realistic account of the molecular structure is made possible by the use of a surface generated from atomic coordinates. We report the molecular expressions obtained in this framework for the ordering, thermodynamic, flexoelectric and dielectric properties of nematic liquid crystals. Given the role played by the molecular flexibility, special attention is devoted to the conformational degrees of freedom. Two different ways are proposed for its inclusion in the model: the Rotational Isomeric State (RIS) approximation, in which only the molecular geometries corresponding to the minima of the torsional potential are considered, or the Monte Carlo (MC) sampling of torsional angles.

In chapter 3 we derive molecular expressions for the bulk and surfacelike elastic constants of nematics, within the framework of the SI model. This requires extensive use of

tensor calculus; after some lengthy algebra, simple expressions are obtained, by exploiting the symmetry of the undeformed nematic phase. From the point of view of the theoretical development, this is the main result of the present thesis. The elastic constants can be calculated as a function of the orientational order, without any free parameter, at low computational cost. It enables us to investigate the role of molecular features and to explore how changes at the atomic level can be conveyed into changes in elastic behaviour, on a quite different length-scale. Therefore it can shed light on the origin, still poorly understood, of the different elasticity of mesogens with different structure. The predictive ability of this method makes it potentially useful for the synthetic design of tailored mesogens: the elastic constants can be easily calculated, if the molecular structure is known. We also derive molecular expressions for the surfacelike elastic constants of nematics. The surface elasticity of nematics has been a subject of intense theoretical and experimental investigation and no consensus has been reached; our analysis can be seen as a preliminary exploration of this problem, which deserves further investigation in the future, and we hope that our atomistic level approach can provide some new insight.

In chapter 5 the elastic behaviour of three typical liquid crystals mesogens (PAA, 5CB, 8CB) is investigated, using the molecular field theory presented in Chapter 3. These have been chosen as representative cases because of their different elasticity, despite the structural similarity. The availability of experimental data allows us to assess the quality of the theoretical predictions. We show that the observed temperature dependence of the splay, twist and bend elastic moduli can be traced back to differences, even not dramatic, in molecular shape. Our calculations also highlight the importance of the flexibility of mesogens, which was generally ignored by previous theories: in view of their different shape, conformers are shown to give different contributions to the elastic moduli. The key role of deviations from a rod-like shape, which is generally assumed by models of mesogens, emerges from the calculations. The bend elastic constant is shown to be particularly sensitive to molecular bending; it can range from high values for rod-like conformers, to low and even negative values for bent conformers of a given compound. These findings could have important implications for bent-core mesogens, which are presently the object of intense investigation because of their unusual and attractive properties. We also report the surfacelike elastic constants of PAA, 5CB, 8CB, whose experimental determination is controversial; we have found that these are generally smaller than the bulk elastic moduli

and even more sensitive to changes in molecular shape.

The results obtained for the LC dimers, taking into account the conformational freedom at the RIS level, are reported in chapter 6. A full overview is provided, comprising order parameters, properties at the nematic-isotropic transition, dielectric permittivity, elastic and flexoelastic moduli. The molecular model enables us to reach an unprecedented insight into the origin of not yet explained experimental findings, and to predict behaviours not yet probed by experiment. Particularly interesting are the results obtained for the flexoelectric and elastic properties of the LC dimers. The common view, which gives electric and steric dipoles the main responsibility for the flexoelectric properties, cannot explain recent experimental findings for LC dimers; our results single out the importance of taking into account the whole distribution of charges and the real molecular shape. Experimental data are available for the splay elastic constants of dimers [Tsvetkov et al, Mol. Cryst. Liq. Cryst.: 331:1901, 1999]: we correctly predict not only magnitude of the elastic constants, but also their dependence on the length of the flexible spacer. No comparison with experiment is possible for the twist and bend elastic moduli; however our results appear very promising, in relation to some intriguing phenomena which have been recently reported for LC dimers [Coles et al, Nature, 436:997, 2005] and bent-core LCs [Görtz et al, Soft Matter, 5:463, 2009].

In chapter 7 we investigate whether the small amplitude fluctuations around the minima of the torsional potential, which are neglected by the RIS approximation, can affect the elastic and dielectric properties of LC dimers. To this purpose, we have performed calculations with MC sampling of the torsional angles. We show that small amplitude fluctuations do play a role for those properties which are particularly sensitive to the balance between elongated and bent conformations; these comprise the bend elasticity and flexoelectricity. Significant, though less subtle effects of torsional oscillations are also found for the dielectric permittivity, when some of the torsional angles are characterised by relatively low barriers between the minima. In this final chapter, collecting all the results obtained for LC dimers, we are able to provide a complete explanation for the experiments performed by Coles and colleagues [Coles et al, J. Mater. Chem.,11:2709, 2001; Morris et al, Phys. Rev. E, 75:041701,2007], which simultaneously involve elastic and flexoelectric properties.

Riassunto

La tesi ha come oggetto lo sviluppo e l'applicazione di una metodologia computazionale, basata su una teoria di campo molecolare e su una modellazione atomistica, per connettere proprietà dielettriche ed elastiche dei nematici alla struttura delle molecole costituenti.

Il capitolo 1 riporta una introduzione generale sull'argomento della tesi. Innanzitutto, il problema della connessione tra le proprietà di materiali e la struttura molecolare dei costituenti, con speciale riferimento al caso dei cristalli liquidi, e si introduce l'obiettivo di questo studio. Vengono poi richiamate le principali caratteristiche dei cristalli liquidi, considerando in particolare le proprietà elastiche e dielettriche, investigate in questo lavoro di tesi, che sono direttamente coinvolte nel comportamento elettro-ottico del materiale. Si riportano, inoltre, i sistemi molecolari ai quali è stata applicata la metodologia sviluppata. Questi hanno in comune una struttura costituita da due unità mesogeniche piuttosto rigide, collegate tramite una catena flessibile e per queste ragioni sono chiamati *dimeri*. Questi mesogeni hanno molteplici ragioni di interesse: le loro proprietà di cristallo liquido sono molto sensibili ai cambiamenti nella struttura molecolare e mostrano comportamenti inusuali e tuttora inspiegati. Quindi, costituiscono un buon banco prova per la modellizzazione molecolare dei cristalli liquidi.

Nel capitolo 2 viene presentato il contesto teorico dello studio. Dopo una rassegna dello stato dell'arte dei metodi computazionali impiegati per lo studio dei cristalli liquidi, viene presentato l'approccio di tipo campo molecolare utilizzato, che è basato sul modello delle 'Interazioni di Superficie'. In esso, la relazione tra livello molecolare e mesoscala è introdotta tramite l'assunzione che ogni elemento della superficie molecolare tenda ad allinearsi al direttore della fase nematica. È possibile rendere conto della struttura molecolare tramite l'uso di una superficie generata dalle coordinate atomiche. Si riportano le espressioni molecolari ottenute nell'ambito del modello SI per le proprietà di ordine, termodinamiche, flessoelettriche e dielettriche dei cristalli liquidi nematici. Al riguardo, data l'importanza della flessibilità molecolare, speciale cura è stata dedicata ai gradi di libertà conformazionali. Due metodi differenti sono stati proposti per la sua inclusione nel modello: l'approssimazione dello stato rotazionale isomerico (Rotational Isomeric State, RIS), nel quale si considerano solo le geometrie corrispondenti ai minimi del potenziale torsionale, e il campionamento Monte Carlo (MC) degli angoli torsionali.

Nel capitolo 3 si derivano le espressioni molecolari per le costanti elastiche di *bulk* e di superficie nel contesto del modello SI. Questo richiede un uso estensivo del calcolo tensoriale; alla fine si ottengono espressioni semplici, sfruttando la simmetria della fase nematica non deformata. Dal punto di vista dello sviluppo teorico, questo è il principale risultato della presente tesi. Le costanti elastiche possono essere calcolate in funzione dell'ordine orientazionale, senza l'uso di parametri liberi, ed a basso costo computazionale. La teoria sviluppata ha permesso di investigare il ruolo svolto dalle caratteristiche molecolari e esplorare come cambiamenti a livello atomistico influiscano sul comportamento elastico, su una scala di lunghezza assai differente. È stato quindi possibile interpretare l'origine, tuttora poco chiara, della differente elasticità della fase nematica formata da mesogeni con differente struttura chimica. L'abilità predittiva di questo metodo lo rende potenzialmente utile come strumento per la guida al *design* sintetico di cristalli liquidi con proprietà desiderate: le costanti elastiche possono essere facilmente calcolate se si conosce la struttura molecolare. In questo capitolo, si derivano inoltre espressioni molecolari per le cosiddette costanti di superficie dei nematici. L'elasticità di superficie dei nematici è stata oggetto di intensa indagine sia sperimentale che teorica senza peraltro raggiungere un consenso comune; la nostra analisi può essere vista come un'esplorazione preliminare di questo problema, che merita ulteriori approfondimenti in futuro, ed è sperabile che l'approccio atomistico qua descritto possa dare un contributo alla comprensione del fenomeno.

Dato il contesto teorico, la possibilità di ottenere predizioni di elevata qualità delle proprietà dei materiali liquido-cristallini risiede nella disponibilità di (i) una procedura computazionale efficiente e flessibile, (ii) accurati valori delle proprietà a livello molecolare (energia, geometria e cariche) per i sistemi in esame. Entrambi i punti sono stati trattati nel capitolo 4. È stata realizzata una procedura computazionale integrata; codici Fortran realizzati *ad hoc* e software di terze parti sono stati collegati tramite programmi Python. In tal modo, si sono sfruttate le specifiche caratteristiche di ciascun linguaggio di programmazione: codice Fortran veloce ed ottimizzato per le parti riguardanti il calcolo intensivo, e programmazione Python ad alto livello per il controllo dell'intera procedura computazionale. Particolare attenzione è stata dedicata alla generazione delle conformazioni molecolari. Queste sono convenientemente assemblate da un limitato numero di unità molecolari, cioè frammenti trasferibili con cariche e geometrie fissate. La definizione accurata dei parametri ha richiesto un'analisi preliminare, basata principalmente su cal-

coli quantomeccanici di singola molecola; i risultati sono riportati nel capitolo 4.

Nel capitolo 5 viene riportata l'analisi del comportamento elastico di tipici mesogeni liquido-cristallini (PAA, 5CB, 8CB), impiegando la teoria di campo molecolare presentata nel capitolo 3. PAA, 5CB e 8CB sono stati scelti come casi rappresentativi a causa della loro differente elasticità, a dispetto delle loro piccole differenze strutturali. La disponibilità di dati sperimentali ha permesso di giudicare la qualità delle predizioni teoriche. Si mostra che la dipendenza dalla temperatura osservata per il modulo elastico di *splay*, *twist* e *bend* può essere ricondotta a differenze, anche se piccole, di forma molecolare. I calcoli riportati evidenziano l'importanza della flessibilità dei mesogeni, che è stata generalmente ignorata dalle precedenti teorie: a causa delle diverse forme, i conformeri danno contributi differenti ai moduli elastici. Dai calcoli emerge il ruolo chiave delle deviazioni della struttura molecolare da una forma cilindrica. La costante elastica di *bend* si mostra particolarmente sensibile al ripiegamento nella struttura molecolare e può variare da alti valori per conformeri approssimatamente cilindrici, a valori bassi e anche negativi per conformeri ripiegati di un dato composto. Questi risultati possono avere importanti implicazioni per i mesogeni formati da unità rigide ripiegate (chiamati *bent-core*), che sono tuttora oggetto di intensa analisi a causa delle loro proprietà inusuali e interessanti dal punto di vista applicativo. Per il PAA, il 5CB e 8CB sono state calcolate anche le costanti elastiche superficiali, la cui determinazione sperimentali è controversa; abbiamo trovato che queste costanti sono generalmente più piccole dei moduli elastici di *bulk* e anche più sensibili ai cambiamenti di forma molecolare.

I risultati ottenuti per i dimeri liquido cristallini, tenendo conto della libertà conformazionale a livello RIS, sono riportati nel capitolo 6. Viene presentata una rassegna completa, comprensiva dei parametri d'ordine, delle proprietà alla transizione nematico-isotropica, della permittività dielettrica, e dei moduli elastici e flessoelastici. Il modello molecolare consente di ottenere una maggiore comprensione dell'origine di risultati sperimentali, e di predire comportamenti ancora non verificati da esperimenti. Particolarmente interessanti sono i risultati ottenuti per le proprietà flessoelettriche ed elastiche dei dimeri liquido-cristallini. La visione comune, che ascrive ai dipoli elettrici e sterici la principale responsabilità delle proprietà flessoelettriche, non permette di spiegare una serie di risultati ottenuti recentemente per tali dimeri; i risultati presentati in questo lavoro di tesi individuano l'importanza di tenere conto dell'intera distribuzione delle cariche e della

reale forma molecolare. Risultati sperimentali sono disponibili per le costanti elastiche di splay dei dimeri [Tsvetkov et al, Mol. Cryst. Liq. Cryst., 331:1901, 1999]; di essi viene correttamente riprodotta sia l'intensità delle costanti elastiche, che la loro dipendenza dalla lunghezza della catena spaziatrice. Non è possibile confrontare con dati sperimentali i moduli elastici di twist e bend; comunque i risultati sembrano molto promettenti in relazione a interessanti fenomeni che sono stati recentemente riportati per i dimeri [Coles et al, Nature, 436:997, 2005] e per cristalli liquidi *bent-core* [Görtz et al, Soft Matter, 5:463, 2009].

Nel capitolo 7 si valuta se le fluttuazioni di piccola ampiezza attorno ai minimi dei potenziali torsionali, trascurati nell'approssimazione RIS, possono avere effetti sulle proprietà elastiche e dielettriche dei dimeri liquido-cristallini. A tal fine, sono stati realizzati calcoli con campionamento MC degli angoli torsionali. Si mostra che le fluttuazioni di piccola ampiezza giocano un ruolo per quelle proprietà che sono particolarmente sensibili all'elequilibrio tra conformazioni allungate e quelle ripiegate; queste comprendono le componenti *bend* dell'elasticità e della flessoelettricità. Significativi effetti delle oscillazioni torsionali si sono trovati anche per la permittività dielettrica, quando alcuni angoli torsionali sono caratterizzati da barriere relativamente basse tra i minimi di energia potenziale. In questo capitolo finale, raccogliendo i risultati ottenuti per dei dimeri liquido cristallini, si è fornita una spiegazione degli esperimenti realizzati da Coles e collaboratori [Coles et al, J. Mater. Chem., 11:2709, 2001; Morris et al, Phys. Rev. E, 75:041701, 2007], che coinvolgono simultaneamente proprietà elastiche e flessoelettriche.

Acknowledgements - Ringraziamenti

Many thanks to all the people I've met in Southampton, especially my lovely housemates Leire, Siphiwe, Filippo, Rita, Claudia, Candice and Matt. Plus, I'm particularly grateful to Mario, Beppe, Nicola, Marco and all the guys of 89 Harefield road.

Pur sapendo come sia impossibile fare una lista di tutte le persone che mi sono state vicine in questo periodo trascorso a Padova mi sentirei veramente in difficoltà a non menzionare tutti i ragazzi della sala calcolo ed in particolare Mirco, Barbara, Silvia, Fabio e Andrea, e tutti i ragazzi della sala dottorandi. Estrema gratitudine va ad i miei amici di Ferrara Edo, Andrea, Fede e Telli, e agli ex compagni di corso (e ora compagni di "shuda") Lara, Manuel, Anna, Alex e Stef.

Infine, su tutti, ringrazio la mia famiglia.

Bibliography

[1] Wilson, M. R. *Int. Rev. Phys. Chem.* **24**, 421 (2005).

[2] Wilson, M. R. *Chem. Soc. Rev.* **36**, 1861 (2007).

[3] Leach, A. R. *Molecular Modelling: Principles and Applications*. Dorset Press, Dorchester, (2001).

[4] Ferrarini, A., Moro, G. J., Nordio, P. L., and Luckhurst, G. R. *Mol. Phys.* **77**, 1 (1992).

[5] Ferrarini, A., Moro, G. J., and Nordio, P. L. *Phys. Rev. E* **53**, 681 (1996).

[6] Ferrarini, A., Moro, G. J., and Nordio, P. L. *Mol. Phys.* **87**, 485 (1996).

[7] Schadt, M. and Helfrich, W. *Appl. Phys. Lett.* **127**, 18 (1971).

[8] Schadt, M. *Annu. Rev. Mater. Sci.* **27**, 305 (1997).

[9] Davidson, A. J. and Mottram, N. J. *Phys. Rev. E* **65**, 051710 (2002).

[10] Meyer, R. B. *Phys. Rev. Lett.* **22**, 918 (1969).

[11] Prost, J. and Marceau, J. P. *J. Phys. (France)* **38**, 315 (1977).

[12] Morris, S. M., Clarke, M. J., Blatch, A. E., and Coles, H. J. *Phys. Rev. E* **75**, 041701 (2007).

[13] Coles, H. J., Musgrave, B., Coles, M. J., and Willmott, J. *J. Mater. Chem.* **11**, 2709 (2001).

[14] Tsvetkov, N. V., Zuev, V. V., Ksenofontov, I. V., and Tsvetkov, V. N. *Liq. Cryst.* **25**, 727 (1998).

[15] Coles, H. J. and Pivnenko, N. *Nature* **436**, 997 (2005).

[16] Urban, S., Gestblom, B., Kuczynski, W., Pawlus, S., and Wurflinger, A. *Phys. Chem. Chem. Phys* **5**, 924 (2003).

[17] Dunmur, D. A., Fukuda, A., and Luckhurst, G. R., editors. *Physical Properties of Liquid Crystals*. EMIS Datareviews Series, IEE, London, (2000).

[18] Emsley, J. W., Luckhurst, G. R., , and Shilstone, G. N. *Mol. Phys.* **53**, 1023 (1984).

[19] Burnell, E. E. and de Lange, C. A. *Chem. Rev.* **98**, 2359 (1998).

[20] Berardi, R., Muccioli, L., and Zannoni, C. *ChemPhysChem* **5**, 104 (2004).

[21] Stimson, L. M. and Wilson, M. R. *J. Chem. Phys.* **123**, 034908 (2005).

[22] Sunaidi, A. A., Otter, W. K. D., and Clarke, J. H. R. *Philos. Trans. R. Soc. London Ser. A* **362**, 1773 (2004).

[23] Allen, M. P., Warren, M. A., Wilson, M. R., Sauron, A., and Smith, W. *J. Chem. Phys.* **105**, 2850 (1996).

[24] Maier, W. and Saupe, A. *Z Naturforsch A* **14**, 882 (1959).

[25] Maier, W. and Saupe, A. *Z Naturforsch A* **15**, 287 (1960).

[26] Luckhurst, G. R., Zannoni, C., Nordio, P. L., and Segre, U. *Mol. Phys.* **30**, 1345 (1975).

[27] Rapini, A. and Papoular, M. *J. de Physique Colloq.* **30**, 54 (1969).

[28] Ferrarini, A., Luckhurst, G. R., Nordio, P. L., and Roskilly, S. J. *J. Chem. Phys.* **100**, 1460 (1994).

[29] Ferrarini, A. *Phys. Rev. E* **64**, 021710 (2000).

[30] Vertogen, G. and de Jeu, W. H. *Thermotropic liquid Crystals: Fundamentals.* Springer, Berlin, (1988).

[31] Flory, P. J. *Statistical mechanics of chain molecules.* Wiley, New York, (1969).

[32] Frisch, M. J., Trucks, G. W., Schlegel, H. B., Scuseria, G. E., Robb, M. A., Cheeseman, J. R., Montgomery, Jr., J. A., Vreven, T., Kudin, K. N., Burant, J. C., Millam, J. M., Iyengar, S. S., Tomasi, J., Barone, V., Mennucci, B., Cossi, M., Scalmani, G., Rega, N., Petersson, G. A., Nakatsuji, H., Hada, M., Ehara, M., Toyota, K., Fukuda, R., Hasegawa, J., Ishida, M., Nakajima, T., Honda, Y., Kitao, O., Nakai, H., Klene, M., Li, X., Knox, J. E., Hratchian, H. P., Cross, J. B., Bakken, V., Adamo, C., Jaramillo, J., Gomperts, R., Stratmann, R. E., Yazyev, O., Austin, A. J., Cammi,

R., Pomelli, C., Ochterski, J. W., Ayala, P. Y., Morokuma, K., Voth, G. A., Salvador, P., Dannenberg, J. J., Zakrzewski, V. G., Dapprich, S., Daniels, A. D., Strain, M. C., Farkas, O., Malick, D. K., Rabuck, A. D., Raghavachari, K., Foresman, J. B., Ortiz, J. V., Cui, Q., Baboul, A. G., Clifford, S., Cioslowski, J., Stefanov, B. B., Liu, G., Liashenko, A., Piskorz, P., Komaromi, I., Martin, R. L., Fox, D. J., Keith, T., Al-Laham, M. A., Peng, C. Y., Nanayakkara, A., Challacombe, M., Gill, P. M. W., Johnson, B., Chen, W., Wong, M. W., Gonzalez, C., and Pople, J. A. Gaussian 03, Revision C.02, Gaussian, Inc., Wallingford, CT, 2004.

[33] Almenningen, A., Bastiansen, O., Fernholt, L., Cyvin, B. N., Cyvin, S. J., and Samdal, S. *J. Mol. Struct.* **128**, 59 (1985).

[34] Bastiansen, O. and Samdal, S. *J. Mol. Struct.* **128**, 115 (1985).

[35] Seip, H. M. and Seip, R. *Acta Chem Scand.* **27**, 4024 (1973).

[36] Carreira, L. A., , and Towns, T. G. *J. Mol. Struct.* **41**, 1 (1977).

[37] Cacelli, I. and Prampolini, G. *J. Phys. Chem. A* **107**, 8665 (2003).

[38] Tsuzuki, S., Uchimaru, T., Matsamura, K., Mikami, M., and Tanabe, K. *J. Chem. Phys.* **110**, 2858 (1999).

[39] Göller, A. and Grummt, U.-W. *Chem. Phys. Lett.* **321**, 399 (2000).

[40] Cinacchi, G. and Prampolini, G. *J. Phys. Chem. A* **107**, 5228 (2003).

[41] Smith, G. D., Jaffe, R. L., and Yoon, D. Y. *J. Phys. Chem. B* **100**, 13439 (1996).

[42] Bultinck, P., Alsenoy, C. V., and Goeminne, A. *J Phys. Chem. A* **105**, 9203 (2001).

[43] Salam, A. and Deleuze, S. *J. Chem. Phys.* **116**, 1296 (2002).

[44] Klauda, J. B., Pastor, R. W., and Brooks, B. R. *J. Phys. Chem. B* **109**, 15684 (2005).

[45] Klauda, J. B., Brooks, B. R., Jr, A. D. M., Venable, R. V., and Pastor, R. W. *J. Phys. Chem. B* **109**, 5300 (2005).

[46] Koglin, E. and Meier, R. J. *Chem. Phys.* **312**, 284 (1999).

[47] Colombo, L. and Zerbi, G. *J. Chem. Phys.* **73**, 2013 (1980).

[48] Kanesaka, I., Snyder, R. G., and Strauss, H. L. *J. Chem. Phys* **84**, 395 (1986).

[49] Herrebout, W. A., van der Veken, B. J., Wang, A., and Durig, J. R. *J Phys. Chem.* **99**, 578 (1995).

[50] Smith, G. D. and Jaffe, R. L. *J. Phys. Chem.* **100**, 18718 (1996).

[51] Ferrarini, A., Luckhurst, G. R., Nordio, P. L., and Roskilly, S. J. *Chem. Phys. Lett.* **214**, 409 (1993).

[52] Malpezzi, L., Bruckner, S., Ferro, D. R., and Luckhurst, G. R. *Liq. Cryst.* **28**, 357 (2001).

[53] Bata, editor. *Advances in liquid crystal research and application*, volume 1. Pergamon Press, New York, (1981).

[54] Picken, S. J., Gunsteren, W. F. V., Duijnen, P. T. V., and Jeu, W. H. D. *Liq. Cryst.* **6**, 357 (1989).

[55] Pelez, J. and Wilson, M. *Phys. Chem. Chem. Phys.* **9**, 2968 (2007).

[56] Tiberio, G., Muccioli, L., Berardi, R., and Zannoni, C. *ChemPhysChem* **10**, 125 (2009).

[57] Besler, B. H., Merz, K. M., and Kollman, P. A. *J. Comput. Chem.* **11**, 431 (1990).

[58] Singh, U. C. and Kollman, P. A. *J. Comput. Chem.* **5**, 129 (1984).

[59] Martin, F. and Zipse, H. *J. Comput. Chem.* **26**, 97 (2004).

[60] Jorgensen, W. L., Maxwell, D. S., , and Tirado-Rives, J. *J. Am. Chem. Soc.* **118**, 11225 (1996).

[61] Metropolis, N., Rosenbluth, A. W., Rosenbluth, M. N., Teller, A. H., and Teller, E. *J. Chem. Phys.* **12**, 1087 (1953).

[62] Stocchero, M., Ferrarini, A., Moro, G. J., Dunmur, D. A., and Luckhurst, G. R. *J. Chem. Phys.* **121**, 8079 (2004).

[63] Ferrarini, A., Luckhurst, G. R., and Nordio, P. L. *Mol. Phys.* **85**, 131 (1995).

[64] GRACE, (2008). Ver. 5.1.22 `http://plasma-gate.weizmann.ac.il/Grace/`.

[65] Cornell, W. D., Cieplak, P., Bayly, C. I., Gould, I. R., Merz, K. M., Ferguson, D. M., Spellmeyer, D. C., Fox, T., Caldwell, J. W., and Kollman, P. A. *J. Am. Chem. Soc.* **117**, 5179 (1995).

[66] Anderson, P. M. and Wilson, M. R. *Mol. Phys.* **103**, 89 (2005).

[67] Cacelli, I., Prampolini, G., and Tani, A. *J. Phys. Chem. B* **109**, 3531 (2005).

[68] Sanner, M. F., Spehner, J. C., and Olson, A. J. *Biopolymers* **38**, 305 (1996).

[69] Langtangen, H. P. *Python scripting for computational science (texts in computational science and engineering).* Springer-Verlag New York, (2005).

[70] Ferrarini, A., Janssen, F., Moro, G. J., and Nordio, P. L. *Liq. Cryst.* **26**, 201 (1999).

[71] Bondi, A. *J. Phys. Chem.* **68**, 441 (1964).

[72] Emsley, J. W., Luckhurst, G. R., Shilstone, G. N., and Sage, I. *Mol. Cryst. Liq. Cryst. Lett.* **102**, 223 (1984).

[73] Barnes, P. J., Douglass, A. G., Heeks, S. K., and Luckhurst, G. R. *Liq. Cryst.* **13**, 603 (1993).

[74] Tsvetkov, V. N., Tsvetkov, N. V., Didenko, S. A., and Zuev, V. V. *Mol. Cryst. Liq. Cryst.* **265**, 341 (1995).

[75] Luckhurst, G. R. and Gray, G. W. *The Molecular Physics of Liquid Crystals.* Academic, London, (1979).

[76] Zare, R. N. *Angular Momentum.* Wiley: New York, (1987).

[77] Petrov, A. G. In *Physical Properties of Liquid Crystals,* Dunmur, D. A., Fukuda, A., and Luckhurst, G. R., editors. EMIS Datareviews Series, IEE, London (2000).

[78] Bauman, D. and Wolarz, E. *Liq. Cryst.* **26**, 45 (1999).

[79] Dunmur, D., Luckhurst, G. R., de la Fuente, M. R., Diez, S., and Jubindo, M. A. P. *J. Chem. Phys.* **115**, 8681 (2001).

[80] Singh, S. *Phys. Rep.* **277**, 283 (1996).

[81] Bradshav, M. J., Ranes, E. P., and Bunning, J. D. *J. Phys (France)* **46**, 1513 (1985).

[82] Ford, A. D., Morris, S. M., Pivnenko, M. N., Gillespie, C., and Coles, H. J. *Phys. Rev. E* **76**, 051703 (2007).

[83] Ionescu, D., Luckhurst, G. R., and de Silva, D. S. *Liq. Cryst.* **23**, 833 (1997).

[84] Dozov, I. *Europhys. Lett.* **56**, 247 (2001).

[85] Görtz, V., Southern, C., Roberts, N. W., Gleeson, H. F., and Goodby, J. W. *Soft. Matter* **5**, 463 (2009).

[86] Eremin, A., Nemes, A., Stannarius, R., Pelzl, G., and Weissflog, W. *Soft. Matter* **4**, 2186 (2008).

[87] Wiant, D., Gleeson, J. T., Eber, N., Fodor-Csorba, K., and andT Toth-Katona, A. J. *Phys. Rev. E* **72**, 041712 (2005).

[88] Dodge, M. R., Rosenblatt, C., Petschek, R. G., Neubert, M. E., and Walsh, M. E. *Phys. Rev. E* **62**, 5056 (2000).

[89] Kundu, B., Pratibha, R., and Madhusudana, N. V. *Phys. Rev. Lett.* **99**, 247802 (2007).

[90] Kitzerow, H.-S. *ChemPhysChem* **7**, 63 (2006).

[91] Alexander, G. P. and Yeomans, J. M. *Phys. Rev. E* **74**, 061706 (2006).

[92] de la Fuente, M. R., Pérez-Jubindo, M. A., López, D. O., Dunmur, D. A., Luckhurst, G. R., Salud, J., and Diez, S. In *Book of Abstracts, 9th European Conference on Liquid Crystals, Lisbon*, PB31, July (2007).